# Re-aligning patient prognosis: the role of collagen in establishing an immunosuppressive microenvironment and facilitating cancer cell dissemination in pancreatic ductal adenocarcinoma

A Dissertation

SUBMITTED TO THE FACULTY OF THE

UNIVERSITY OF MINNESOTA

BY

Mackenzie Kate Callaway

IN PARTIAL FULFILLMENT OF THE REQUIREMENTS

FOR THE DEGREE OF

DOCTOR OF PHILOSOPHY

Paolo Provenzano, PhD

Degree conferred October 2021

© Mackenzie Kate Callaway 2021

## BIOGRAPHICAL SKETCH

Mackenzie Kate Callaway is originally from Lee's Summit, MO. In August 2011, Mackenzie began attending the University of Missouri-Columbia as an Engineering Dean's Scholar and Howard Hughes Medical Institute Apprentice. Mackenzie worked in Dr. Donald Burke's laboratory during the entirety of her undergraduate career studying Human Immunodeficiency Virus (HIV), and under the guidance of Dr. Margaret Lange-Osborn, she earned two additional HHMI Fellowships with an emphasis on communicating science to the public. In 2015, she graduated *Cum Laude* with University Honors, earning her Bachelor of Science in Biological Engineering with a Biology minor. Mackenzie began pursuing her Doctor of Philosophy in Biomedical Engineering at the University of Minnesota and received a National Science Foundation Graduate Research Fellowship and an Engineering in Oncology Fellowship through the Physical Sciences in Oncology Center. Outside the lab, she has served her department, University, and community as Co-Chair of the Student Health Advisory Committee, President of the Graduate Women in Biomedical Engineering, Vice President of GWBME Outreach, Graduate Women's Coordinator for the College of Science and Engineering, and Representative to the Council of Graduate Students. In 2019, Mackenzie's dedication was recognized as a recipient of the President's Student Leadership and Service Award from University of Minnesota, an award presented to less than

< 0.1% of students. She is motivated by helping others achieve professional success, physical and mental wellness, and—above all—personal fulfillment.

## ACKNOWLEDGEMENTS

This dissertation would not have been possible without the consistent optimism and encouragement from my advisor, Dr. Paolo Provenzano. I also give my thanks to Dr. Kaylee Schwertfeger and the scientists in her lab for their contributions and support over the years. I thank my mentors Dr. Donald Burke-Aguero and Dr. Margaret Lange-Osborn from the University of Missouri, who went above and beyond to provide me with an outstanding undergraduate research experience and continue to be role models to me now. In Minnesota, I have been grateful to have the support of my lab mates and friends who have shared in my misery and joy in graduate school, and in particular, my lab mates Rachel, Rachel and Demi with whom I've shared a few tears, lots of nachos, and even more laughs. I thank previously graduated lab mates Kianna Elahi-Gedwillo and Nelson Rodriguez for their warmth, intelligence, and laughter, and Arja Ray without whom this dissertation would not exist. I emphatically thank Boynton Health leadership, Dave and Dr. K in particular—for working tirelessly to improve student health, and for their continuous encouragement and astoundingly positive attitudes—they embody the leader I can only hope to become. I thank my partner's parents, Dennis and Sharon, for their love, support and selflessness. I also thank my parents, Sam and Vicki, for their fierce support—they have always pushed me to be fearless, to persevere, to be bold, to speak up, to own it, and to try to do the right thing. I would be remiss to not acknowledge my cat, Hank, for his company and unconditional love during the COVID-19 pandemic and, finally, am forever indebted to my partner

and biggest advocate, Dan, for his limitless love and faith in me. I am glad he followed me to Minnesota in 2015 and look forward to joining him in New York as a postdoctoral fellow in the dos Santos Lab at Cold Spring Harbor Laboratory.

## DEDICATION

In memory of those we have lost, and with hope for the ones we may still help.

## ABSTRACT

Pancreatic ductal adenocarcinoma (PDA) is an aggressive cancer with particularly poor clinical outcomes, in part, because of a dramatically altered stromal environment and striking immune dysfunction. Physical properties within tumors—such as aligned fiber architectures—are fundamental to cancer progression and invasion, and negatively correlate with survival in cancers like those of the breast. However, the influence of aligned architectures in PDA remains unexplored. Here, we elucidate the role extracellular matrix alignment has in establishing an immunosuppressive, metastasis-conducive tumor microenvironment in early, preinvasive PDA, as well as in precursory pancreatic inflammation. Using both mouse and human samples, we demonstrate an inextricable link between collagen, alignment, and 1) immunosuppressive macrophage localization, phenotype, and function (Chapter 2); 2) epithelial cell extrusion and subsequent invasion from intact ductal structures (Chapter 3). The contribution of alignment in both driving macrophage polarization and tumor cell dissemination could be attributed to altered focal adhesion dynamics, as targeting FAK *in vivo* resulted in a concomitant decrease in aligned collagen architectures, disseminated tumor cells, metastatic burden, and elongated, immunosuppressive macrophages. In Chapter 4, we explore the interplay between macrophages, collagen, and cancer cell extrusion using novel 3D microtissue co-cultures and human biopsies to reveal contributions of macrophages to dissemination *in vitro* and *in vivo*. Importantly, we show aligned collagen signatures and immunosuppressive macrophages are

abundantly prevalent in pancreatitis, a known risk factor for PDA, suggesting that pancreatic precursory disease may create stromal memory that is later conducive to early immunosuppression and dissemination of PDA. This work highlights the opportunity to utilize FAK inhibitors to target stromal immunity and architectures and supports a model in which collagen architecture drives the early involution of an immunosuppressive, malignant microenvironment. Further, this thesis underscores the importance of targeting stromal matrices in precursor inflammation, limit cancer progression, and “reprogram” stromal immunity.

# TABLE OF CONTENTS

# LIST OF FIGURES

## Chapter 1



## Chapter 2

## Chapter 3



## Chapter 4



## Supplemental Figures

## LIST OF ACRONYMS

| | |
|---|---|
| **ADM** | Acinar-to-Ductal Metaplasia |
| **Arg-1** | Arginase-1, canonical M2 marker |
| **APC** | Antigen Presenting Cell |
| **BMDM** | Bone Marrow Derived Macrophage |
| **CAN** | Cancer Adjacent Normal |
| **CD4 T cell** | Helper T lymphocyte (i.e., T regulatory cells) |
| **CD8 T cell** | Cytotoxic, anti-tumor lymphocyte |
| **CHC** | Circulating Hybrid Cell (Immune/Epithelial fusion) |
| **CP** | Chronic Pancreatitis |
| **CTC** | Circulating Tumor Cell |
| **ECM** | Extracellular Matrix |
| **EMT** | Epithelial to Mesenchymal Transition |
| **FAK** | Focal Adhesion Kinase |
| **FFPE** | Formalin Fixed Paraffin Embedded |
| ***KPC*** | *Kras*$^{LSLG12D/+}$ *;p53*$^{LSL-R172H/+}$ *;Pdx-1-Cre* mouse model |
| ***KPCT, G, Y*** | Labeled *KPC* models for tracing pancreas epithelia |
| **LSMPM** | Laser Scanning Multiphoton Microscopy |
| **MDSC** | Myeloid Derived Suppressor Cell |
| **MHC** | Major Histocompatibility Complex |
| **MMP** | Matrix Metalloproteinase |
| **M1** | Inflammatory, anti-tumor macrophage |

| | |
|---|---|
| **M2** | Immunosuppressive, pro-tumor macrophage |
| **PanIN** | Pancreatic Intraepithelial Neoplasia (preinvasive) |
| **PDA** | Pancreatic Ductal Adenocarcinoma |
| **ROS** | Reactive Oxygen Species |
| **SHG** | Second Harmonic Generation |
| **STT** | Stroma Targeted Therapy |
| **TAM** | Tumor Associated Macrophage |
| **TACS** | Tumor Associated Collagen Signatures |
| **TCM** | Tumor Conditioned Media |
| **TME** | Tumor Microenvironment (“stroma”) |

# 1. INTRODUCTION

## Pancreatic ductal adenocarcinoma and its clinical implications

Pancreatic ductal adenocarcinoma (PDA) is an extremely aggressive and highly lethal form of pancreatic cancer with a 5-year survival rate of 9% [1]. Despite the 5-year survival rate having doubled over the last several decades from <5% to <10%, the majority of patients are not diagnosed until after their cancer has spread to distant organs. Metastatic disease is the number one killer in nearly all solid tumors [2, 3], and points to an overarching need across cancer types to determine the factors promoting metastasis, and identify strategies to target these components to slow or stop cancer spread. PDA presents unique challenges in that it begins spreading very early in disease onset, and our ability to screen at-risk patients or detect PDA is severely lacking; patients rarely present clinical symptoms for diagnosis until late-stage disease at which point the survival rate is a grueling 3% [1].

## The purpose of the pancreas

The pancreas is primarily responsible for generating and secreting compounds to assist with digestion and regulate blood glucose levels. Pancreatic function is maintained by three distinct cellular components: acinar cells, pancreatic islands, and ducts (**Figure 1.1A**). Acinar cells are the predominant cell type in the pancreas and are responsible for secreting digestive enzymes like lipase, amylase, and trypsin for the breakdown of fats, carbohydrates, and proteins in other digestive organs. Pancreatic islets are small distinct groups of cells responsible for secreting

insulin and glucagon in response to elevated or diminished blood glucose (**Figure 1.1A, dashed margin**). Finally, pancreatic ducts—the namesake of PDA—transport pancreas secretions to other organs in the digestive tract (**Figure 1.1A, arrowhead**).

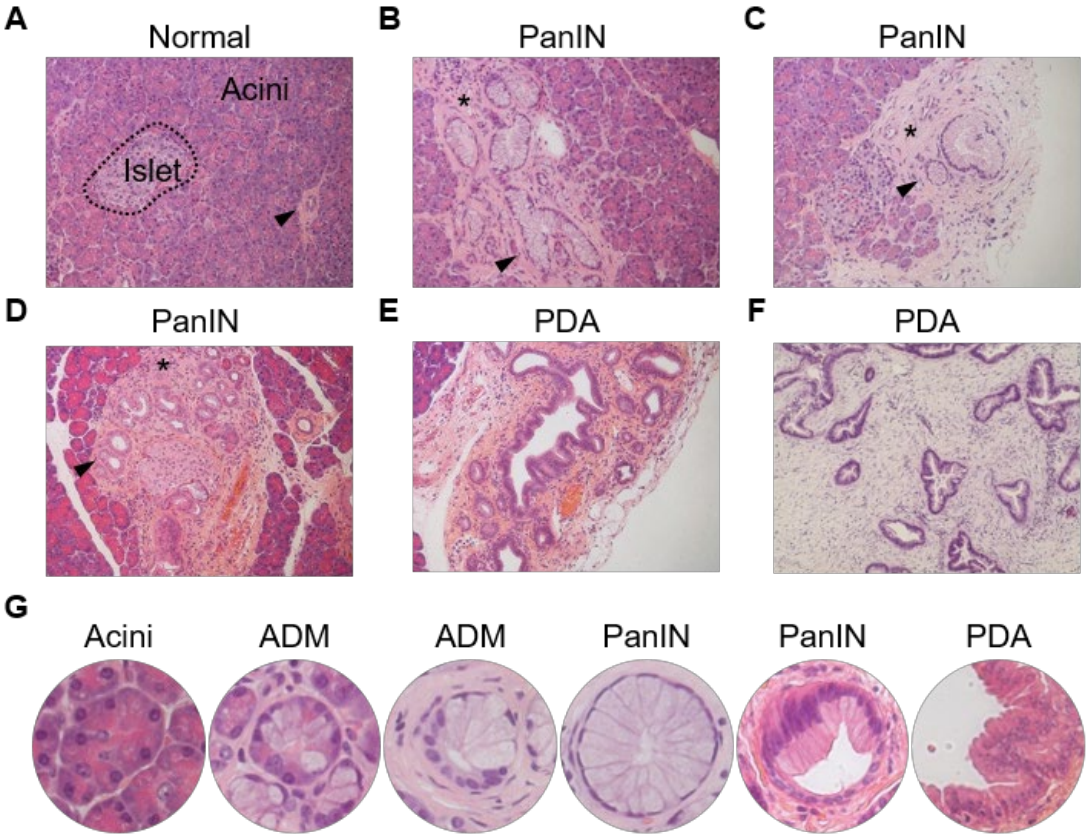


**Figure 1.1 Histological depictions of normal, preinvasive, and invasive pancreas tissue. A)** Image of normal pancreas with distinct acinar clusters, islets (margin) and sparsely distributed ducts with typical benign nuclear and cellular morphology (arrow head). **B), C)** and **D)** Low grade PanIN lesions and accumulation of ducts (arrow head) with fibrosis and acinar dropout (asterisk). **E)** Depiction of well-differentiated PDA with high-grade PanIN lesions and loss of nuclear polarity, severe acinar dropout and fibrosis. **F)** Advanced PDA with complete loss of acini and islets. **G)** Depiction of various stages of acinar to ductal metaplasia, from normal acinar clusters to well-differentiated PDA.

## Pancreas pathology

Ducts are typically very sparsely distributed within a healthy pancreas, and the elevated histological prevalence of ducts serves as a tell-tale indication of pancreatic pathology. In fact, the diagnosis of various grades of preinvasive lesions—called pancreatic intraepithelial neoplasia(s) (PanIN)—and the various stages of pancreas cancer are based on the evaluation of ductal prevalence and appearance (**Figures 1.1B through 1.1F**) [4-7]. Chronic inflammation of the pancreas, called chronic pancreatitis (CP), also displays histological features very similar to PDA (discussed in "Pancreatitis" section below). Histological features like acinar drop-out (**Figures 1.1B-1.1D, asterisks)**, expansion of ductal cells **(Figures 1.1B-1.1D, arrow heads)**, and the conversion of acinar cells to ductal cells—termed "acinar-to-ductal metaplasia" (ADM, depicted in **Figure 1.1G**)—are conserved in both disease contexts making it challenging to discern between resolvable but severe inflammation and signs of malignancy. However, key genetic aberrations observed reproducibly across human PDA are responsible for the neoplastic transformation of pancreas tissue and serve as markers for pancreas cancer identification. Nearly all PDA tumors (>90%) harbor oncogenic *KRAS* mutations, resulting in constitutive cell growth and proliferation [7, 8]. While cells possess pre-programmed responses to quell uncontrolled growth, 50-70% of pancreas tumors develop a mechanism of escape via dominant-negative mutations in *p53* [7, 8], a gene encoding a tumor suppressive protein normally responsible for inhibiting proliferation, inducing genetic repair, and instigating

apoptosis of aberrant cells. These core mutations are transformative events, not only bestowing advantages to pre-malignant epithelial cells, but also driving local alterations in non-neoplastic pancreas tissue [9, 10]. The composition of this local environment, referred to as the tumor microenvironment (TME), is highly linked to patient outcomes and offers a multitude of novel targets to consider for the treatment of PDA.

## Pancreatic tumor microenvironment: a clinical barrier

From its inception, PDA presents a fibrotic, inflammatory TME (also referred to throughout as the “stroma”). The stroma constitutes all non-neoplastic components of the tumor, both living and non-living, which support tumor cell growth and metastasis, exacerbate disease severity, and protect tumors from both host immune and therapeutic intervention [11-18]. Remarkably, the stroma can comprise over 90% of the pancreas tumor volume. Summarized in **Figure 1.2** [19], stromal components include 1) soluble factors like growth factors, cytokines, and chemokines, 2) a myriad of supportive cells that all serve the tumor, and 3) a densely fibrotic network of extracellular matrix components like hyaluronic acid and collagen which supports aggressive, invasive behavior. While there is a more comprehensive understanding of how both stromal- and tumor-derived soluble factors contribute to PDA, there is a fundamental disparity in knowledge relating to the interplay between stromal cells and ECM, and how this relationship contributes to the onset and severity of PDA.

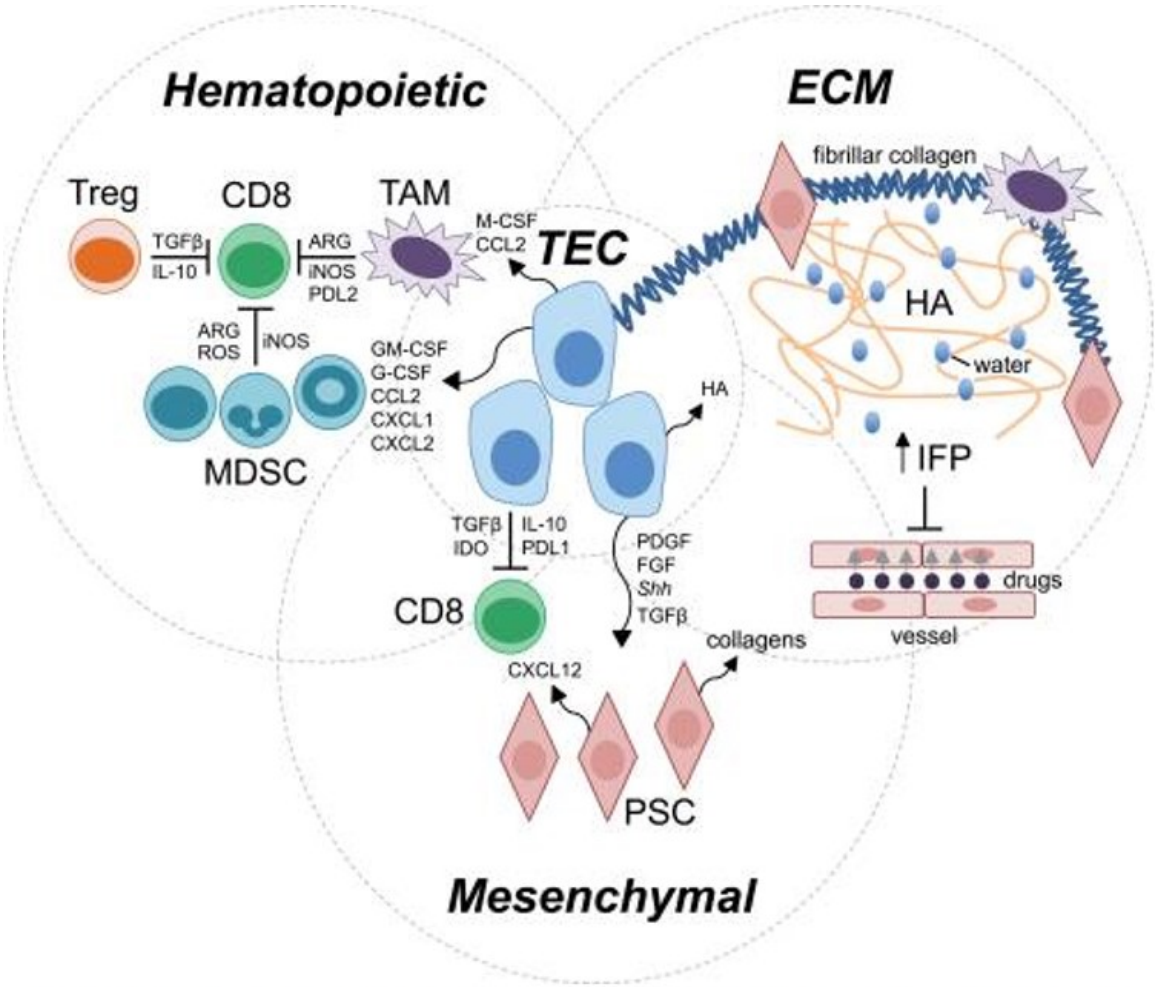


**Figure 1.2 The pancreatic tumor microenvironment.** Tumor epithelial cells are supported by signals from hematopoietic immunosuppressive cells like regulatory T cells, tumor associated macrophages and myeloid derived suppressor cells, all which contribute to the suppression of CD8+ T cells. Tumor cells also receive support from ECMs like collagen and HA, which increase interstitial fluid pressure to inhibit drug delivery. Finally, support from the mesenchymal compartment helps facilitate tumor progression via pancreatic stellate cells (fibroblasts) which assist in maintaining an immunosuppressive fibrotic environment. *Figure used with permission: Stromnes et al., 2014, Carcinogenesis.*

## *Stromal cells*

Stromal cells include any non-neoplastic cell type found within the TME and often support tumor progression by promoting processes like angiogenesis, tumor cell

growth, extracellular matrix deposition and reorganization, tumor cell metastasis, immune evasion and immune suppression [11, 12, 14, 19-24]. Due to the critical amount of support stromal cells provide tumors, they serve as an attractive target for novel therapeutics and combination regimes—is it possible to render tumors vulnerable to therapeutic intervention by cutting off tumor support? Indeed, studies have shown that traditional chemotherapies exhibit increased efficacy when used in combination with stroma targeted therapies (STTs), resulting in improved survival and anti-tumor immune responses in murine models of PDA [25-27]. Moreover, STTs which directly target stromal fibrosis, like halofuginone, have shown promise in their ability to alter stromal mechanics resulting in increased vessel patency, drug delivery, necrosis, and infiltration of anti-tumor immune cells [13]. Conversely, other groups have observed detrimental impacts from targeting stromal cells, suggesting the stroma may exert a tumor suppressive role in some contexts [28, 29]. For example, the depletion of stromal fibroblasts has been shown to increase immune suppression via the accumulation of regulatory T cells in mouse models deficient of myofibroblasts. These animals also exhibited poor survival compared to mice with stromal fibroblasts, as well as enhanced EMT signatures. Moreover, this study determined the prevalence of stromal myofibroblast in human PDA samples correlates with diminished survival [30]. An additional study showed deletion of collagen I specifically in stromal fibroblasts was sufficient to exacerbate PDA onset, immune suppression, and survival *in vivo* [29]. Another set of studies from Jiang, et al. highlights the utility in targeting stromal mechanics [31], yet also that this depletion is responsible for development

of stromal resistance to inhibition after continued treatment [32]. Even identical combination strategies have resulted in differential conclusions in human clinical trials, with one particular combination scheme showing striking benefits in phase II trials [33], and the following phase III trial showing no benefit, resulting in the abandonment of this particular drug, PEGPH20, altogether [28]. In fact, the inclusion of STTs in some clinical trials actually resulted in worse survival outcomes compared to control regime and thus were terminated before conclusion of trial [28]. This controversy highlights an urgent need to better understand which stromal components impact PDA progression, and how these components may be harnessed and altered to improve patient prognosis, or conversely, how promising therapies may inadvertently exacerbate disease without proper consideration of their impact on, for example, stromal immune cells.

Immune cells

Interestingly, despite a remarkable influx of immune cells beginning early and persisting throughout PDA progression, pancreas tumors notoriously fail to elicit anti-tumor responses [11, 15, 18, 34]. Much of this is due to the immune landscape in PDA, and the spatio-temporal dynamics of immune infiltration, polarization, and suppression [15, 18].

*T cells*

T cells are a major defense against pathogens, often involved with recognizing and mounting a response against host cells displaying foreign antigens. Antigens can be derived from pathogens like viruses or bacterium as well as from mutated host

proteins which may be indicative of neoplastic transformation. While both CD4 helper T and CD8 cytotoxic T cells can recognize foreign material, cytotoxic T cells are the only adaptive immune cell capable of recognizing and destroying aberrant *host* cells. Given the gravity of this responsibility, cytotoxic T cell activation is closely regulated to avoid unwarranted immune responses toward host organs, and inadequate regulation is linked to autoimmune disorders. The mechanisms used to naturally blunt T cell responses can be harnessed by tumors and utilized as mechanisms to shunt anti-tumor immune responses: cancer inherently finds ways around cytotoxic T cell recognition and death by imposing a multitude of barriers to T cell recruitment, migration, proliferation, function, and survival. These mechanisms are highlighted in **Figure 1.3** [35] and include creating chemically immunosuppressive environments, consuming T cell nutrients and metabolites necessary for their survival and cytotoxic functions, expressing compounds like FasL to promote CD8 T cell death, upregulating immune receptors like CTLA-4 and PD-L1, hijacking CD4 helper T cells to support tumors, down-regulating antigen presentation, and physically trapping CD8 T cells in extensive extracellular matrix networks [17, 35, 36]. In this way, CD8 T cells become physically constrained by ECM, blinded to host signals of abnormality, and/or destined for death due to lack of sufficient resources and stimulation. Taken together, these processes culminate to render cytotoxic T cells useless in PDA, regardless of their numbers.

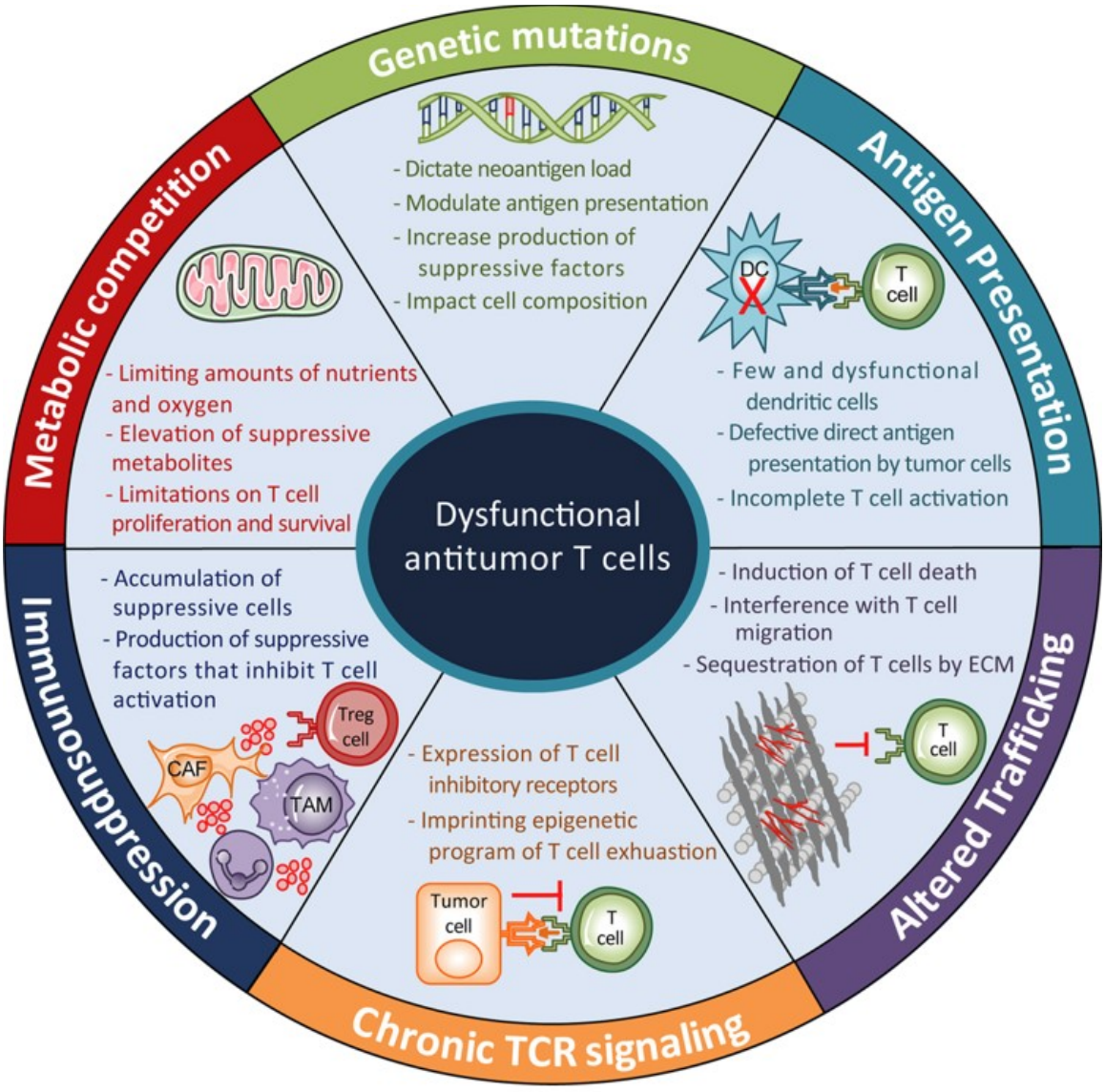


**Figure 1.3 Overview of mechanisms underlying T cell dysfunction in PDA.** Moving clockwise, and in summary, key points like the increase in expression and secretion of immunosuppressive cytokines, poor antigen presentation by aberrant tumor cells, inhibition of T cell migration via dense ECM, T cell inhibition and exhaustion, the development of an immunosuppressive TME, and the inhibition of T cell expansion and survival all contribute to the gruesome outcome associated with PDA and highlight the need for combination therapies which target multiple facets of cancer progression and immune modulation. *Figure used with permission: Anderson et al., 2017, Cancer Cell.*

Of no surprise, many therapeutics seek to reharness patient immunity. For example, some therapies seek to restore immunity by re-engineering T cells to recognize specific antigens, and while this approach has worked in other solid tumors, these therapies have had minimal success in human PDA, likely due at least in part to the stark absence of anti-tumor T cells altogether [37, 38]. Similarly, other immunotherapies have shown promising *in vitro* and *in vivo* in murine models, yet often result in clinical failure when progressed to human trials [18]. Perhaps by targeting stromal barriers, the utility of these failed immunotherapies will be revived [18, 35]. For example, freeing sequestered T cells from ECM, decreasing chemical immune suppression, and reeducating immune cells towards a potent anti-tumor state could all serve as more efficacious solutions compared to existing toxic therapeutics. One target garnering much recent attention to alleviate immune suppression and slow cancer progression across multiple contexts is the macrophage. In several solid tumors, macrophages have become an attractive target given their generally highly immunosuppressive role in cancer.

*Macrophages*

Macrophages are innate immune cells originating from the myeloid lineage and are one of the first lines of defense against pathogens [39]. In normal physiology, macrophages may be found sparsely distributed throughout the pancreas [15], existing in a quiescent state but ready to respond to injury or pathogens. Macrophages play a crucial role in the recognition, destruction, and clearance of foreign, pathogenic, or aberrant material, and possess the means to both mount

and dissolve immune reactions. At first sign of injury, macrophages exhibit a more alert, inflammatory phenotype, and are involved with activities centered around secreting toxic factors to kill pathogens, engulfing debris, and calling on other immune cells to assist in the response. Macrophages are one of few innate immune cells capable of presenting antigens to naïve T cells in the thymus or lymph nodes, a process necessary for initiating T cell immobilization and expansion. In this way, “antigen presenting cells,” (APCs) like macrophages are at the crux of controlled yet rapid and robust antigen-specific T cell responses [40]. The role of macrophages in responding to pathogens is balanced by their ability to suppress and resolve inflammation [41]. As an immune response is mounted, there is a tipping point where macrophages shift to a more immunosuppressive state to blunt and resolve this reaction, acting on other immune cells nearby to quiet their response. From a reductionist perspective, these two respective phenotypes are often discussed as “classically activated” or “M1” inflammatory macrophages, and “alternatively activated” or “M2” immunosuppressive macrophages. Although an oversimplification of the functional spectrum macrophages exhibit, this binary nomenclature allows us to distinguish between two broad populations of macrophages, their canonical gene expression, and their differential roles in both normal physiology and disease (compared in **Figure 1.4**).

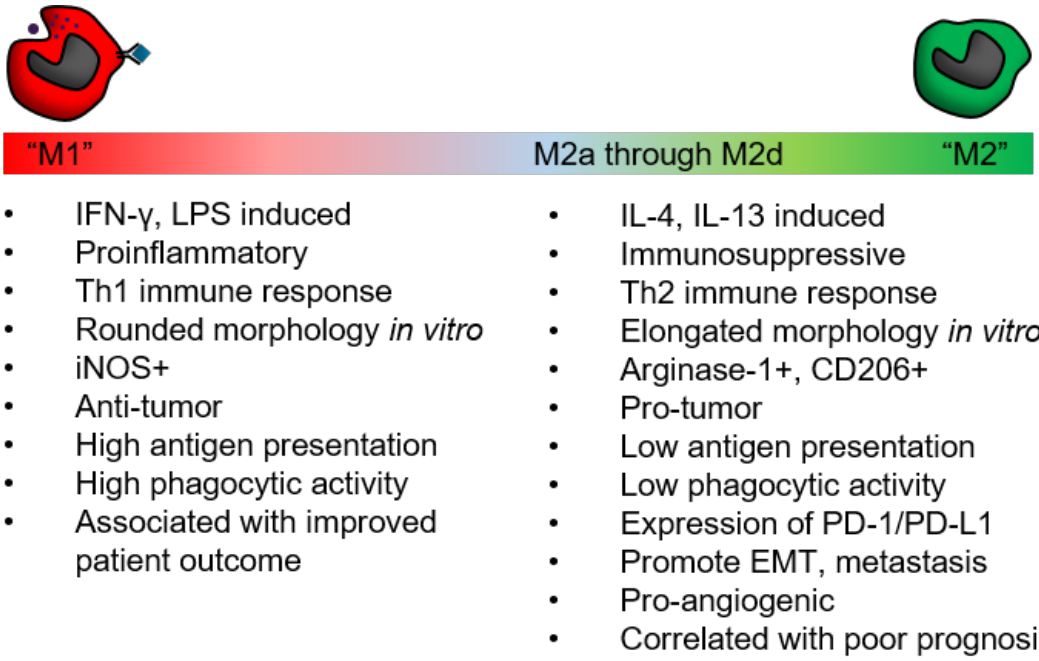


**Figure 1.4 Reductionist comparison of canonical macrophage phenotypes.** Macrophages exhibit a spectrum of behaviors that have canonically been distilled down to "M1" or "M2." M1 macrophages in the context of cancer are typically associated with inflammation and antitumor activity, whereas M2 macrophages typically assist tumor development and dissemination.

In the context of cancer, these M1 and M2 macrophages are thought of more as anti-tumor or pro-tumor, respectively [42]. There are many terms to describe M2 macrophages—this thesis will interchangeably refer to them as either M2 or tumor-associated macrophages (TAMs). TAMs have long been appreciated for their contributions to cancer, highlighted in **Figure 1.5** [43].

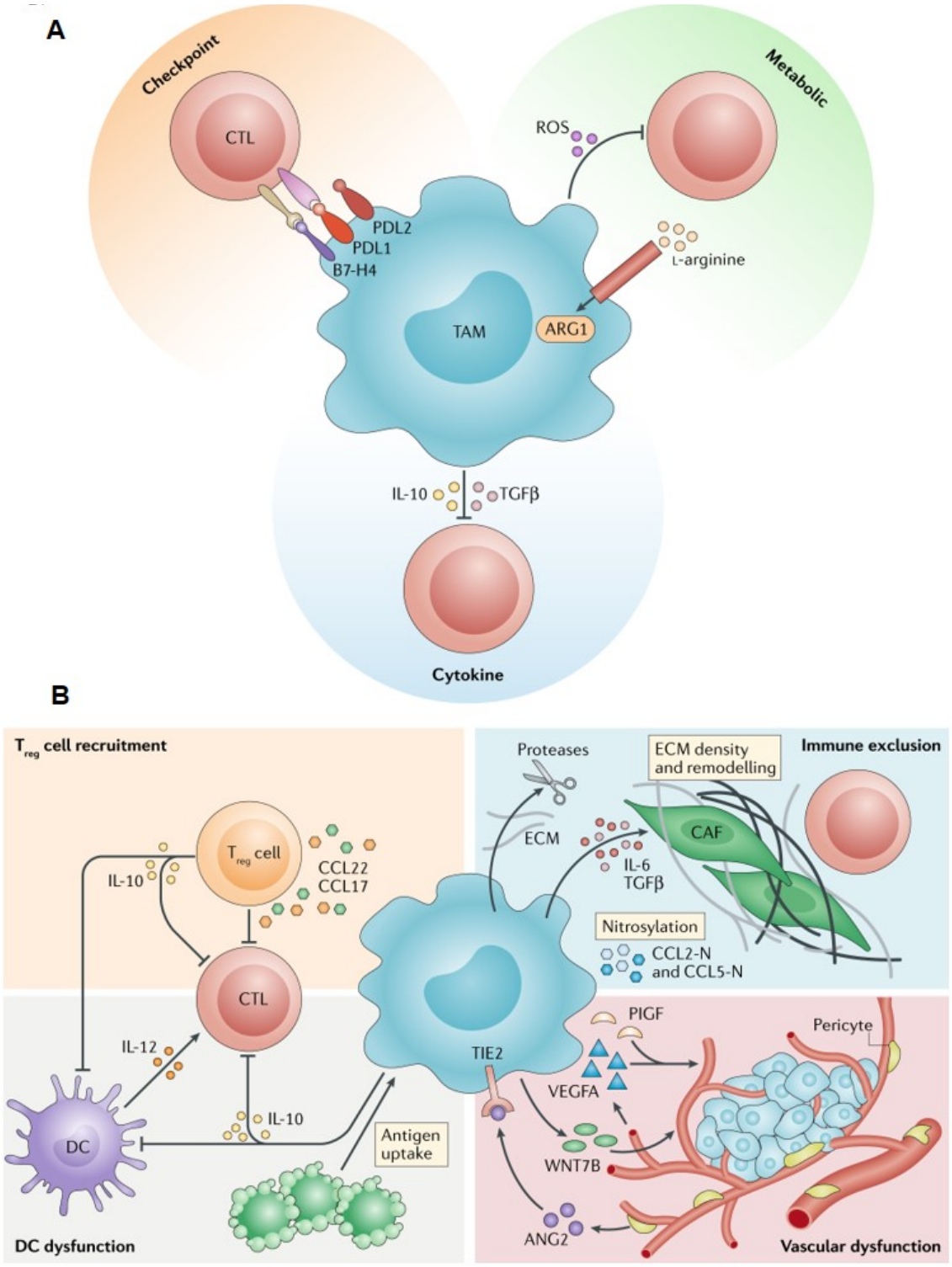


**Figure 1.5 Direct and indirect mechanisms of macrophage-mediated immune suppression and tumor promotion.** *Figure used with permission: DeNardo et al., 2019, Nature Reviews Immunology.*

TAMs are a hallmark of cancer progression across solid tumors, and their numbers correlate with poor prognosis and decreased patient survival in many solid tumors, including those of the pancreas [44-47]. The involvement of TAMs in cancer is extensive. TAMs are known to promote matrix deposition and remodeling, angiogenesis, metastasis, drug resistance, immune evasion, and tumor cell growth and survival [42, 45-52]. Interestingly, TAMs may even travel with tumor cells through the blood stream to provide protection and contribute to establishing immunosuppressed metastatic lesions [53] similar to lesions found in well-differentiated primary PDA. Of relevance to this dissertation are the mechanisms by which TAMs 1) suppress anti-tumor immunity, and 2) facilitate metastasis.

TAMing the TME: Macrophage-mediated immunosuppression

TAMs are potent suppressors of both adaptive and innate anti-tumor immunity and have been shown to blunt immunosurveillance by abrogating cytotoxic T cell and dendritic cell trafficking, downregulating expression of and antigen presentation through MHC class I and II surface proteins, increasing the expression of immune inhibitory surface PD-1/PD-L1 and CTLA-4 (“checkpoints”), secreting suppressive cytokines, and consuming nutrients necessary for cytotoxic T cell survival and function [43, 54]. For example, arginase-1, a canonical marker for suppressive macrophages, is an enzyme responsible for consuming key T-cell nutrient L-arginine. In the TME, arginase-1 expression has been linked to decreased CD3g T cell receptor expression, a surface protein critical for antigen recognition and thus antigen-specific T cell-mediated cytotoxicity [55]. Moreover, arginase-1 has

also been linked to decreased T cell proliferation, likely also through the consumption and conversion of L-arginine [56]. Another mechanism through which macrophages abrogate immunosurveillance is via increased production of reactive oxygen species (ROS) like hydrogen peroxide and superoxides. Though physiologically relevant in the context of macrophages killing foreign pathogens like bacteria, ROS accumulation in the TME can result in unhealthy levels of chronic oxidative stress, ultimately resulting in impaired T cell function, survival, proliferation, and signaling. Moreover, ROS production has been shown to impair T cell production of cytokine IL-2, a key signaling molecule for cytotoxic T cell activation, expansion, recruitment, and differentiation into effector T cells [56]. Interestingly, despite widespread macrophage-mediated CD8 T cell suppression, macrophages can also actively recruit additional T cell populations, like CD4 regulatory T cells [15, 42, 43, 56, 57]. Tregs are another key immunosuppressive cell type in the TME, and their immunosuppressive function is enhanced and sustained via stromal TAMs, adding yet another complex barrier to anti-tumor immunity. Taken together, these and many other studies highlight the role immunosuppressive macrophages play in dismantling anti-tumor immunity.

In PDA specifically, immunosuppressive myeloid cells dominate the TME from the earliest point of disease inception. In fact, macrophages are the first immune population to expand during disease onset, localizing to PanINs of even the lowest grade and persisting as the most abundant immune cell throughout PDA progression [14, 15, 44, 58-61]. In contrast, anti-tumor macrophages are sparsely

found. It is evident macrophages are preferentially skewed toward M2 phenotypes from early in progression, but the factors influencing this early polarization are elusive. Interestingly, data from Calderon, et al. highlights macrophage heterogeneity within the normal pancreas and attributes their differential polarization to local environmental cues [62]. They found macrophages associated with islets exhibited a more M1 phenotype compared to stromal macrophages, which displayed a more M2 phenotype. Upon macrophage ablation via irradiation, donor stem cells could fully replenish both islet- and stroma-associated macrophages which displayed phenotypes identical to the original resident cells. This work suggests local, niche-specific cues regulate the phenotype of macrophages and highlights our need to better assess the local environment and environmental cues informing macrophage fate.

TAMing the TME: Macrophage-mediated metastasis

In addition to their capacity to suppress anti-tumor immunity, TAMs also support the dissemination of tumor cells at essentially every step of the metastatic cascade (**Figure 1.6** [63]). Of note, many models in which macrophages are selectively targeted result in reduction of metastasis, decreased rates of extravasation, and improved anti-tumor immune responses [22, 26, 37, 52, 54, 59, 64-69]. While their exact roles in metastasis aren't fully defined, a summary of their known influence has been reviewed extensively. A summary overview is provided below based primarily on two of the more recent, thorough reviews of TAMs in metastasis [70, 71].

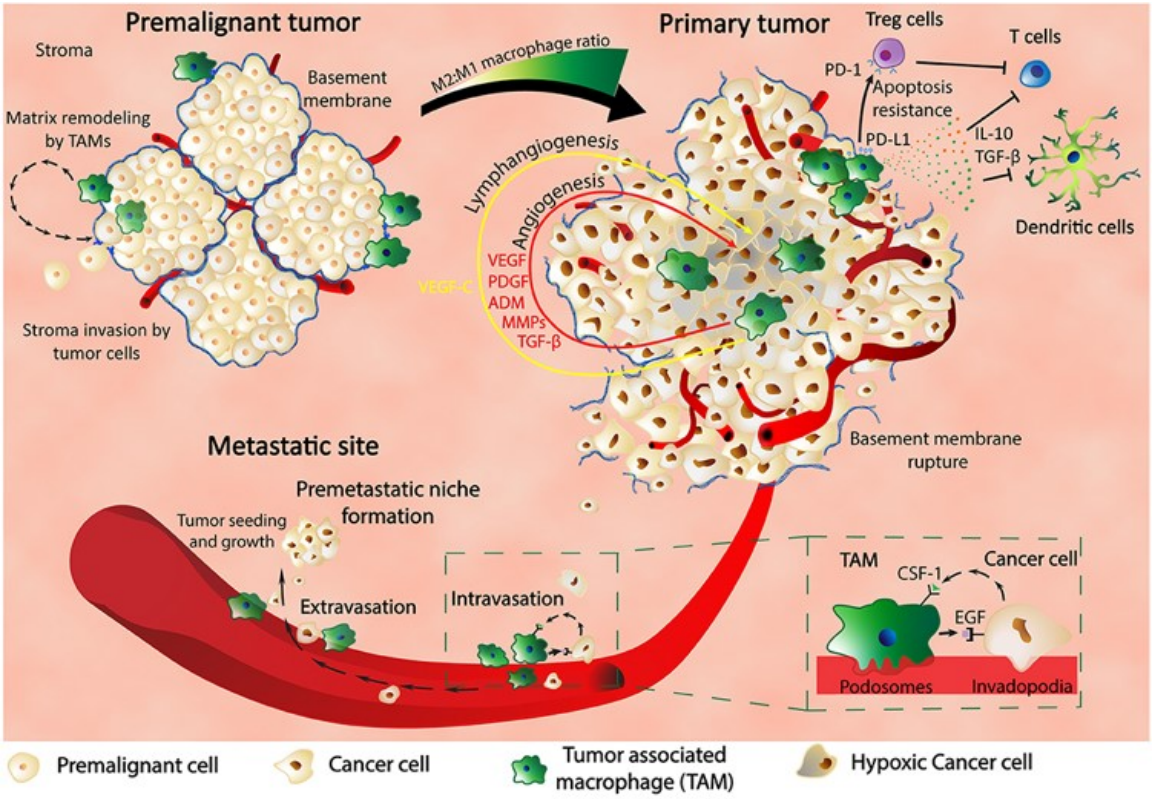


**Figure 1.6 The contribution of TAMs in metastasis.** Depiction of the contribution of TAMs to cancer cell dissemination, from premalignant disease to circulation and colonization of secondary sites. *Figure used with permission: Iurca et al., 2020, Frontiers in Immunology.*

**Priming the pre-metastatic niche**: Before tumor cells are immobilized from primary sites, emerging evidence suggests macrophages are already hard at work preparing secondary sites to support eventual tumor cell colonization and growth. Both resident and infiltrating macrophages serve as sources of pre-metastatic niche macrophages and have been shown to cluster and begin creating an immunosuppressed niche via production of CCL2, CSF-1, VEGF, exosomes, and other cytokines necessary for establishment of metastases [46, 70-72].

Macrophages also begin suppressing immune cells likely to recognize and kill CTCs, like dendritic cells and T cells.

**Invasion**: In the primary tumor, macrophages secrete proteases which cleave ECM, creating pathways for invasion and moreover releasing sequestered growth factors and other tumor-supportive cues. Moreover, TAMs correlate with tumor cells undergoing epithelial to mesenchymal transition (EMT) *in vivo* [73, 74] and can induce expression of EMT markers *in vitro* across multiple cancers. Likewise, *in vitro* co-culture of pancreas cancer cell lines with TAMs increased expression of EMT markers like vimentin and decreased expression of the epithelial cell-cell adhesion molecule E-Cadherin [75]. Macrophages are also known to mediate tumor cell migration by secreting EGF, establishing a chemokine gradient for tumor cells to respond to and migrate toward [76-78]. These studies suggest macrophages directly influence the migratory, mesenchymal, and metastatic propensity of tumor cells.

**Intravasation**: Once tumor cells are migrating in the stroma, macrophages can facilitate spreading by promoting angiogenesis and lymphoangiogenesis [79, 80], which serve as conduits to transport tumor cells into circulation, to local lymph nodes, and to distal organs. Not only do macrophages promote the growth of vessels and lymphatics, but they are also known to increase vascular permeability via VEGF secretion [45], allowing tumor cells to transverse the endothelium with increased ease. Macrophages also increase tumor cell expression of cell adhesion molecules like VCAM-1, which macrophages then engage through integrins,

effectively tethering macrophages and cancer cells together and resulting in the initiation of internal tumor cell survival signaling, protection which persists through circulation [81].

**Circulation**: Many studies have suggested widely varying ways in which macrophages support tumor cells once en route to a secondary site. Intravital imaging has shown macrophages and tumor cells are often found in proximity in circulation, allowing macrophages to continue shielding and supporting tumor cells via production of cytokines, chemokines. More complex hypotheses involve tumor cells traveling in clusters with ECM and other stromal cell types like macrophages tagging along, essentially forming a satellite TME with a miniature, immune privileged stroma. More recently, studies report evidence of circulating hybrid cells (CHCs), fusions between cancer cells and macrophages which acquire enhanced metastatic potential and immune privilege while en route [82-85].

**Extravasation and colonization:** Upon encountering a hospitable environment for secondary tumor establishment (or, upon becoming physically constrained in, for example, small capillaries), cancer cells will traverse the endothelia yet again to migrate through and colonize secondary sites. In this process, macrophages assist by regulating vascular permeability and the expression of cell-cell adhesion molecules on the endothelia which ultimately allow tumor cells to adhere to and squeeze through vessels once again, this time entering their primed and protected secondary site [52, 86]. Macrophages facilitate colonization similarly to how they prime the pre-metastatic niche—via establishing an immunosuppressive, tumor-

supportive TME. Of note, without macrophages, rates of metastasis dramatically decrease due, in part, to diminished tumor cell ability to extrude from vasculature.

Targeting macrophages

Given the macrophage's vast contribution to cancer and metastasis, these observations culminate in an obvious and urgent need to understand how to target macrophages. Extensive studies and reviews suggest targeting TAMs can increase the efficacy of traditional therapies, decrease metastasis, and increase the infiltration and activity of anti-tumor immune cells [22, 37, 43, 45, 48, 59, 66-69]. One approach to targeting TAMs includes eradicating macrophages from tumors and preventing their replacement by monocytes derived from the bone marrow [48, 58, 68, 69]. These strategies have been shown to reduce tumor growth, abrogate monocyte differentiation into TAMs, reduce angiogenesis and ultimately slow progression in some contexts. Some studies have further observed improved function of CD8 T cells and other anti-tumor immune cells, suggesting the removal of TAMs alleviates immunosuppressive barriers [37, 58, 59, 64, 67, 69]. However, this approach in PDA seemed to elicit compensatory action from tumor associated neutrophils and failed to target tissue resident sources of TAMs. To circumvent this, Nywening, et al. demonstrated combinatorial approaches to inhibit both neutrophils and macrophages through simultaneous inhibition of CXCR2 and CCR2 alleviated this compensation and rendered PDA more vulnerable to FOLFIRINOX treatment [26], suggesting therapies which fail initially still offer promise when administered with an appropriate partner. However, given

the vast presence of macrophages and their broad distribution throughout PDA tumors [15, 60], total elimination of macrophages seems a waste of a great opportunity to revert them from a tumor-permissive to a tumor-destructive state.

More recent therapies and combination regimes seek to re-educate macrophages to become more immune-stimulatory and show exciting results [65, 67, 87]. Multiple ongoing clinical trials seek to assess how targeting the programmed cell death ligand-1 (PD-1/PD-L1) signaling axis on TAMs specifically. PD-L1 is a surface ligand that serves as a checkpoint for PD-1 receptors expressed on immune cells and serves as a "stop" signal for immune responses. Recent literature suggests TAMs may be a source of PD-L1 in tumors [88], and that targeting is sufficient to repolarize TAMs. In human hepatocellular carcinoma, monocytes in tumors exhibited high expression of PD-L1, were capable of blunting T cell activity, and correlated with disease severity and patient prognosis. Blocking this signaling axis *in vivo* resulted in decreased tumor volume, likely due to improved tumor-specific T cell activity [89].

In other studies, TAMs have been shown to express PD-1 receptor rather than ligand, again with expression correlating with disease stage. Gordon, et al. observed targeting TAMs *in vivo* decreased tumor volume, improved animal survival, and elicited phagocytic ability of TAMs, an activity associated with anti-tumor phenotypes [90]. Macrophage re-education via PD-1/PD-L1 targeting has also been successful in glioblastoma [57]. Other therapies, like CD40 agonists, appear to also improve phagocytic ability, MHC expression and thus antigen presentation, and a switch to the production of inflammatory cytokines when used

in combination with other macrophage-targeting antibodies, like those targeted to CSF1R. Moreover, CD40 agonism has been shown to increase engineered T cell longevity in mouse models of PDA [37]. Further, the delivery of nanoparticles also not only stimulates antitumor activity and phagocytosis, but also offers some utility in delivering therapeutics directly to macrophages as they have been shown to phagocytose nanoparticles at 10x the rate of cancer cells [91-94]. Moreover, nanoparticles offer a broad range of options for conjugation of therapeutics or other compounds, and thus would provide enhanced opportunity to deliver compounds to macrophages. However, there is still a vast disparity in our understanding of how and when macrophages become immunosuppressive in the TME, and moreover whether the factors driving macrophage function can be altered to redirect macrophage behavior.

Fibroblasts

Fibroblasts are widely accepted as a formidable contributor to pancreas cancer. Known best for their role in collagen deposition and remodeling, they are responsible for much of the fibrosis that occurs in pancreas inflammation and cancer [11, 12, 14, 16, 20, 23, 95-97]. This accumulation of extracellular matrix results in a host of undesirable events, and importantly, establishes a self-perpetuating loop to sustain fibrosis. As ECM deposition increases, the surrounding microenvironment stiffens, resulting in, for example, alterations of stromal and cancer cell gene expression, ultimately exacerbating cancer cell invasive behavior and dissemination. Moreover, fibroblasts are one of the few cell types responsible for reorganizing collagen via matrix metalloproteinase (MMP)

production the exertion of significant tensile forces on collagen fibers. This ultimately gives rise to the aligned ECM architectures that are known predictors of recurrence and characterized contributors to dissemination (discussed below).

## *Extracellular matrix*

Pancreas tumors exhibit robust ECM deposition and present dense networks of various ECM proteins and glycosaminoglycans—namely, collagen and hyaluronic acid, respectively. ECMs act as structural scaffolding for cells which constitute tissues and are critical for normal development, homeostasis, and wound healing. However, the deposition of ECM becomes dysregulated early in PDA onset via the constitutive activation of stromal fibroblasts, and ultimately results in physical and mechanical changes in the pancreas which exacerbate disease. For example, dense stromal collagen networks have been shown to sterically restrict antitumor T cell migration [17, 36], which blocks physical contact with tumor cells and subsequent receptor-mediated cytotoxicity. In addition to serving as a physical barricade to host immunity, local mechanics broadly influence cellular behavior and gene expression [98, 99]. From bone remodeling to stem cell differentiation, physical properties of tissues regulate the shape and function of many cell types, even in the absence of biochemical factors [100, 101]. It is not surprising that variables which influence tumor mechanics—like matrix density, alignment, and crosslinking—contribute to tumor progression [17, 48, 75, 99, 102-114] and correlate negatively with patient survival in both breast cancer and PDA [115-117].

Stiffening

Early in disease, quiescent stromal fibroblasts are constitutively activated and begin depositing robust amounts of ECM. The accumulation and subsequent crosslinking and/or remodeling of ECM by fibroblasts, macrophages, and cancer cells ultimately results in matrix stiffening, or an increase in the physical hardness of the pancreas [98, 99]. Tissue stiffness is an accepted risk factor for breast cancer and clinically correlates with poor progression and disease severity, and of note is one of the oldest methods used to detect masses in the breast via physical breast exams [109-112, 114, 118], although the implications of how stiffness drives disease has only recently come to light. For example, in pancreas cancer, *in vitro* cell lines upregulated EMT expression profiles, displayed more mesenchymal morphologies, and developed enhanced therapeutic resistance in response to increased matrix stiffness [104]. A 3D coculture model of lung carcinoma cells with macrophages mimicked these results, with matrix stiffness increasing the invasive, proliferative potential of cancer cells, and the addition of macrophage conditioned media notably influenced tumor cell EMT only in cells cultured with higher stiffness [75]. Another 3D coculture system of macrophages and T cells showed macrophages cultured in higher density and thus stiffer collagen matrices were more immunosuppressive, decreasing T cell proliferation and recruitment compared to macrophages in softer environments [119]. Moreover, matrix crosslinking and thus enhanced stiffness has been shown to enhance focal adhesions and invasive capacity of breast epithelia via integrin engagement, and targeted depletion of crosslinking via lysyl oxidase abrogated tumor incidence and

spreading [102]. More recent studies confirm these observations and note stromal-derived lysyl oxidase is responsible for subsequent crosslinking and stiffening, and that elevated expression of lysyl oxidase is highly (negatively) correlative with patient survival [48]. Moreover, this study identifies macrophage-derived lysyl oxidase to be the primary driver of stromal stiffening and crosslinking, a surprising observation given the attention widely accepted and anticipated role of fibroblasts and cancer cells in altering matrix mechanics.

Pressures

Fibroblasts also play a role in the robust deposition of HA, a glycosaminoglycan capable of retaining vast amounts of liquid. Previous studies from our lab and others have shown increased HA, and thus increased fluid retention, results in elevated interstitial fluid pressures consequently leading to vascular and lymphatic collapse, the former which diminishes drug delivery to PDA [11, 13, 21, 27]. The influence of lymphatic collapse is less understood but has been hypothesized to decrease lymphocyte access to tumors and thus may decrease subsequent antigen presentation in local lymph nodes. While HA is outside of the scope of this work presented here, it is worth noting there is a precedence for ECM abrogating immune surveillance and drug delivery, and moreover a proven history and success of targeting ECM to stunt immune suppression, decrease metastasis, recruit anti-tumor immune cells, enhance chemotherapeutic efficacy, extend survival, and elicit more effective immune responses.

Remodeling

As ECM accumulates, it will subsequently be remodeled by fibroblasts, macrophages, and cancer cells both chemically via secretion of MMPs and other proteases, and/or physically through applied tensional force.

*Tumor-Associated Collagen Signatures*

The remodeling of ECM results in distinct patters of collagen orientation and alignment, termed “Tumor Associated Collagen Signatures” (TACS), and can be distilled down to three general architectures (**Figure 1.7**). Originally discovered in breast cancer, TACS were defined with respect to a tumor, or epithelial cell cluster, boundary. TACS-1 signatures generally display sparse, loose collagen networks lacking distinct orientation (not depicted). TACS-2 regions exhibit circumferentially

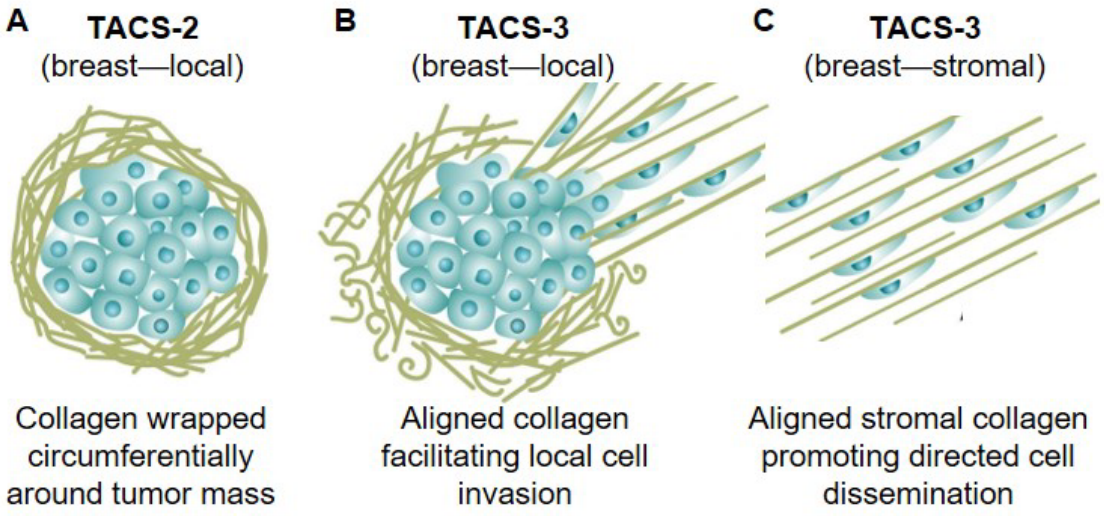


**Figure 1.7 Defining tumor-associated collagen signatures.** Schematics of collagen signatures originally identified in the breast.. **A)** Classical TACS-2 signatures oriented parallel/circumferentially around tumor mass. **B)** Classical TACS-3 signatures oriented perpendicular to tumor mass, facilitating local tumor cell invasion into TACS-3 collagen tracts. **C)** TACS-3 signatures in the stroma, oriented parallel to one another and promoting directed cell migration within the breast TME.

aligned collagen around ductal structures and parallel to epithelial cells (**Figure 1.7A**), and TACS-3 architectures are characteristically aligned perpendicular to ductal structures and epithelial cells (**Figure 1.7B**). While perhaps not classically defined, it is relevant to this thesis to point out TACS-3 architectures also exist in the stroma, appearing as aligned stromal collagen fibrils promoting directed cell dissemination through the TME (**Figure 1.7C**). Previous studies from our lab and others have shown TACS-2 and TACS-3 architectures are crucial in facilitating dissemination of breast cancer cells, promoting invasion and migration via contact guidance cues [105-108]. ECM alignment is a known negative prognostic factor for survival in breast cancer [115] and is a predictor of disease recurrence in pancreas cancer [116, 117]. The prevalence and significance of TACS in PDA, and their role in facilitating dissemination, is unknown, as is the influence of TACS on stromal cells. However, there is a definite relationship between cell shape and phenotype *in vitro* [105, 108, 120-123]. Given the cues alignment provides, and the ways in which these cues inevitably influence cell shape, aligned collagen may very well be a driving force behind stromal and cancer cell behavior in PDA.

## *Mechanotransduction: connecting cells to local mechanics*

Physical cues influence cell behavior via mechanotransduction, the process by which cells sense and respond to local mechanical signals. Much of this is regulated through integrins, cell shape, focal adhesions, the actin cytoskeleton, etc. and involves changes in gene expression, cell signaling, epigenetics, phosphorylation, protein localization, cell function and behavior [98, 124].

Importantly, several key mechanotransducive proteins have been directly linked to immunosuppression and disease progression in PDA.

Focal Adhesion Kinase

Focal adhesion kinase (FAK) is a critical contributor to cellular mechano-sensing and -signaling (**Figure 1.8** [125]). Situated directly downstream from external signal transducers like extracellular growth factor receptors and ECM-binding integrins, FAK directly links receptors at the cell surface to the cell's actin cytoskeleton [126]. Moreover, FAK can translocate to the nucleus to regulate transcriptional responses to stimuli like stiffness, and therefore effectively synchronizes a cell with its external environment. Upregulated in many solid tumors, FAK has an established role in promoting processes like tumor cell invasion, migration, proliferation (**Figure 1.9** [127]) and has thus become an attractive target for anti-cancer therapies.

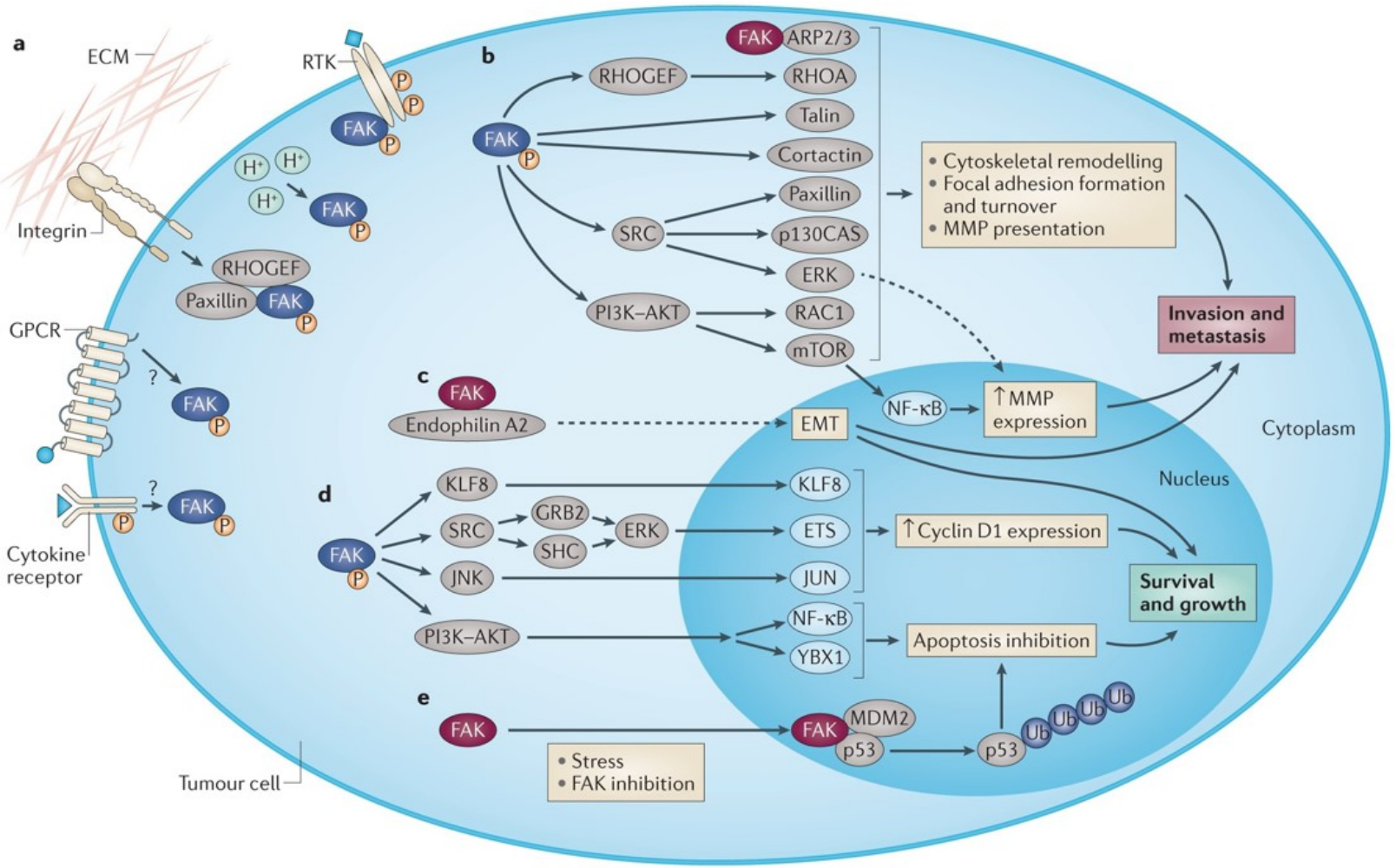


**Figure 1.8 FAK signaling as a driver of tumor cell behavior.** *Figure used with permission: Sulzmaier, et al. 2014, Nature Reviews Cancer.*

Nature Reviews | Cancer

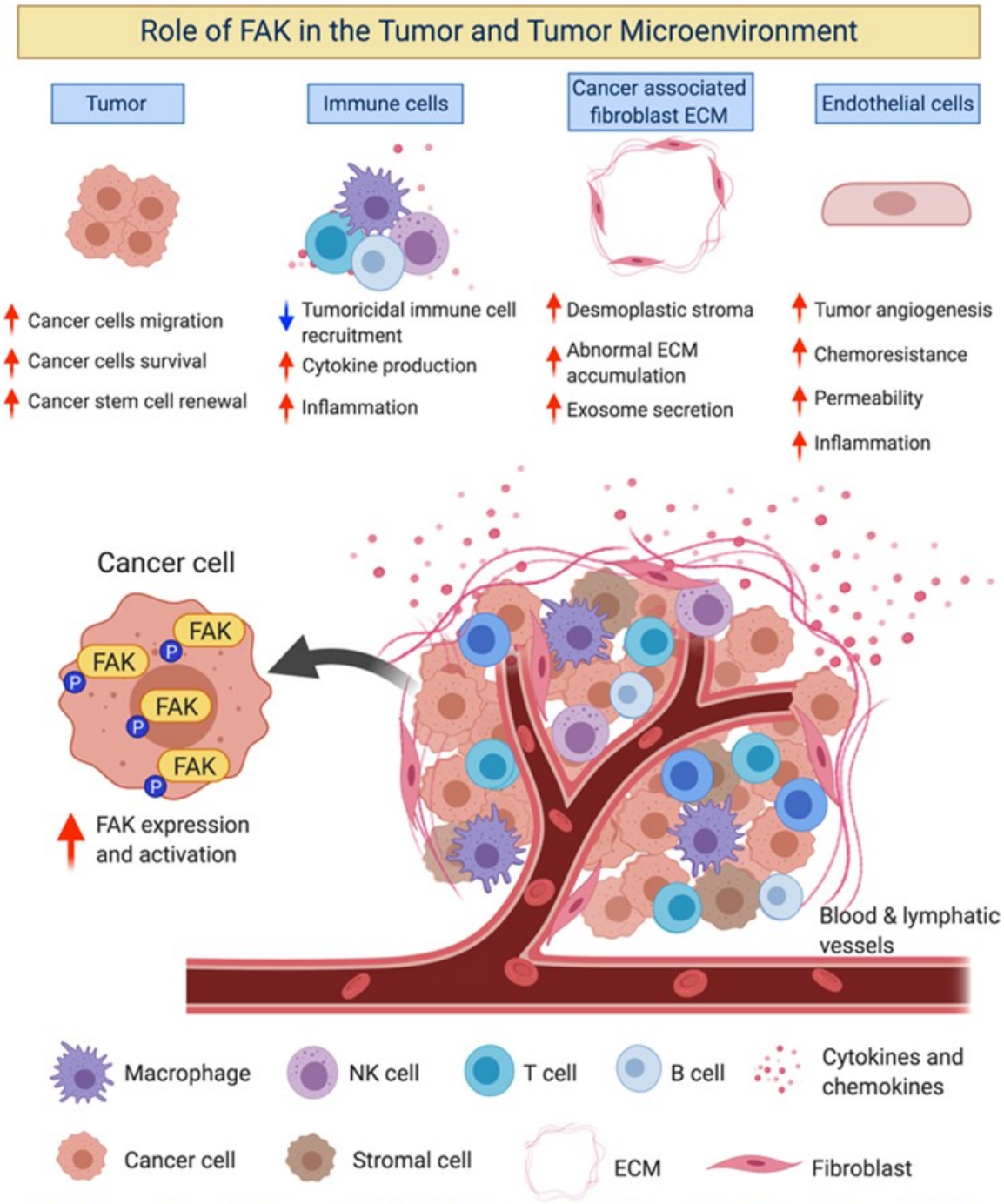


**Figure 1.9 FAK contributions broadly across the tumor microenvironment.** *Figure used with permission: Murphy et al., 2020, Experimental Molecular Medicine.*

FAK is the main culprit behind orchestrating cellular responses to mechanical stimuli such as matrix deposition, stiffening, and crosslinking, and its activity and localization are known to be regulated at least in part by matrix stiffness [124]. It is therefore of no surprise FAK is elevated in PDA and contributes to the generation and maintenance of a desmoplastic TME by promoting collagen deposition, resistance to immunotherapy, and immune evasion [31]. Interestingly, inhibition of FAK diminishes fibroblast activation; the recruitment of immunosuppressive cells like myeloid derived suppressor cells (MDSCs), T regulatory cells, and TAMs; collagen deposition; and tumor cell proliferation [31]. Further, a study in squamous cell carcinoma implicated FAK in the recruitment of suppressive T regulatory cells via FAK's modulation of chemokine expression and showed targeting FAK resulted in tumor regression and improved CD8 T cell function [128]. These studies strongly support the idea that PDA progression and immunosuppression are influenced and potentially perpetuated by mechanotransduction.

## Pancreatitis

Precursory fibrosis and inflammation are known to increase risk of developing cancer in many solid tumor types, including PDA [49, 129, 130]. In fact, fibrosis has long been a mechanism to diagnose palpable cancers like those of the breast as the stiffness and thus qualitative fibrosis is indicative of an increased risk of developing breast cancer in the future. Clinical assessment of fibrosis via medical imaging like MRI is highly correlated with disease severity, dissemination, and chance of recurrence [4, 49, 115-117]. In the pancreas, precursory fibrosis and

inflammation may occur both acutely and chronically, the latter of which is considered “unresolved” fibrosis and is a known risk factor of developing PDA, increasing likelihood of developing PDA by roughly 13-16 fold [4, 131]. Moreover, patients with hereditary chronic pancreatitis (CP) have an increased risk for developing PDA, with multiple reports observing a 50-80 fold increase in risk [4, 5]. While the direct conversion of CP to PDA is debated, we suspect precursory pancreas fibrosis occurs in most cases of PDA whether diagnosed or not.

Similar to PDA, pancreatitis is accompanied by an accumulation of immunosuppressive macrophages [132], ductal structures, acinar drop out, and robust stromal collagen deposition [133]. **Figure 1.10** highlights the histological and architectural similarities between CP and PDA in the human pancreas. **Figure 1.10A** shows acinar dropout (asterisks) and the accumulation of islets (dashed margins) in CP and in PDA. Arrows in **Figure 1.10B** highlight the accumulation of ductal structures, and the presence of higher grade PanIN and PanIN-like lesions (**Figure 1.10C**). These lesions show cells displaying mucinous phenotypes and some signs of nuclear atypia, further highlighted in **Figure 1.10D** (arrow heads) in high-grade PanIN lesions with complete loss of cell polarity. **Figure 1.10E** depicts similarities in collagen architecture in CP and PDA, with an accumulation of fibrillar, aligned collagen occurring in both inter- and intralobular spaces.

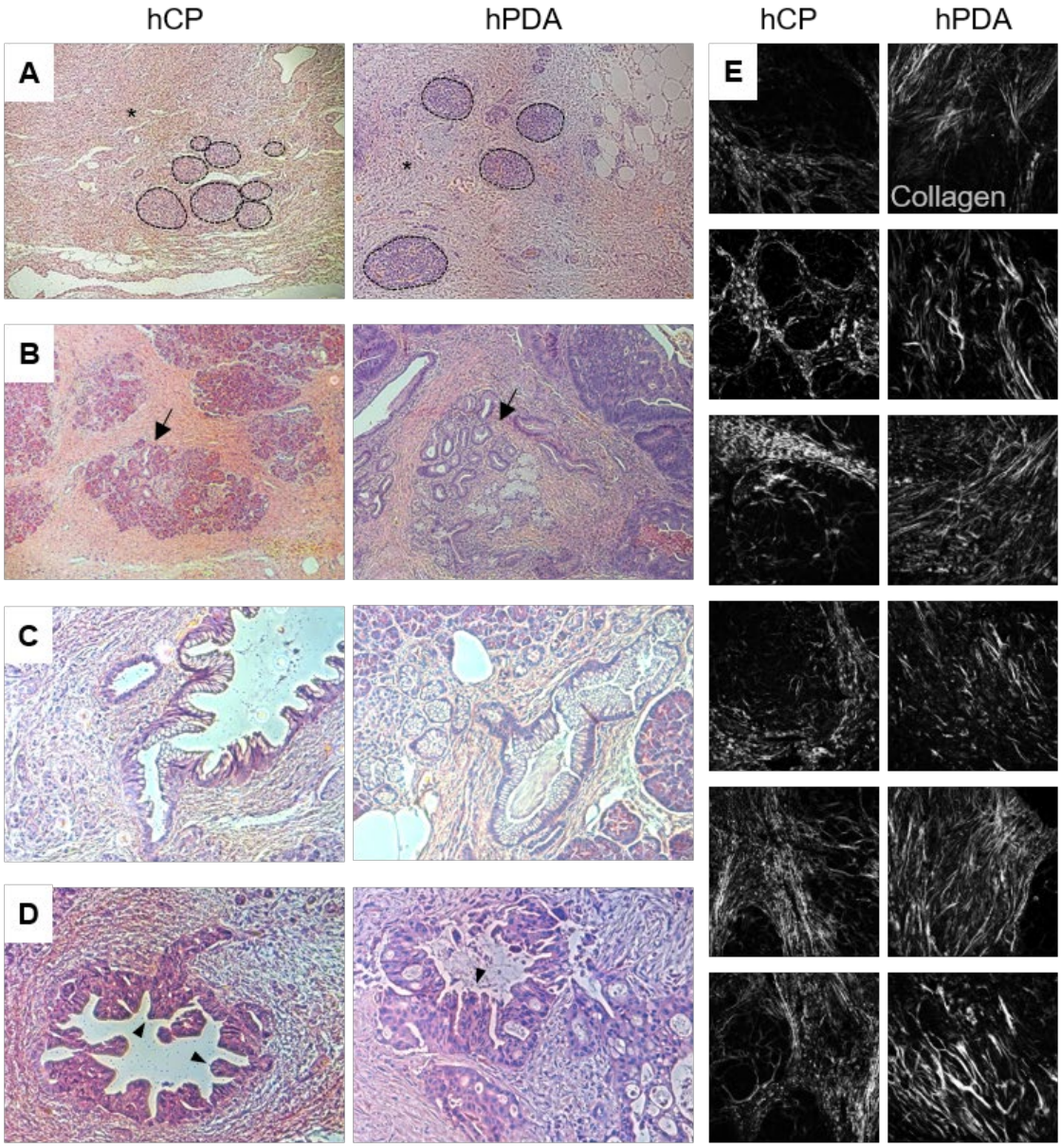


**Figure 1.10 Human chronic pancreatitis exhibits lesions and collagen architectures similar to PDA.** Qualitative comparison of human chronic pancreatitis (hCP) and human PDA (hPDA). **A)** Histological depiction of acinar dropout (asterisks) and islet "island" accumulation (dashed margins) in hCP and hPDA. **B)** Accumulation of ducts in hCP and hPDA (arrows). **C)** Mucinous PanIN-like lesion in hCP and mucinous PanIN lesion in PDA. **D)** PanIN-like lesion with nuclear abnormalities (arrow heads) in CP and high-grade PanIN lesion in PDA. **E)** Depiction of aligned collagen architectures present in hCP and hPDA (SHG).

These fibrillar collagen structures are reminiscent of TACS observed in breast cancer; however, the organization of stromal collagen, the spatio-temporal occurrence of TACS in CP, and the role TACS may play in pancreatic inflammation has not been explored. Importantly, pancreatitis samples allow the study of how collagen architectures and macrophages correlate in the absence of an apparent transformation event, given the striking similarities in the fibro-inflammatory compartments of pancreatitis and PDA. Interestingly, studies reviewing cohorts from as early as the 70s observed that patients who underwent resection surgery for the removal of chronically inflamed pancreata still developed metastatic PDA despite a histological absence of PDA in the pancreas [134]. This would be consistent with the early timeline in which we know PDA to spread, and with the known role of inflammation in promoting more aggressive cancer. Moreover, mouse models of pancreatitis exhibited epithelial cells reminiscent of CTCs circulating in the blood stream after induction of pancreatitis [135]. Other studies have shown human CP samples display expression profiles consistent with EMT [136], or have identified circulating epithelial cells in patients with pancreatic cystic lesions [137], further supporting the existence of circulating epithelial cells before pancreas cancer presentation. Ultimately, these clinical and experimental observations support the notion that the pancreas may be primed to support tumorigenesis and early tumor cell dissemination before frank disease is present, begging the question of whether more aggressive treatment of chronic pancreatitis and pancreas inflammation would alleviate the levity of diagnosis with PDA via decreasing cancer cell dissemination and dissolving immunosuppressive barriers.

Indeed, one interesting study observed that, in mouse models, attenuation of inflammation was observed to accelerate pancreas tissue repair and diminish PanIN prevalence [138]. Moreover, this study shows human patients with pancreatitis who received anti-inflammatory drugs displayed more senescent PanINs, suggesting attenuation of inflammation in the clinic may reduce risk of developing PDA. Studies in mouse models have corroborated this connection, observing that pancreatitis induced ADM and expedited pancreas cancer in mice with oncogenic *KRAS* [9, 138, 139].

## *KPC* mice to study PDA

Of note, genetically engineered mouse models of PDA have allowed for closer study of the dynamics of PDA, contributors to disease progression and severity, and the response to potential therapies *in vivo*. Perhaps one of the best models available to study the spontaneous development of cancer near identical to human disease is the *KPC* model, which harbors driving mutations in *KRAS* and *p53* spontaneously induced by Cre expression under pancreas-specific promoter Pdx-1. *KPC* mice spontaneously develop disease consistent with human PDA which closely mimics the fibroinflammatory TME [10, 15, 60, 140], allowing study of the temporal dynamics of stromal cell activation and influx, as well as how perturbation of stromal compartments influences progression. Lineage tracing fluorescent reporters tdTomato (*KPCT*), zsGreen (*KPCG*), and YFP (*KPCY*) have facilitated the study of disseminating pancreas-derived fluorescent epithelial cells in the blood and at distal secondary sites, and provide a phenomenal opportunity to study how

fibrosis, or targeting of fibrosis, impacts dissemination locally within the pancreas. This dissertation hence utilizes these models, along with human biopsies, 3D culture systems, and LSMPM to interrogate our central hypothesis: collagen architectures emerge early in pancreas inflammation, direct immunosuppression by altering macrophage cell shape and phenotype, and facilitate epithelial cell dissemination all through FAK-dependent mechanisms.

# 2. ALIGNED STROMAL ARCHITECTURES DRIVE THE ESTABLISHMENT OF AN IMMUNOSUPPRESSIVE TME

## Summary

This chapter seeks to identify the influence of matrix architectures on stromal macrophages in PDA. Analysis of mouse and human biopsies revealed an inextricable link between collagen architecture and the distribution of immunosuppressive macrophages in both early preinvasive disease and invasive carcinoma. *In vitro* characterization of primary macrophages demonstrates alignment alone is sufficient to induce elongation, polarization, and immunosuppressive function. Immunofluorescence revealed differential focal adhesion kinase activity and subcellular localization in both primary and immortalized macrophages in response to alignment as well as to polarization with recombinant IL-4 and IL-13, implicating FAK in the maintenance of immunosuppressive macrophage phenotypes. FAK inhibition *in vivo* dramatically reduced the correlation between elongated CD206+ macrophages in aligned collagen, highlighting the opportunity to utilize FAK inhibitors to target stromal immunity. Importantly, the correlation between aligned collagen and immunosuppressive macrophages is observed in human chronic pancreatitis, a known risk factor for PDA, suggesting that pancreatic precursory disease may create stromal memory conducive to subsequent immunosuppression and dissemination early in PDA. Taken together, these results support a model in which collagen architecture drives the early establishment of an immunosuppressive

microenvironment and underscore the importance of targeting stromal matrices in precursor inflammation to limit cancer progression and “reprogram” patient immunity.

## Introduction

In PDA, a remarkable influx of leukocytes begins very early in disease and persists through disease progression. This infiltrate is primarily comprised of macrophages and other myeloid cells educated to exacerbate disease and hinder productive anti-tumor immune responses [15, 22, 34, 43]. Macrophages are accepted drivers of severity in cancer and in PDA, contributing to fibrosis, angiogenesis, dissemination, and drug resistance [22, 37, 43, 64, 65, 67, 141]. More recently, macrophages have been revealed to have a role in limiting performance of promising immunotherapies [22, 37, 43, 64, 65, 67] in solid tumors including PDA, especially given their potential as potent immune suppressors. Macrophages are largely responsible for maintaining tumor-permissive microenvironments which protect tumor cells by abrogating T cell trafficking and T cell mediated tumor cell killing, as well as altering antigen presentation and the expression of checkpoint markers, and attracting and/or polarizing other stromal cells to support tumor progression [42, 44, 46, 50, 59, 61, 64, 66, 68, 142]. As such, therapeutic interventions to selectively target, deplete, or repolarize macrophages in PDA have resulted in increased immunotherapy efficacy and survival in pre-clinical models [65, 67, 69].

However, despite our advances in understanding the impact of myeloid cells in PDA, our awareness of the physical and molecular mechanisms which regulate immunosuppressive function is incomplete. Chemical cues like cytokines are known regulators of macrophage polarization and function. An emerging body of evidence, however, suggests mechanical and physical cues also play a role in dictating macrophage phenotype and function *in vitro* and may even supersede chemical cues in some cases [75, 120, 121, 123, 143-146]. For example, macrophages have been shown to polarize in response to both perceived mechanics, like surface roughness and stiffness, and applied mechanics, like pressure and stretching, reviewed by Meli, et al. [145]. Of note, many of these biophysical cues are present in tumors and have been shown to directly influence the behavior of cancerous cells and stromal cells such as carcinoma-associated fibroblasts [147-149]. These physical changes are largely perpetuated by the deposition, organization and mechanics of ECM components like collagen and hyaluronan, and ultimately manifest as barriers to patient survival [21, 147, 148]. Interestingly, aligned collagen signatures also appear early in PDA progression [150], and temporally coincide with the accumulation of alternatively activated macrophages [15, 151, 152]. Yet, while recent studies demonstrate the presence of TACS architectures in PDA [108, 150, 153] and their influence on T cell migration [36, 154], our understanding of the role of ECM architecture in immune cell regulation, and in particular myeloid cell behavior, in PDA is extremely limited. Given the evidence that macrophages are responsive to mechanical and architectural cues, and the early robust accumulation of both macrophages and

aligned collagen, we hypothesized a relationship between macrophage distribution, shape, orientation, and function and collagen alignment, and further anticipate any observed relationships will likely be attributable to mechanotransduction.

In this study, we show that immunosuppressive macrophages colocalize with aligned stromal collagen in pre-invasive and invasive PDA. Moreover, we demonstrate that alignment alone is sufficient to drive macrophage polarization toward an immunosuppressive phenotype, increasing their ability to suppress T cell migration and proliferation. This suppressive phenotype can be attributed to differential FAK signaling dynamics in macrophages, where the inhibition of FAK both *in vitro* and *in vivo* diminishes the prevalence of elongated immunosuppressive macrophages. Interestingly, these observations are conserved in human pancreatitis suggesting that precursor diseases may generate stromal memory and highlight the utility of targeting the matrix in precursory pathology to alleviate immunosuppressive tumor-conducive boundaries in PDA.

## Experimental Procedures

### Human patient samples

Human normal, normal adjacent, chronic pancreatitis, and PDA samples were obtained from BioNet core facility through the University of Minnesota as either FFPE sections, or as freshly resected tissues obtained in compliance with approved Institutional Review Board protocols which were processed immediate

after receipt. Tissues were accompanied with pathological assessment of disease staging and other relevant information when available.

**Mouse models**

Animal studies were approved by the Institutional Animal Care and Use Committee of the University of Minnesota. C57BL/6 mice of 10-16 weeks of age were obtained from Jackson Labs for all primary immune cell isolation. Both male and female mice were utilized to account for any possible sex-based differences. Primary live tumor slices and tumor cell lines were derived from the *Kras$^{G12D/+}$;p53$^{R172H/+}$;Pdx1-Cre* (*KPC*) mouse model, as well as from derivatives of this line expressing fluorescent reporters specifically expressed in pancreas tissue *Kras$^{G12D/+}$;p53$^{R172H/+}$;Pdx1-Cre;TdTomato* (*KPCT), Kras$^{G12D/+}$;p53$^{R172H/+}$;Pdx1-Cre;YFP* (*KPCY)* and *Kras$^{G12D/+}$;p53$^{R172H/+}$;Pdx1-Cre;ZsGreen* (*KPCG).* The *KPC, KPCT, KPCY,* and *KPCG* models are genetically engineered mice which develop spontaneous genetic aberrations specifically within pancreatic epithelial cells, giving rise to disease that is highly faithful to the human condition.

**Cell lines and culture**

L929 fibroblasts were used to generate conditioned media for macrophage differentiation by culturing L929 cells in 100 mL complete DMEM in T-150 flasks. Conditioned media was collected in large batches 7-10 days post-confluence, combined, filter sterilized and stored at -20°. Raw 264.7 and J774 murine macrophages were cultured in T-75 flasks and passaged using cell scraping. Primary bone marrow derived macrophages were obtained by harvesting and

resuspending bone marrow from wild type C57BL/6 mice of at least 10 weeks of age. BMDMs were differentiated by plating bone marrow suspension on ultra-low adhesion plates (Corning, Cat# 29443-030) and culturing with complete medium supplemented with 20% L929 conditioned media for seven days, except in the case of the paired T cell cocultures (see below). BMDMs were passaged using gentle pipetting. Primary splenic CD8+ T cells were isolated from C57BL/6 mice using the EasySep mouse CD8+ T cell Isolation Kit following manufacturer's instructions (Stemcell technologies, Cat# 19853). T cells were then activated and expanded in 96 well round bottom plates (Corning, Cat# 0720095) for either 5 or 6 days using Dynabeads mouse T-activator CD3/CD28 (Life Technologies, Cat# 11452D). Half media changes were used to supplement 30 units IL-2 on days 3 and 4. On day 5, T cells were prepared differentially according to their future use described below. T cells were expanded in RPMI 1640 medium with L-glutamine (Fisher, Cat# mt10040cv), with 10% FBS (Fisher, Cat# SH3007103), 1X Antibiotic-antimycotic (Thermo Fisher, Cat#15240062), 25mg/mL plasmocin (Invivogen, Cat# ant-mpt). All other cell lines were cultured in complete media (Dulbecco's Modified Eagle's Media (media tech, Cat#MT10013CV), 10% fetal bovine serum, 2mM L-glutamine (Life Technologies, Cat# 25030081), 1X Antibiotic-Antimycotic, and 25mg/mL Plasmocin) unless otherwise specified. All culture reagents and conditioned media were filter sterilized prior to use.

**2D alignment studies**

BMDMs were seeded onto control glass insets of 35mm flat control dishes (MatTek, P35G-1.0-20-C) or aligned dishes (Curibio, ANFS-0001-10) [108] at 300,000 cells per dish in 600uL media for 6 hours to allow adherence to inset. After 6 hours, 1.4mL complete media was overlayed, and cells were cultured for 24-48 hours for assessment of arginase-1 expression, 7-16 hours for assessment of phospho-FAK, and 24 hours for assessment of total FAK.

**3D slice studies**

Live tumor slices were isolated and prepared following methods described previously [155]. Briefly, 250-300um slices were cut from freshly isolated *KPC* or *KPCT/G* pancreas tumors using a vibrotome. Unlabeled live *KPC* slices were stained with CellTracker Red CMTPX Dye (Thermo Fisher, C34552) following manufacturer's instructions to allow visualization of host tissue. Staining of *KPCT*/G slices is not necessary as these mice exhibit pancreas-specific fluorescence. BMDMs or Raw 264.7 cells were seeded on top of slices and cultured 24 hours before fixing and staining.

**Macrophage stimulation protocol**

Macrophages were stimulated for 24 hours with complete medium supplemented 1:1 with tumor conditioned media collected from primary tumor cells previously isolated from *KPC* tumors using methods previously described [13]. Tumor cells were grown 3 days past confluence in T-75 flasks, media was collected, filtered, and mixed 1:1 with complete DMEM. Macrophages were stimulated with 20ng/mL

mouse recombinant IL-4 (MilliporeSigma, Cat# I1020-5ug) and 20ng/mL recombinant mouse IL-13 (Fisher Scientific, Cat# 413ML005) for 24 or 48 hours depending on subsequent experiments.

**Paired T cell and BMDM experiments**

Spleens and matched bone marrow were isolated from C57BL/6 mice. BMDMs were isolated as described above and cultured in 20% L929 for 5 days after which they were harvested, plated at (200,000 cells in 600uL) into 24 well patterned (Curibio, Cat# anfs-0024) or unpatterned (Cellvis, Cat# NC0397150) plates, and left to adhere overnight in complete medium. T cells were isolated and expanded as described above for 5 days, after which they were differentially prepared for coculture experiments:

*T cell migration*

On day 5, T cells were collected, magnetic beads were removed, and T cells were reseeded in RPMI with 1% FBS overnight. On day 6, 8um 6.5mm transwell inserts (Fisher Cat# 07-200-174) were prepared by coating with 100uL 50ug/mL high protein rat tail collagen I (Fisher, Cat# CB35249) suspended in sterile 1X PBS (Gibco, Cat# 10010-049) for 1 hour at RT. Membranes were gently washed with PBS and placed above BMDMs. Prepared membranes were overlaid with 100uL 1% RPMI containing 500,000 T cells and incubated at 37° for 6 hours. Membranes were fixed with ethanol and stained using 0.2% crystal violet (sigma, Cat# C0775-25g) and imaged. FIJI was used to process images and quantify percent area positive for crystal violet in each field of view.

*T cell proliferation*

On day 5, T cells were supplemented with IL-2. T cells were harvested on day 6, magnetic beads were removed, and cells were stained in serum free RPMI using CellTrace™ CFSE Cell Proliferation Kit (Invitrogen) at 1:1000 for 15 minutes in a 37° water bath. Cells were rinsed with complete RPMI, resuspended in complete DMEM at a density of 1.5 million T cells per 100uL. 100uL T cell suspension was added directly on top of BMDMs. After 3 days of coculture, T cells were harvested using gentle pipetting and stained 1:100 with PerCP/Cyanine5.5 anti-mouse CD8a antibody (Biolegend, Clone 53-6.7) for 30 minutes on ice protected from light. Proliferation was quantified using a BD Accuri C6 flow cytometer by measuring fluorescence dilution by CD8+ cells.

**Immunofluorescence**

Formalin fixed paraffin embedded (FFPE) tissues were stained for CD206 (1:100), arginase-1 (1:50), F4/80 (1:100), CD68 (1:100), and phospho-FAK Y925 (1:100). Briefly, sections were baked, dewaxed with xylene, and rehydrated with ethanol. Heat-mediated antigen retrieval was performed by boiling Trilogy buffer and slides for 20 minutes. Samples were permeabilized using 0.3% Triton X-100 in 1X TBS, and blocked using 10% goat serum and 1% BSA for 1 hour at RT. Primary antibodies incubated overnight at 4° in 1% serum + TBST. Secondary antibodies were incubated at 1:200 with Draq5 (Biolegend, Cat# 424101) at 1:500 for 1 hour at RT. Slides were mounted with Prolong Gold Antifade Reagent (Fisher, Cat# P36934) and imaged using laser scanning multi-photon microscopy (LSMPM) and

second harmonic generation (SHG) to visualize collagen. Microscope is equipped with 4-channel detection, interchangeable 440/20, 460/50, 525/50, 525/70, 595/50, 605/70, and 690/50 filters, (Prairie Technologies/Bruker) and a Mai Tai Ti:Sapphire laser (Spectra-Physics).

Slices were washed with PBS, fixed with 0.02% PFA for 30 minutes, permeabilized with 0.3% Triton X-100 in PBS for at least 30 minutes, and blocked overnight with 2% fatty acid free BSA + 5% goat serum at 4°. Primary antibody was incubated overnight at 4° at 1:100, with consideration of the added volume of the tissue. Slices were washed for one hour in PBS-Triton, and were stained for 2 hours using secondary antibody at 1:100. Sections were washed for at least 30 minutes before imaging using LSMPM.

Adherent cultures were fixed with either ice cold methanol or PFA for 10-15 minutes, permeabilized with 0.3% Triton X-100 in 1X PBS, and blocked for 1 hour at RT with 1% BSA, 10% serum, 0.3M glycine, and in PBS-Triton. Hoescht dye was used at 1:10,000 to visualize nuclei.

**FAK inhibition in *KPC* mice**

Control and FAKi samples have been previously described [31]. Briefly, 50mg/kg VS-4718 was administered by oral gavage twice a day in a formulation with 0.5% carboxymethyl cellulose and 0.1% Tween-80 (Sigma) in sterile inhibitor.

## Results

**General characterization of BMDM morphology and canonical M1 and M2 marker expression.** Given the general heterogeneity of BMDMs, inconsistencies across the literature, and the broad complexity of working with primary immune cells, we first sought to simply characterize BMDM morphology in various culture conditions, as well as their baseline and stimulated expression of markers associated with canonical M1 and M2 polarization. BMDMs cultured on ultra-low adhesion tissue culture plates display primarily adherent morphologies (**Figure 2.1A**) but without any striking indication of polarization at baseline compared to M1 stimulation with LPS and IFNγ (**Figure 2.1B**) or M2 stimulation with IL-4 and IL-13 (**Figure 2.1C**). Consistent with literature, M1-skewed BMDMs display more rounded pancake-like morphologies compared to M2-skewed BMDMs, which become strikingly elongated in response to stimulation with thin, spindle-like protrusions. Stiffness has been shown to impact macrophage behavior and given most of the experiments in this chapter use glass as a control, we sought to characterize morphology on flat versus aligned glass (**Figures 2.1D and 2.1E**). On flat glass, macrophages do exhibit slight elongation, but with mixed phenotypes and to a lesser extent than with M2 stimulation on plastic (**Figure 2.1C**). Macrophages on aligned nanopatterned substrates exhibit striking elongation consistent with topography. Baseline expression of M1 and M2 markers was also assessed on glass culture plates with and without stimulation (**Figure 2.1F,** quantified in **Figure 2.1G**). As expected, macrophages on glass express virtually

no arginase-1 (M2 marker), moderate CD206 (M2 marker), and again essentially no iNOS (M1 marker) at baseline. However, with M2 stimulation, macrophages significantly increase arginase-1 and CD206 expression, and with M1 stimulation, macrophages strongly upregulate iNOS. These results simply validate our culture,

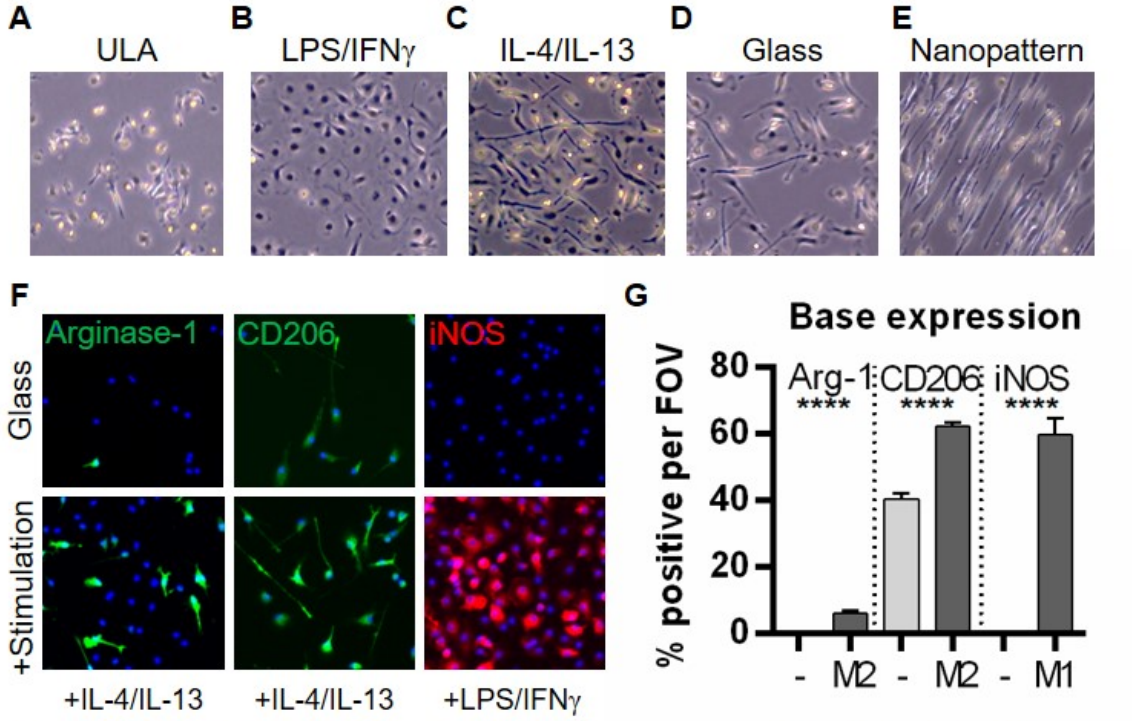


**Figure 2.1 Characterization of bone marrow-derived macrophages.** Macrophages display minimal polarization at baseline with mixed morphology, but respond drastically to topography and stimulation. **(A-E)** Panel of BMDM morphology in various culture conditions. **A)** BMDMs on ultra-low adhesion (ULA) tissue culture plates. **B)** BMDMs exhibiting rounded morphologies after "M1" stimulation with LPS and IFNγ. **C)** BMDMs exhibiting elongated morphology after "M2" stimulation with IL-4 and IL-13. **D)** BMDM morphology on flat glass controls compared to **(E)** on glass nanopatterned substrates with aligned architectures. **(A)** after 1 week of differentiation with L929 conditioned media. **(B-E)** BMDMs after 1 week differentiation and subsequent culture in respective condition for 24 hours. **F)** BMDMs without (top row) and with (bottom row) stimulation for 24 hours to gauge basal polarity after differentiation and culture on glass. Stimulation with either IL-4 and IL-13 (left, "M2"), or with LPS and IFNγ (right, "M1"). Quantified in **(G)** ($p<0.0001$ Student's t-test).

differentiation and stimulation protocols, and confirm low basal expression of canonical markers in culture on glass.

**Macrophage location, morphology, and phenotype correlate with collagen density and fiber alignment.** To define macrophage morphology and distribution throughout disease progression in PDA, we first examined murine pancreata isolated from the *Kras$^{G12D/+}$;p53$^{R172H/+}$;Pdx1-Cre* (*KPC*) mice. This model is ideal for studying PDA because it faithfully recapitulates the histological and clinical progression of human disease, and closely mimics the fibrotic and immunosuppressive TMEs characteristic of human PDA [10, 15, 60, 140]. Of note, the deposition and remodeling of collagen in *KPC* mice gives rise to collagen architectures similar to those observed in human disease [150], allowing the interrogation of how TACS influence disease dynamics. While it is clear these architectures direct carcinoma cell migration in other contexts [106-108], their role in directing immune cell motility and phenotype is less defined.

Consistent with previous reports [15, 22, 60], we observed immunosuppressive myeloid expansion early in disease progression, beginning around PanIN lesions in mice as young as 8 weeks and persisting throughout PDA (**Figure 2.2**). Interestingly, macrophages positive for F4/80 and immunosuppressive markers CD206 or arginase-1 were strongly correlated with both collagen content and fiber alignment at all stages of disease examined.

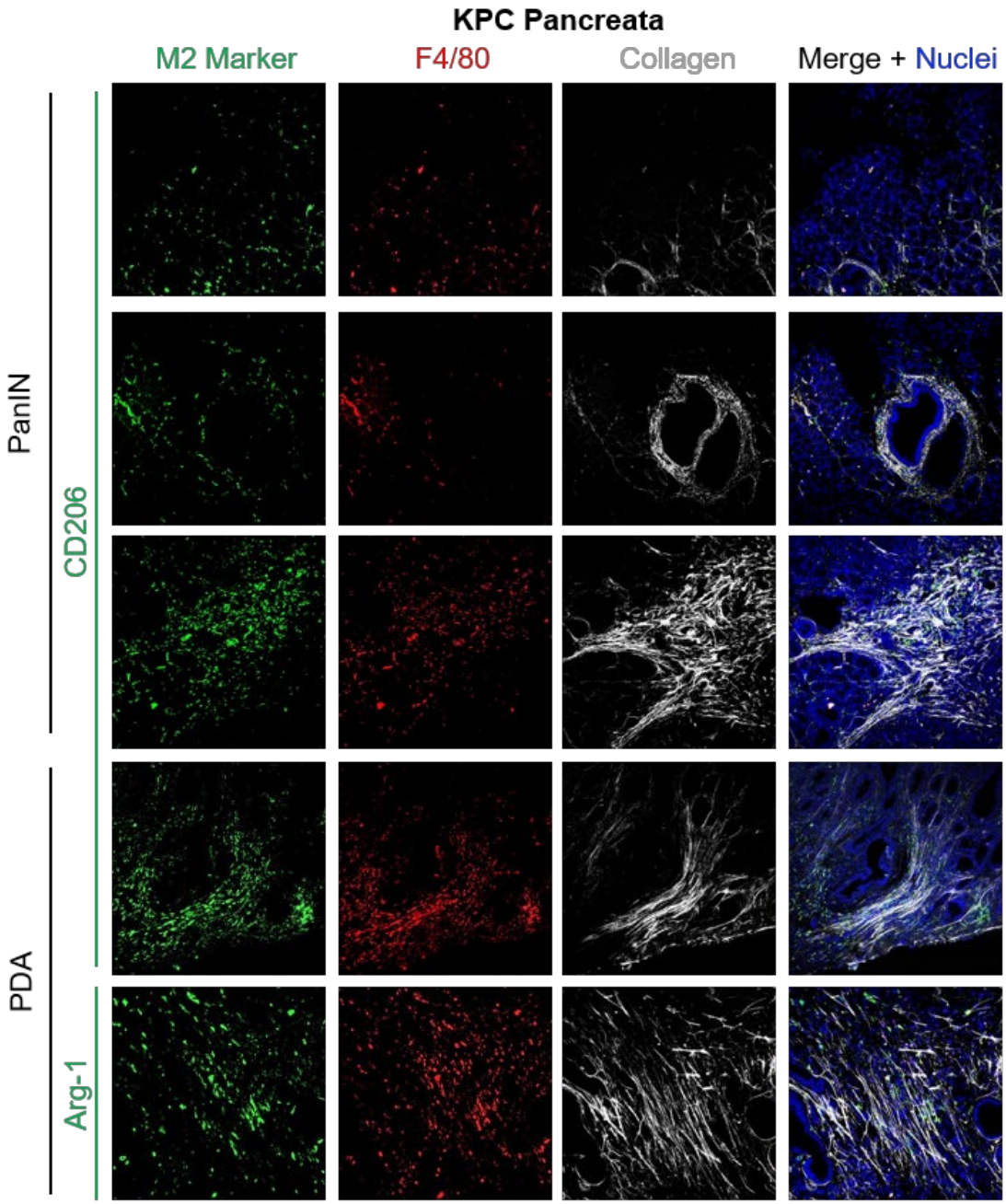


**Figure 2.2 Macrophages correlate with collagen in mouse pancreata.** Samples from both pre-invasive and invasive stage KPC mice were stained for immunosuppressive markers CD206 or Arginase-1, and pan-macrophage marker F4/80. LSMPM/SHG was used to assess macrophage correlation with collagen. Immunosuppressive macrophages correlate with collagen in all stages of disease examined, even in early dysplasia (PanIN).

Utilizing a reductionist perspective where macrophages display two phenotypes within tumors - an anti-tumor “classically activated” or “M1”, or the pro-tumor “alternatively activated” or “M2” phenotype [42, 50] - these data suggest a more M2 phenotype is associated with aligned collagen, supportive of the notion that suppressive macrophages are primed to support tumor progression even in preinvasive inflammation. Furthermore, macrophages near collagen fibers displayed extreme elongation in the direction of fiber orientation, in stark contrast to cells in distal regions that appear rounded and lacked directionality (**Figure 2.3A**). Moreover, cell orientation was highly correlated with collagen angle in regions with elevated, aligned collagen (**Figure 2.3B**) compared to macrophage shape in regions with low or unaligned collagen (**Figure 2.3C**). These observations raise interesting questions regarding the influence of shape on macrophage function as work by Mcwhorter and colleagues [121] suggests a link between macrophage aspect ratio and phenotype *in vitro*. Here, on average, macrophages observed in close proximity to aligned fibers exhibited a significantly higher aspect ratio compared to isotropic regions, with a maximum ratio roughly 8-times higher than the isotropic average (**Figure 2.3D**). Together, these observations suggest collagen architectures may direct macrophage phenotype *in vivo*.

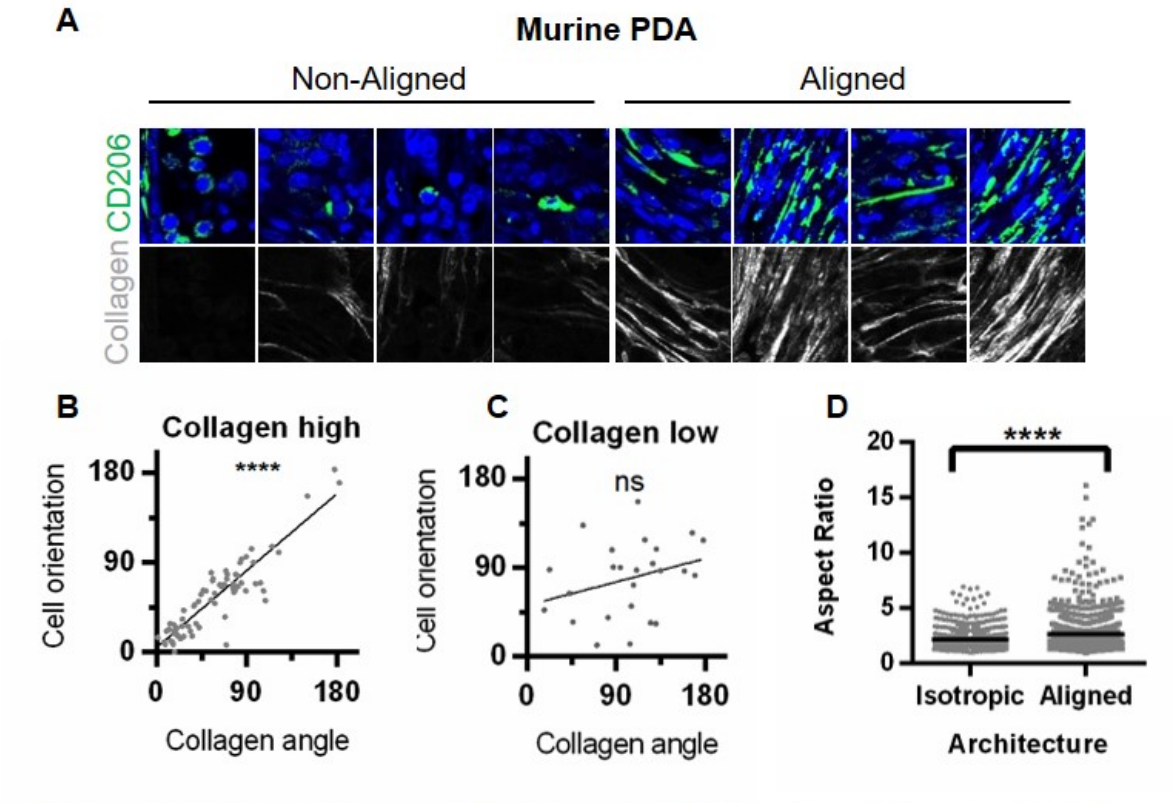


**Figure 2.3 Macrophage morphology correlates with collagen orientation in murine PDA. A)** Enlarged images of immunosuppressive macrophages in PDA in non-aligned versus aligned collagen. **B) and C)** Quantification of correlation between cell orientation and collagen angle using linear regression and Pearson's correlation. Cell orientation in regions with aligned collagen **(B)** strongly correlates with collagen angle (blue, R=0.9, p<0.0001) compared to cells in regions with little to no collagen **(C)** (grey, R=0.3, not significant). **D)** The aspect ratio of immunosuppressive macrophages is significantly higher in PDA in regions with aligned collagen architectures compared to isotropic regions with no distinct TACS-2 or -3 (p<0.0001, Student's t-test).

To determine if these observations were also characteristic of human PDA, patient-derived biopsies were obtained to assess macrophage location, morphology, and polarization state. As expected, the prevalence of immunosuppressive CD206+/CD68+ macrophages increased with disease progression from normal pancreas, to PanIN lesions, to PDA (**Figure 2.4A and 2.4B**).

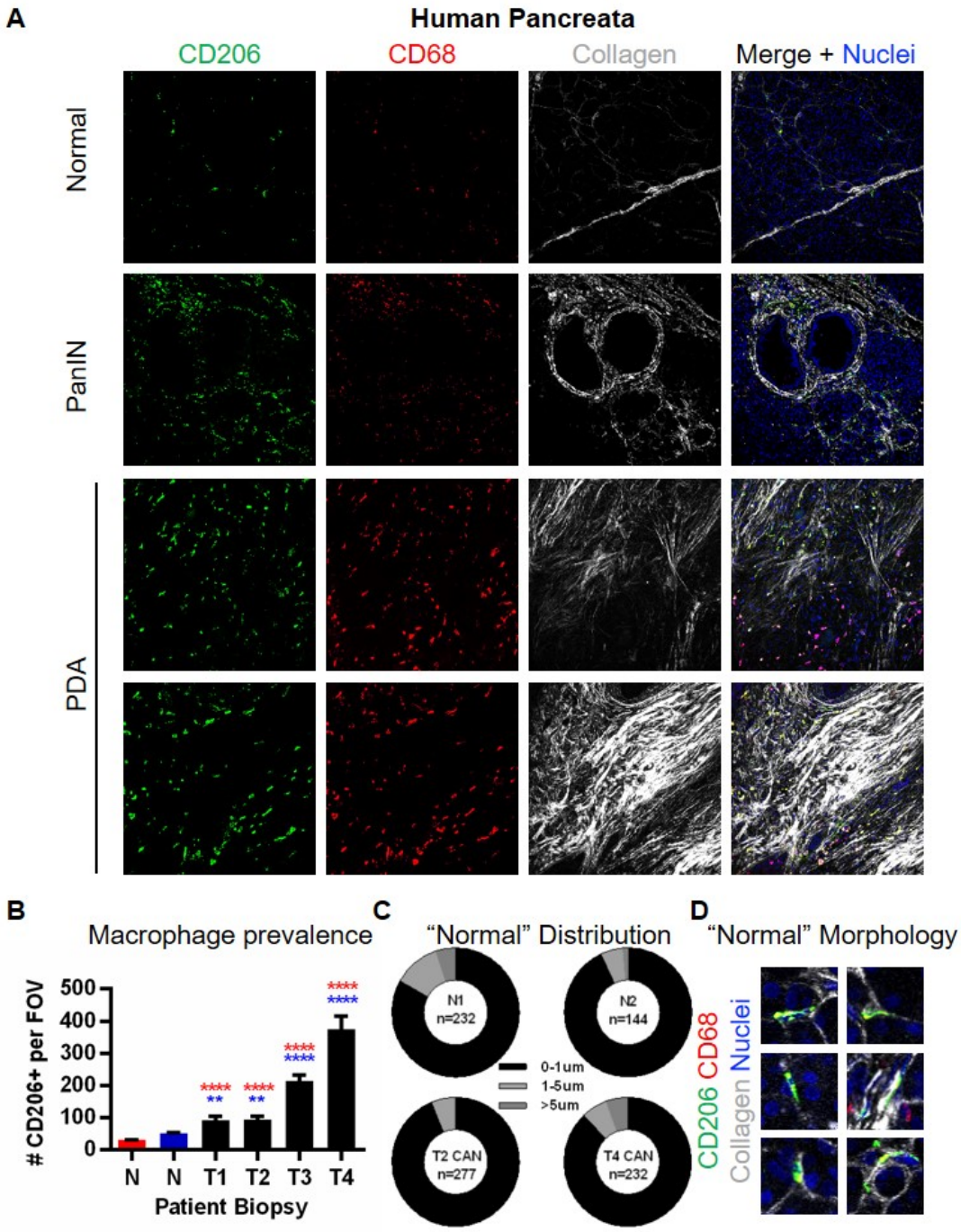


**Figure 2.4 Macrophages correlate with collagen content and alignment in human PDA. A)** Samples from both pre-invasive and invasive human disease were stained and imaged using LSMPH/SHG to assess the number of CD206+ macrophages per 20X field of view **(B).** Assessment revealed significant increases in the number of immunosuppressive macrophages in all four patient PDA biopsies examined compared independently to each normal case (** $p<0.01$, **** $p<0.0001$, Student's t-test). **C)** CD206+ CD68+ macrophages in normal and normal adjacent samples were observed to be within 0-5um of a collagen fiber, with majority within 0-1um, shown in **(D).**

In agreement with our findings from murine pancreata, immunosuppressive macrophages in human disease were observed in close proximity to collagen fibers and were enriched in regions with aligned collagen (**Figure 2.4A**, *PDA panels*). While macrophages were sparsely distributed in two independent normal and two independent cancer-adjacent normal (CAN) pancreas samples, 97% of these macrophages were within 5 microns of a collagen fiber, with an overwhelming majority located within 1 micron (>90%; **Figure 2.4C**). Furthermore, virtually all macrophages in normal tissues were observed directly interacting with collagen fibers and elongated in the direction of fiber orientation (**Figure 2.4D**). Taken together, these results suggest that aligned stromal collagen serves as a mechanical cue to direct macrophage shape and influence phenotype through early to late various disease stages of disease.

**Alignment influences macrophage morphology and phenotype *in vitro* and in live tumors.** The evident link between collagen alignment and macrophage phenotype suggests a direct cause-and-effect relationship. Therefore, to understand how collagen architecture influences macrophage behavior, we first seeded primary bone marrow derived macrophages (BMDM) differentiated with L929 conditioned media into live *KPC* tumor slices. Importantly, these macrophages are capable of polarizing toward both M1 and M2 phenotypes in response to canonical stimulation *in vitro* (**Figure 2.1**). Because the live tumor slices contain pre-existing ECM architectures, we hypothesized that the *ex vivo* applied macrophages would home to sites of dense and aligned collagen and

subsequently undergo extensive elongation. In support of our hypothesis, BMDMs do in fact home to areas with increased collagen density and become CD206-positive (images in **Figure 2.5A**, quantification in **Figure 2.5B**). Moreover, within

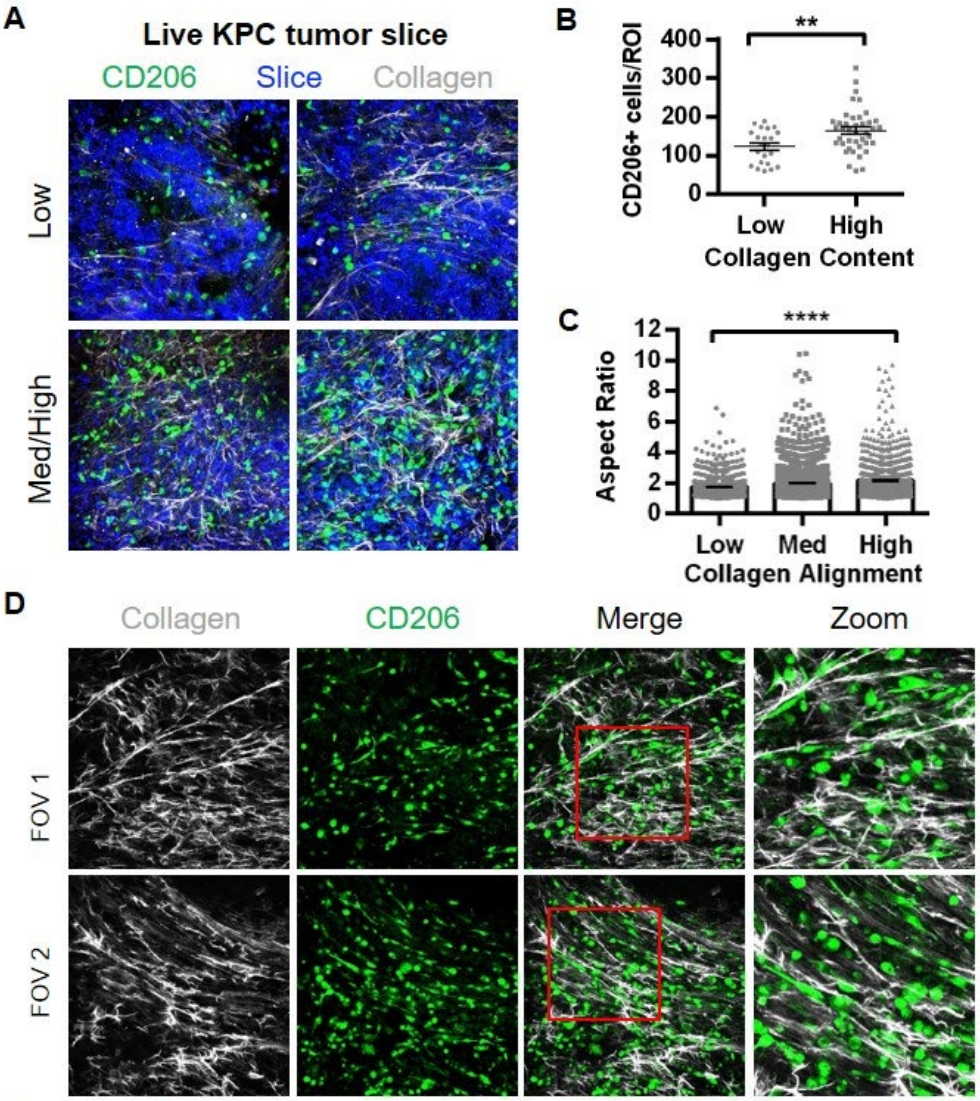


**Figure 2.5 Macrophages home to and elongate in response to alignment *ex vivo*. A)** Live KPC tumor slices were sectioned using a vibratome at 300um thickness and seeded with primary BMDMs for 24 hours after which CD206+ macrophages can be observed to preferentially home to regions with higher collagen content, quantified in **(B)** (Student's t-test, p<.01)**.** Moreover, cells within regions of medium and high collagen alignment exhibited higher aspect ratios than macrophages in regions with low or no collagen alignment **(C)** (p<.0001, one-way ANOVA), shown in **(D)**.

24 hours of seeding, macrophages transitioned to the more elongated phenotypes in regions with moderate to high collagen alignment compared to regions with little or no alignment (quantification in **Figure 2.5C,** images in **Figure 2.5D**), with aspect ratios similar to those determined from analysis of intact tumors (**Figure 2.2)**. To independently verify these results, we seeded macrophage-like Raw 264.7 cells onto live *KPC* tumor slices and assessed location and phenotype. Consistent with our observations using BMDMs, we observed the Raw 264.7 cells home to collagen and express arginase-1 and CD206 (**Supplemental S2.1**).

As the stroma in live tumor environments is quite complex, we sought to perform more reductionist experiments to test the hypothesis that ECM alignment is sufficient to drive macrophage behavior. Therefore, to directly test whether alignment regulates macrophage phenotype, we employed “2.5D” nanopatterned culture systems which mimic physiologically relevant ECM alignment, spacing, and texture and allow study of large numbers of cellular events in defined microenvironments that reasonably capture key 3D behaviors [108, 154]. Thus, with these systems we can analyze large cell numbers in a biomimetic environment to directly define how physical cues impact macrophage phenotype. We seeded primary macrophages onto aligned or flat control topographies and observed that BMDMs on aligned topographies exhibited striking elongation in contrast to macrophages on flat surfaces which showed more rounded, randomly oriented morphologies (**Figure 2.6A**).

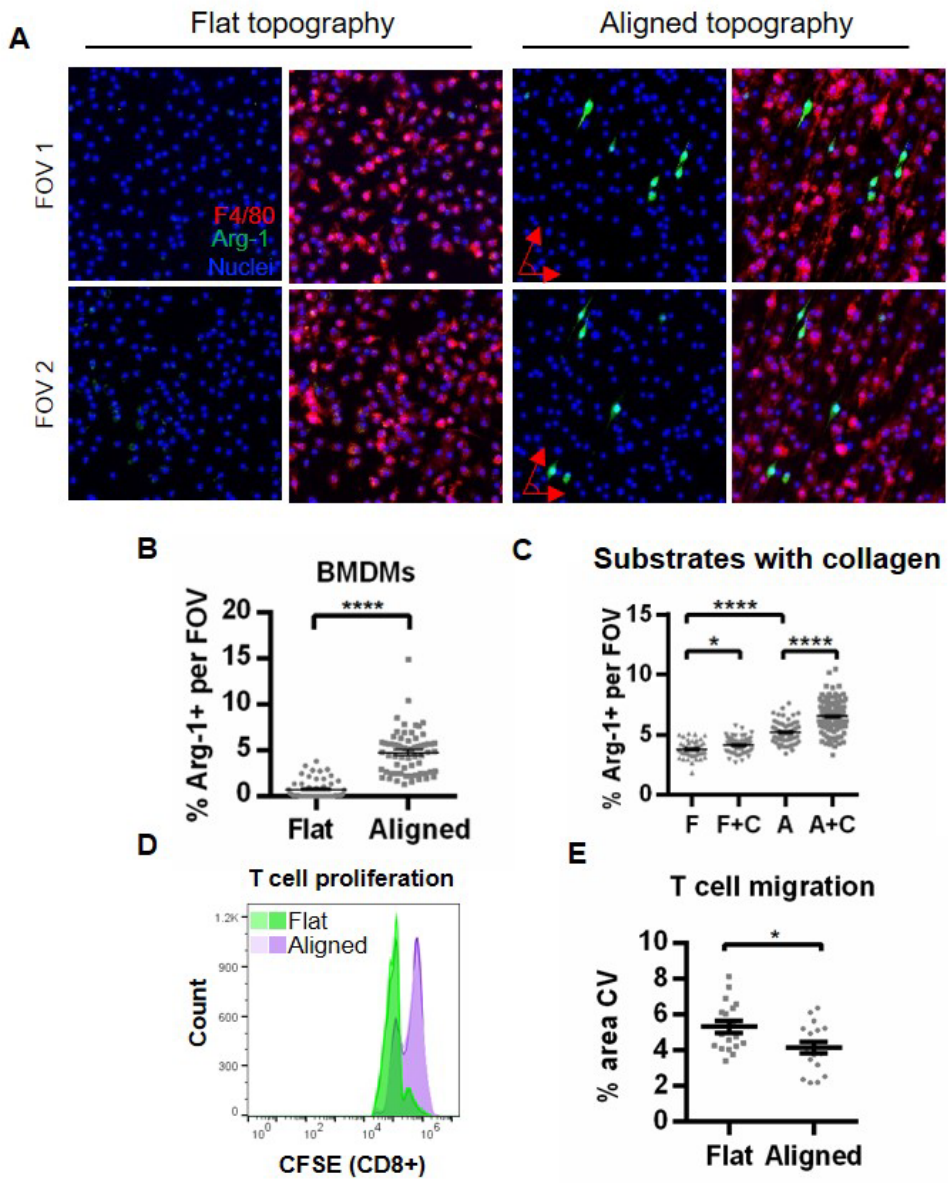


**Figure 2.6 Alignment induces immunosuppressive behavior in primary macrophages. A)** Primary BMDMs seeded onto aligned nanopatterned substrates exhibit increased arginase-1 expression, quantified in **(B)** ($p<0.0001$, Student's t-test), suggesting polarization toward an immunosuppressive state. **C)** Addition of collagen to nanopatterned substrates elicits even stronger increase in arginase-1 expression in both conditions ($p<0.0001$ and $p<0.1$, Student's t-test). **D)** Direct coculture of BMDMs and paired activated T cells on aligned nanopatterns abrogates T cell proliferation compared to flat control coculture as measured by CFSE dye dilution after three days of coculture. **E)** Transwell assays demonstrate activated T cells cultured above paired BMDMs on aligned substrates exhibit diminished migration compared to flat controls. Migration was quantified by measuring the fraction of the membrane positive for crystal violet ($p<0.1$, Student's t-test).

This behavior is consistent with findings of robust contact guidance of carcinoma cells along nanopatterns [108, 154, 156], and with previous studies characterizing macrophage elongation in response to M2 stimulation with cytokines IL-4 and IL-13 [121]. Thus, our results suggest aligned topographies alone are capable of regulating macrophage phenotype, even in the absence of specific chemical cues. Moreover, BMDMs on aligned topographies displayed significantly increased expression of the canonical pro-tumor marker arginase-1 (images in **Figure 2.6A,** quantification in **Figure 2.6B**), consistent with results found by McWhorter [121] where the elongated cell shape promotes a M2 state. Interestingly, coating flat and aligned substrates elicited an even more robust increase in arginase-1, suggesting not only topography, but also the addition of collagen, even to flat controls, can induce skewing toward an M2 phenotype (**Figure 2.6C**). Thus, our data suggests that matrix alignment may be directly promoting immunosuppressive macrophage behavior.

In many solid tumors, myeloid cells attenuate or abolish nearly every facet of CD8+ T cell cytotoxicity, including their recruitment, trafficking, stimulation, expansion, antigen recognition, and even survival. Known to be an immunologically “cold” tumor, PDA contains sparse CD8+ T cells, even at the earliest points of inception [15, 60], and this stark absence can be largely attributed to stromal fibrosis and immunosuppressive macrophages. We therefore sought to determine whether matrix alignment drives immunosuppressive macrophage behavior. To test the hypothesis that guidance of macrophages along aligned topographies impacts

both CD8+ T cell proliferation and migration, activated primary CD8+ T cells were cocultured with BMDMs. Both populations were derived from the same mouse to remove any possibility of immune cross-reactivity. Proliferation was assessed by directly coculturing activated CD8+ T cells on top of BMDMs on flat or aligned topographies. Indeed, T cells overlaid on macrophages in aligned conditions exhibited decreased proliferation compared to flat controls (**Figure 2.6D**) as evidenced by their attenuated dilution of carboxyfluorescein succinimidyl ester (CFSE) proliferation dye. This suggests macrophages on aligned substrates have a heightened ability to abrogate T cell expansion. Moreover, activated CD8+ T cells seeded into the upper chamber of collagen-coated transwell inserts exhibited decreased migration toward BMDMs on aligned topographies when compared to flat controls (**Figure 2.6E**), suggesting alignment not only impedes expansion, but T cell trafficking as well. Given other literature suggesting glass can skew macrophages toward an M1 phenotype, we referred to our baseline characterization of iNOS expression in macrophages on glass in **Figure 2.1F** and **2.1G**. Given their low basal expression of iNOS in response to glass, we do not attribute the difference in T cell proliferation and migration to M1-skewing with stiffness. Interestingly, even whole undifferentiated bone marrow elongated and upregulated arginase-1 in response to aligned topography (**Figure 2.7A, quantified in Figure 2.7B**) to an even greater extent than differentiated BMDMs in **Figure 2.6**. Taken together, these data implicate alignment as a direct regulator of not only macrophage polarization, but also of macrophage function. Thus, it is evident alignment skews macrophages toward a functionally suppressive state.

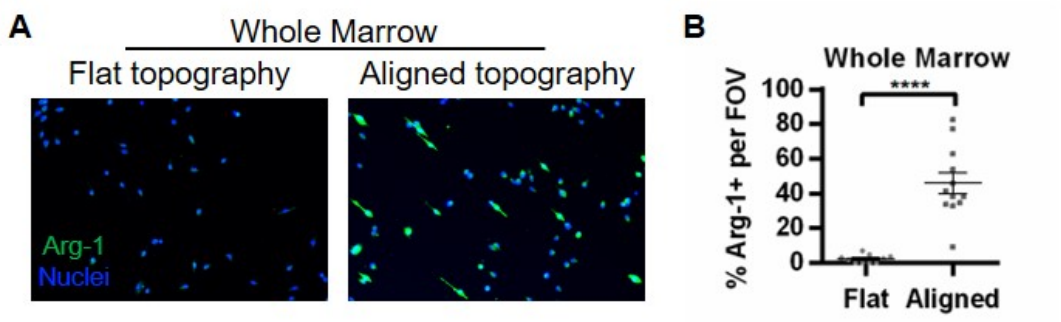


**Figure 2.7 Alignment induces Arginase-1 expression in whole, undifferentiated bone marrow. A)** Whole, undifferentiated bone marrow was isolated and seeded onto flat or aligned nanopatterned substrates for 48 hours after which expression of Arginase-1 was assessed. Surprisingly, bone marrow exhibited an even greater shift in arginase-1 expression, quantified in **(B)** ($p<0.0001$, Student's t-test), than differentiated BMDMs shown in **Figure 2.6**.

**Focal adhesions are enriched and striated in macrophages on aligned topographies.** Cells utilize surface receptors such as integrins to sense and respond to their external environment via focal adhesion dynamics. In fact, anisotropic distribution of mature focal adhesions is known to govern spontaneous sensing of guidance cues by carcinoma cells. As such, we sought to determine the role of focal adhesions as regulators of the link between macrophage shape and function. Recent studies from our group and others have implicated FAK as a key driver of fibrosis, macrophage accumulation, and cancer cell dissemination, and suggest a link between FAK, collagen alignment, and disease severity [31, 32, 103, 105, 125-128, 157]. Thus, FAK seemed a likely influencer of macrophage polarization in response to alignment.

To inspect the level, localization, and phosphorylation status of FAK in macrophages, BMDMs were cultured on aligned nanopatterns. First, we evaluated active FAK by examining FAK phosphorylation at tyrosine 925 (pY925), one of several sites phosphorylated downstream of FAK activation. Compellingly, BMDMs on aligned topographies exhibited high levels of pY925 compared to BMDMs on flat control substrates (**Figure 2.8A**). Moreover, the distribution of pY925 was strikingly striated along aligned substrates, forming long stretches of

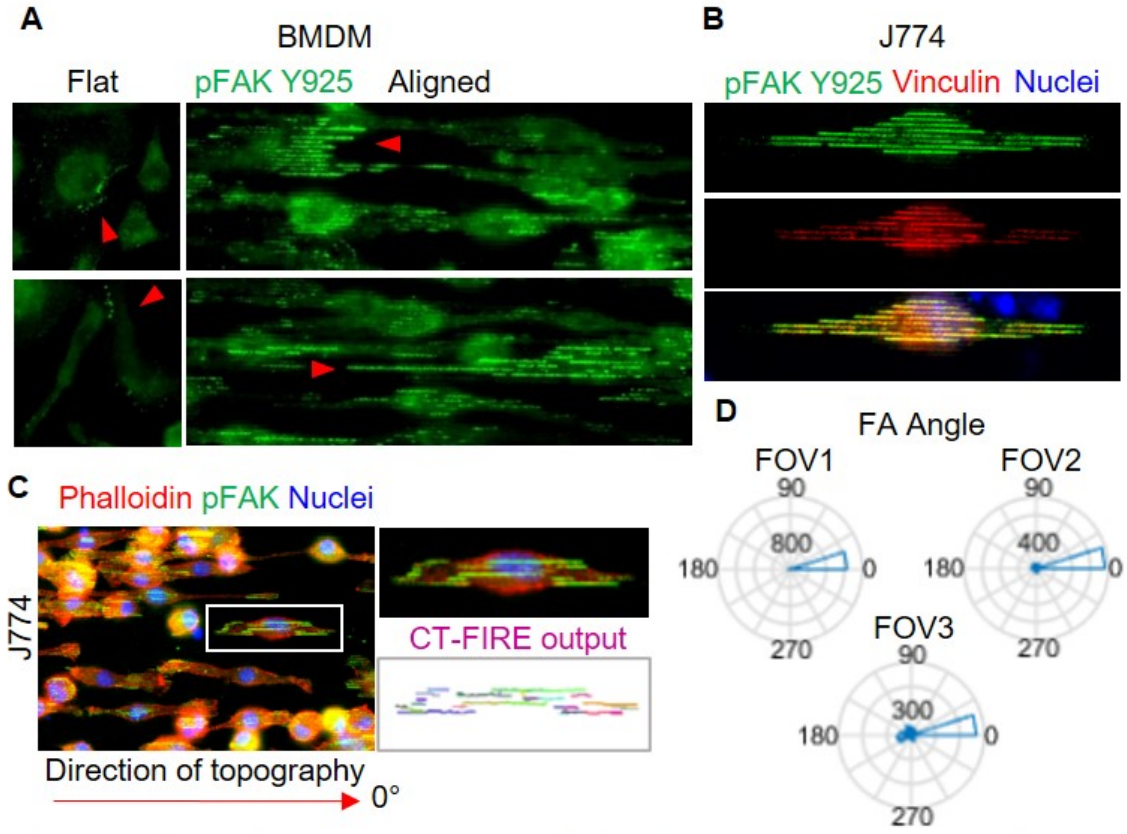


**Figure 2.8 Alignment alters focal adhesion dynamics in primary macrophages. A)** Primary BMDMS seeded on aligned nanopatterns exhibit increased phosphorylated FAK at tyrosine 925 compared to on flat conditions. **B)** Immortalized macrophage-like J774 cells also exhibited straited focal adhesion patterns on aligned surfaces, and their focal adhesions were characterized using CT-FIRE, depicted in **(C)**. **D)** CT-Fire was used to quantify focal adhesion angle in 3 fields of view, all showing majority of the detectable focal adhesion striations are oriented along the direction of topography (0*).

highly aligned focal adhesions along aligned nanopatterns (**Figure 2.8A**, arrow heads), distinct from more localized focal adhesions at the leading edge in carcinoma cells responding to nanopatterned contact guidance [108, 158]. In contrast, on flat conditions, pY925 was dispersed diffusely within the cell, with little to no pY925 near the cell membrane. Rarely, pY925 could be observed at the membrane in small, punctate clusters with no apparent pattern or orientation. Phospho-tyrosine 397 (pY397), another indicator of FAK activity, also exhibited similar patterns localized to and oriented along aligned nanogrooves. To confirm our findings, we further validated this phenotype in immortalized J774 macrophages. Interestingly, J774 cells exhibited a similar increase in and organization of pY925 with long, highly aligned focal adhesions along the length of the cell (**Figure 2.8B** and **Supplemental Figure S2.2**) versus more random and diffuse signal on flat. To confirm pY925 is indeed associated with mature focal adhesions, we performed dual-immunofluorescence and evaluated colocalization of pY925 with vinculin. Consistent with FAK staining, striated vinculin was observed suggesting these are indeed mature focal adhesions. To confirm these visual findings, quantitative analysis was performed to characterize focal adhesion orientation and straightness. Focal adhesions in aligned cultures were overwhelmingly oriented in the direction of alignment (**Figure 2.8C** and **2.8D**, explanation of analysis and additional examples in **Supplemental Figure S2.2**), and were uniformly perfectly straight, S=1. We note this phenotype is distinct from our previous observations in carcinoma cells, prompting us to evaluate cell shape and adhesions in greater detail.

Alternatively-activated macrophages are known to display more elongated morphologies *in vitro* as a result of canonical “M2” stimulation with IL-4 and IL-13, though the significance of this phenotype has yet to be understood. Given the evidence that alignment and elongation alone are sufficient to direct macrophage polarization (**Figures 2.6 and 2.7**), and the apparent accumulation of pY925 in response to alignment, we speculated stimulating macrophages with IL-4 + IL-13 may also alter FAK dynamics. As anticipated, BMDMs stimulated with IL-4 + IL-13 exhibited significantly elevated Y925 phosphorylation (**Figure 2.9A**, quantified in **Figure 2.9B**). J774 cells independently recapitulated this increase in pY925 (**Figure 2.9C**, quantified in **Figure 2.9D**), further implicating pY925 as a key player in this elongation-polarization axis. To gain a broader understanding of how chemical stimulation influences macrophage global FAK dynamics, BMDMs were cultured with either complete media alone (“Cont”), complete supplemented 1:1 with tumor conditioned media (“TCM”), or complete with IL-4 + IL-13. Immunofluorescence was used to compare pY925. Consistent with the pY925 patterns, BMDMs in tumor conditioned media exhibited an increase in pY397, and those with M2 stimulation exhibited even higher levels of pY397 (**Figure 2.9E**). Total FAK levels increased with a similar trend (**Figure 2.9E**), reaching the highest levels with M2 stimulation.

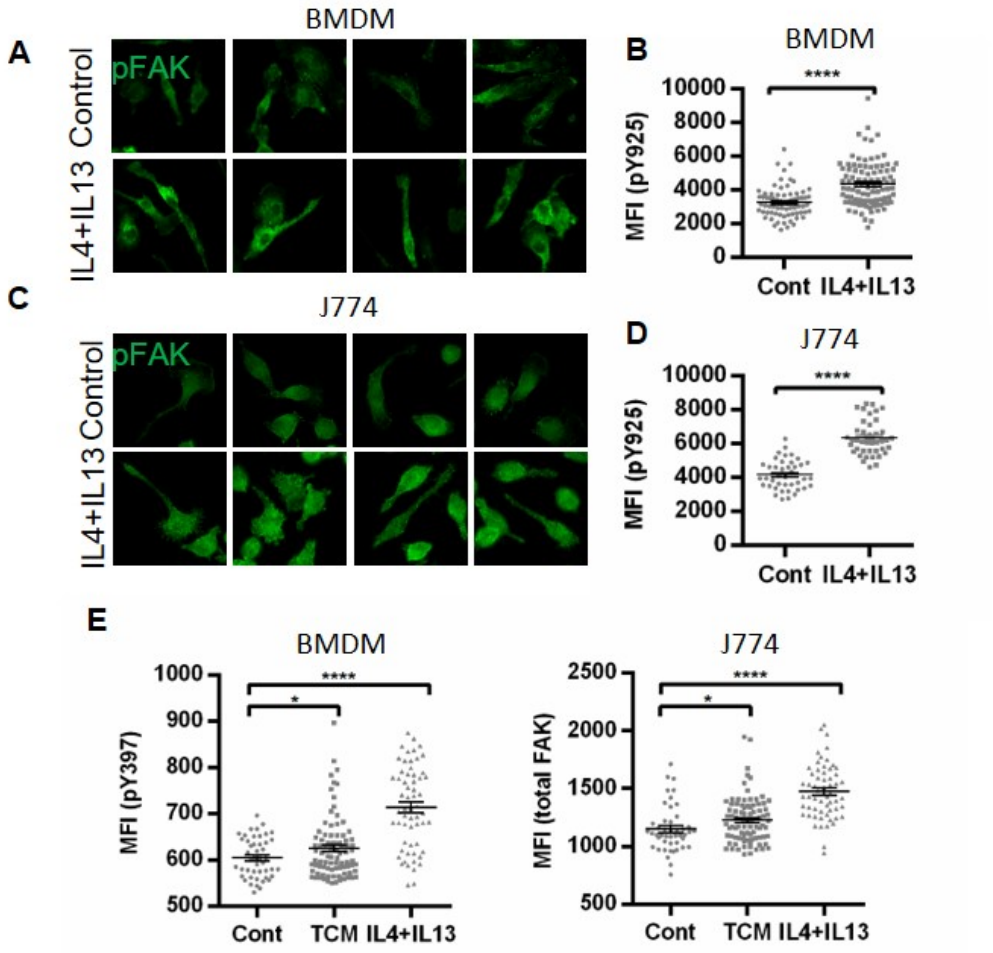


**Figure 2.9 Alternatively-activated macrophages exhibit increased FAK signaling. A)** Primary BMDMs were stimulated with IL-4 and IL-13 for 24 hours, then fixed and stained for pFAK Y925. **B)** M2 stimulation increased expression of pY925 ($p<0.0001$, Student's t-test). Immortalized J774 cells independently recapitulated this observation **(C, D)** ($p<0.0001$, Student's t-test). **E)** BMDMs also increased pY397 and total FAK in response to KPC primary tumor cell conditioned media, and even more so with M2 stimulation with IL4+IL13. The same was observed with J774 macrophages. (* $p<0.1$, **** $p<0.0001$, Welch t-test).

To further probe this interaction, selective FAK inhibitors were employed to understand whether macrophages can still polarize in response to alignment with abrogated FAK signaling. BMDMs were seeded into ultra-low adhesion plates and allowed to adhere for at least 24 hours after which they were subjected to either

1uM/mL VS-4718 or DMSO control treatment. BMDMs were then collected and seeded onto aligned nanopatterned substrates and cultured for 24 hours with continued FAKi or DMSO treatment and were then fixed and stained to assess arginase-1 expression and morphology. Indeed, FAK inhibition *in vitro* diminished BMDM ability to adhere, elongate, and polarize in response to alignment. BMDMs under FAKi exhibited a drastic fold change in arginase-1 expression normalized to vehicle control (**Figure 2.10A**). Moreover, despite an incomplete abolishment of arginase-1 expression in the FAK inhibited samples, we also observed arginase-1+ cells displayed much smaller aspect ratios than those in DMSO, suggesting these cells are not fully adhered to nanopatterned substrates, likely due to

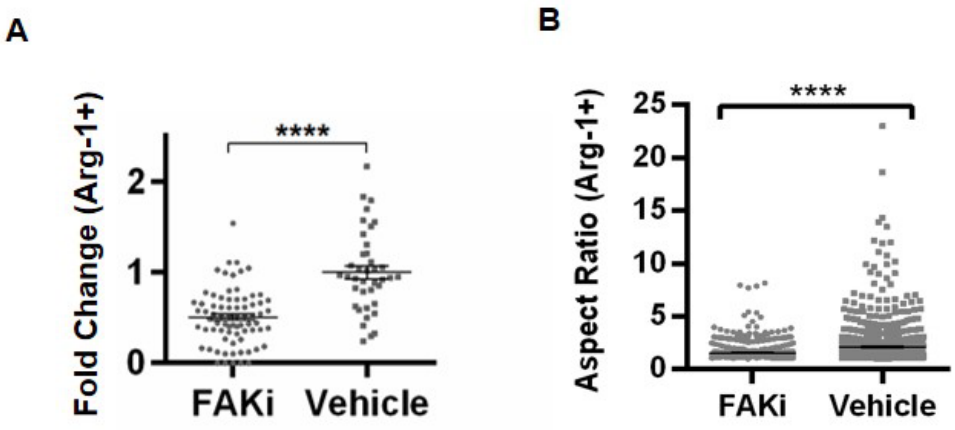


**Figure 2.10 FAK inhibition in vitro abrogates response to alignment.** BMDMs were pretreated with VS-4718 FAK inhibitor or vehicle control (DMSO) for 24 hours before plating on aligned nanopatterned substrates. Cells were grown for 24 hours to allow adherence and response to alignment in the presence of inhibitor or control. **A)** FAK inhibition strongly decreases BMDM ability to increase arginase in response to alignment compared to vehicle (normalized to the mean of the vehicle). **B)** Cells in the FAKi conditions which remained Arginase-1+ had significantly lower aspect ratios, with morphologies much closer to perfectly spherical (AR~1). (Welch t-test, $p<0.0001$)

abrogated integrin signaling and impeded contact guidance. These results collectively implicate FAK as a key regulator of macrophage polarization in response to both chemical and physical cues *in vitro.*

To determine if our results linking cell shape, FAK signaling, and the M2 phenotype *in vitro* are maintained *in vivo*, we obtained samples from a previous study treating *KPC* mice with either FAK inhibitor VS-4718 or control vehicle in order to characterize macrophage cell shape and distribution. DeNardo and colleagues previously characterized these samples and noted FAK treated samples exhibited drastically reduced numbers of CD206+ macrophages, but the localization and aspect ratios of these macrophages was not assessed. As expected, vehicle treated *KPC* mice exhibited a spectrum of significantly higher aspect ratios in regions with collagen alignment compared to regions with no alignment (**Figure 2.11A,** quantified in **2.11B**), consistent with our observations in murine and human samples (**Figures 2.2** through **2.4**). However, tissues from age-matched *KPC* mice treated with FAK inhibitor VS-4718 exhibited no significant difference in their aspect ratio when comparing aligned versus non-aligned regions, suggesting FAK is required for the elongated macrophage phenotype which supports immunosuppressive M2 function. Furthermore, these results support the utility of FAK inhibitors in combination with other stroma targeted or immune therapies to not only target cancer cells, but also to reengineer extracellular matrix architectures and stromal immunity.

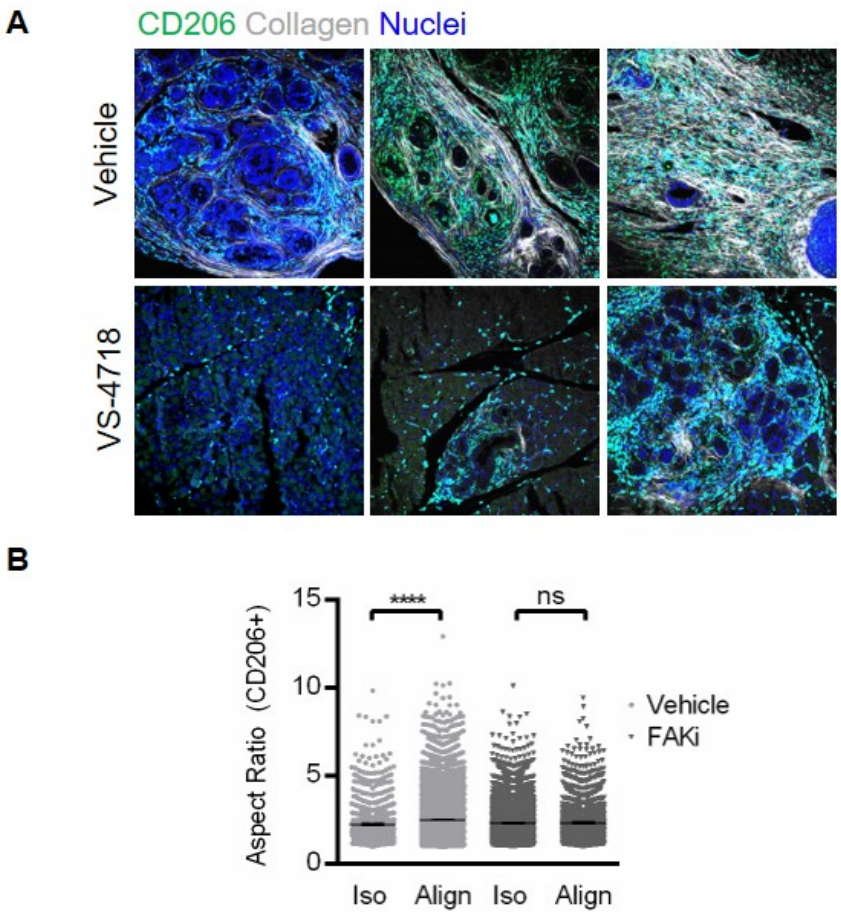


**Figure 2.11 FAK inhibition *in vivo* significantly alters aspect ratio of cells in aligned collagen. A)** Three fields of view exhibiting varied levels of fibroinflammation from KPCY mice treated with either VS-4718 or vehicle control show FAK inhibition drastically decreases collagen, alignment, and the number of CD206+ macrophages. **B)** FAK inhibition abrogates CD206+ macrophage elongation and decreases CD206+ macrophage aspect ratio in aligned collagen compared to macrophages in the vehicle control samples (Student's t-test, **** $p<0.0001$ in vehicle, not significant in FAK treated mice).

**Myeloid-collagen landscape in chronic pancreatitis is similar to PDA.** Pancreatitis is a well-known risk factor for PDA [4, 130, 133, 138, 139]. However, changes to ECM architecture and macrophage number and localization during pancreatitis that may precede transformation and development of robust, malignancy-associated, desmoplasia are not well defined. As such, we sought to

define the myeloid-collagen landscape in pancreatitis to determine if architectures emerge which could provide a form of stromal memory in the pancreas conducive to promoting early PDA. To answer this question, we obtained human chronic pancreatitis (CP) samples to determine if collagen architectures are similar to those present in PDA (shown in **Figure 1.10**), and whether these architectures correlate with macrophage accumulation, localization, and phenotype in the absence of transformation. In four independent CP patient biopsies, we note a strong correlation between CD206+/CD68+ macrophages and aligned stromal collagen (**Figure 2.12A**). Moreover, the number of immunosuppressive macrophages was greatly increased in CP compared to normal patient biopsies (**Figure 2.12B**), and in some cases, higher than previously observed in PDA (**Figure 2.4B**). Further, the fraction of CD68+ cells expressing CD206 greatly increased when examining regions with increased collagen content (**Figure 2.12C**). CD206+ cells also displayed significantly higher aspect ratios in regions with aligned collagen, with a maximum ratio roughly 8-times higher than the average ratio of cells in regions with low to no aligned collagen (**Figure 2.12D**).

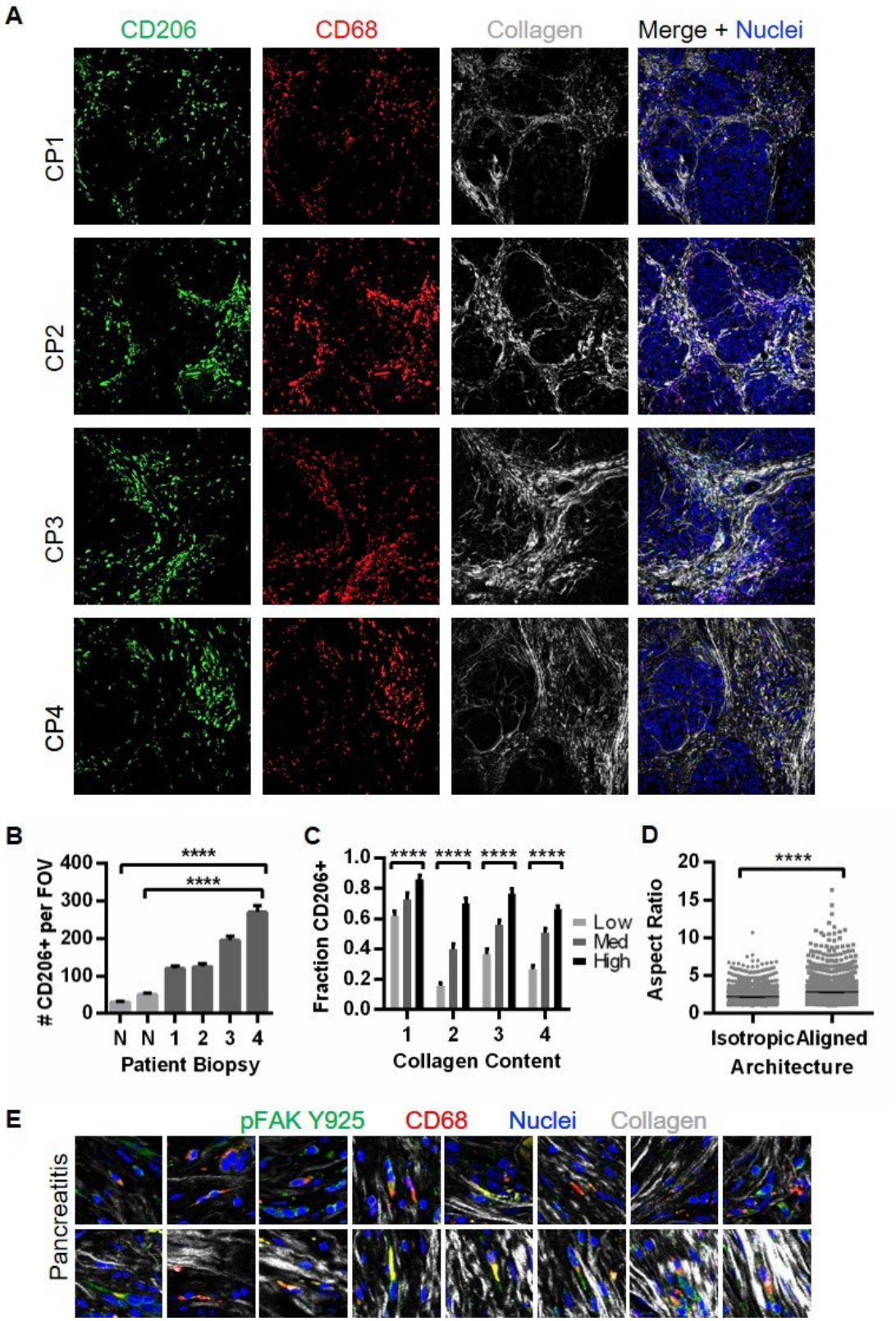


**Figure 2.12 Macrophages correlate with collagen in human chronic pancreatitis.**

These ratios, and their correlation with collagen alignment, are consistent with findings from macrophages in fixed mouse PDA samples and on live PDA slices (**Figures 2.3D and 2.5C**), a surprising result given these samples were isolated from chronically inflamed tissues with no histological signs of PDA, as determined by clinical pathologist evaluation, suggesting key stromal dynamics in CP are similar to PDA and could help establish and robustly promote early PDA.

Given the evident role of FAK in facilitating myeloid response to alignment, and the coinciding, colocalized accumulation of immunosuppressive macrophages and aligned collagen in CP, we sought to identify the presence of elongated, phospho-FAK+ macrophages in pancreatitis. Corroborating our *in vitro* results, CD68+ macrophages did indeed express pY925 at the cell membrane in all three biopsies examined (**Figure 2.12E**). Moreover, these pY925+/CD68+ cells were often found in regions of highly aligned collagen, although specific localization of pFAK to cell:collagen adhesions *in vivo* could not be assessed. These data suggest FAK plays a novel role in the regulation of macrophage shape and function, as well as in the connectivity of extracellular matrix architecture and immune dysfunction in early PDA onset and precursory fibroinflammatory disease.

---

**Figure 2.12 Macrophages correlate with collagen in human chronic pancreatitis. A)** Four human chronic pancreatitis biopsies were stained for CD206 and pan-macrophage marker CD68. LSMPM/SHG was used to assess the number of CD206+ macrophages per 20X field of view **(B)**. Assessment revealed significant increases in the number of immunosuppressive macrophages in all four CP biopsies examined compared independently to each normal case ($p<0.0001$, one-way ANOVA). **C)** The fraction of CD68+ macrophages that were immunosuppressive (CD206+) increased significantly in regions with higher collagen content ($p<0.0001$, one-way ANOVA for each case). **D)** The aspect ratio of CD206+ macrophages in regions with aligned collagen was significantly higher compared to isotropic regions with low collagen alignment ($p<0.0001$, Student's t-test). **E)** CD68+ macrophages could be found in stromal collagen expressing phospho-FAK Y925 in human CP biopsies.

Moreover, given the heightened risk of developing PDA during CP and the rapid timeline in which PDA spreads after inception, this study collectively supports the notion that stromal architectures are priming the microenvironment to support immune suppression, evasion of anti-tumor immunity, and tumor cell dissemination from the earliest stages of pancreas cancer [135, 150].

## Conclusions

The multitude of ways in which TAMs support cancer is striking—it is abundantly clear macrophages are a critical driver of disease, and thus make an incredibly attractive target for therapeutic intervention. Their transient functionality poses an interesting possibility to reprogram native patient immunity toward an anti-tumor state. However, to truly harness the power of macrophages and convert them to the heroes they could be, we must fully understand exactly what influences their polarization, and the timing and context in which this occurs.

In this chapter, we establish an inextricable cause-and-effect relationship between stromal architecture and macrophage behavior. Interrogation of both fixed and live murine pancreas samples revealed extensive macrophage elongation at sites of dense, aligned collagen. Moreover, macrophage localization and morphology also correlated with increased expression of canonical pro-tumor immunosuppressive markers. These observations were conserved in human patient samples, which also exhibited extensive macrophage infiltration and elongation in regions with increased collagen and alignment. *Ex vivo* slice cultures of live tumor samples possessing native collagen architectures were utilized to study how exogenous

macrophages respond to architecture; we found macrophages to home to, elongate in, and respond to increased collagen and collagen alignment in live samples within as little as 24 hours of seeding. Further studies to dismantle these architectures in slices with matrix-targeting compounds like collagenase should be done to elucidate the role collagen plays in macrophage homing *ex vivo.*

To characterize how alignment alone influences macrophage behavior, macrophages were cultured on aligned nanopatterned substrates and their expression of canonical M2 markers was assessed. Alignment alone was sufficient to induce M2-skewing, as measured by expression of arginase-1. Interestingly, the addition of collagen exacerbated M2-skewing even more robustly compared to alignment alone. This data suggests alignment and collagen both contribute to driving macrophages toward an immunosuppressive phenotype, and show alignment alone is sufficient to induce this shift. Additional functional studies *in vitro* revealed aligned topographies increase macrophage-mediated suppression of cytotoxic T cell expansion and chemotaxis as measured by diminished T cell proliferation and migration in conditions with macrophages cultured on aligned nanopatterned substrates. M2 skewing of macrophage behavior was at least partially attributable to increased expression and activity of focal adhesion kinase in response to topography, as expected. FAK inhibition *in vitro* abrogated macrophage ability to adhere, elongate, and polarize in response to aligned topography, although the impact of FAK inhibition on macrophage *function* should be assessed in future studies—namely, whether FAK inhibition in the myeloid compartment is sufficient to diminish their immunosuppressive influence on T cells.

Regardless, *in vivo* inhibition of FAK led to alterations of cell morphology in mouse models of PDA, and as previously published by our collaborators Jiang and DeNardo, a decrease in macrophages in general [31]. Further work should also be conducted to better understand how FAK inhibitors could be utilized *in vivo*, as well as the on- and off-target impact of FAK inhibition in both cancer cells and stromal cells.

Lastly, this chapter establishes a novel relationship between collagen alignment and macrophage function in the pancreas, and is the only to our knowledge to establish a link between physical cues and myeloid cells not only in PDA, but also in chronic pancreatitis. While the connections between chronic pancreatitis and PDA are controversial, CP is a long-accepted risk factor of PDA and parallels PDA involution in many facets. We establish here a clear link between collagen architecture, macrophage distribution and macrophage phenotype in human CP biopsies which closely mimics the correlation observed in frank PDA in both mouse and human biopsies, suggesting macrophages in CP are already primed to carry out immunosuppressive functions in the inflamed pancreas. The broader significance of this work indicates macrophage elongation and their resultant immunosuppressive phenotype is driven by stromal architectures, beginning early in preceding and parallel inflammatory disease states, irrespective of cancer onset, and highlights an opportunity to rethink how CP is treated clinically from the perspective of preventing PDA.

# 3. ALIGNED STROMAL ARCHITECTURES AND FOCAL ADHESION KINASE FACILITATE EARLY DISSEMINATION

## Summary

In this chapter, we demonstrate in both human and mouse PDA that extracellular matrix architectures (TACS) discussed in the previous chapter also regulate epithelial cell extrusion and subsequent invasion from intact ductal structures. This results in early dissemination from histologically pre-malignant lesions and continual invasion from well-differentiated disease, suggesting TACS could be used clinically as a biomarker in pathologic assessment of pancreas tissue. Furthermore, we show that pancreatitis results in invasion-conducive architectures, which may prime the stroma to support dissemination prior to malignant disease. Studies *in vitro* using novel microfluidics-derived microtissues and *in vivo* demonstrated decreased extrusion and invasion following focal adhesion kinase inhibition, consistent with decreased metastasis *in vivo* previously reported by Jiang, et al. [31] The data presented in this chapter further support the conclusions from Chapter 2, reiterating the utility of targeting FAK, the stroma, and ECM architectures, as well as the potential to resolve precursory fibrosis and dismantle architectures conducive to early dissemination. However, the data in this chapter take into consideration how architectures facilitate epithelial extrusion, rather than how they direct macrophage phenotype.

**Acknowledgement**: We acknowledge Dr. Arja Ray for his contributions to this Chapter as co-first author for this manuscript, as well as Nelson Rodriguez and other collaborators who contributed to this chapter's content, design and text. Data presenting in Dr. Arja Ray's thesis is provided in the supplement for this chapter for context.

## Introduction

The ECM which comprises PDA's desmoplastic stroma plays a fundamental role in the extensive metastasis frequently observed in PDA [108, 159], and may directly influence early tumor cell dissemination. Recent studies using the *KPC* mouse model demonstrate single epithelial cells can disseminate into the stroma and peripheral blood even before frank histologically-detectable malignancy [135]. This is consistent with early disseminated cancer cells (DCCs) observed in breast cancer [160, 161], and decreased efficiency of dissemination in PDA following treatment with antifibrotic or anti-inflammatory agents [31, 135]. These studies challenge the traditional notion of metastasis occurring late in cancer progression and are consistent with the early timeline in which we know PDA to metastasize clinically. The stroma is inevitably a key player in early metastatic cell dissemination, yet the mechanisms by which the fibrotic stroma aids early dissemination in PDA are unknown.

Excessive fibrillar collagen is a hallmark of several solid tumors, including those of the breast, where collagen is associated with elevated stiffness, hyperproliferation, increased invasion and metastasis [98, 102, 103, 113]. In the context of invasion, both collagen content and fibrillar architectures are important, and distinct patterns of collagen organization—TACS-2 and TACS-3—are critical to dissemination in breast cancer. For TACS-2, collagen fibers of variable density are mainly organized approximately parallel to either the ductal or carcinoma *in situ* boundary, around carcinoma cell clusters within the tumor mass, or at the tumor boundary.

For TACS-3, fibers orient perpendicularly to the cell clusters or ductal boundary, or result in aligned collagen regions throughout the tumor mass in later stages, often providing a conduit for carcinoma cell invasion [107, 162]. Cancer cells utilize anisotropy from these aligned ECM fibers via a process termed “contact guidance” to orient themselves and migrate along single fibers. Consequently, TACS-3-like aligned collagen patterns lead to increased focal and local invasion and metastasis [107, 162], and correlate with worse survival in human patients [115]. While recent studies suggest the presence of TACS architectures in PDA [108, 153], the prevalence of TACS in PDA—particularly relative to disease stage and early dissemination—remains largely unexplored. Thus, we hypothesized that TACS or TACS-like collagen architectures are involved in early dissemination and invasion in PDA.

Here, we employ an autochthonous mouse model of PDA, highly faithful to the human disease [10] and expressing carcinoma cell-specific fluorophores [108], as well as human PDA samples to define a key link between early dissemination in PDA and periductal collagen organization. We utilize LSMPM/SHG imaging on archival and live tumor samples to characterize the prevalence of TACS in PDA and demonstrate that periductal collagen patterns drive carcinoma cell dissemination. We further identify these patterns in pancreatitis and inflamed “normal” adjacent tissue, suggesting that precancerous fibroinflammatory disease can precondition the stroma for early dissemination prior to transformation. Moreover, we identify FAK as a regulator of ECM-guided extrusion from ductal

epithelium and subsequent stromal invasion and observe FAK inhibition reduces efficiency of single cell dissemination in PDA.

## Experimental Procedures

### Human and mouse pancreatic tissues and tumors

These samples were acquired and processed as described in Chapter 2.

### Cell Culture

Primary PDA cell lines were derived from pancreatic tumors in *KPCG* or *KPCT* mice as previously described [27]. Briefly, tumors were excised and minced before incubating with slight agitation in complete medium with 2mg/mL collagenase at 37°. Primary lines were maintained in high glucose DMEM supplemented with 10% FBS. 3D microtissue-culture was conducted as described previously [103, 163]. Primary tumor cell microtissues were then embedded in 3mg/mL collagen-I (Corning) (see the “Engineering microtissues to analyze cell extrusion and invasion” for details on generating collagen matrices) or Matrigel (Corning) diluted in complete medium to 4mg/mL.

### Staining and imaging of archival tissues

Mouse and human FFPE samples were stained and imaged following protocols outlined in Chapter 2, with the following additions: for human samples, tissue architectures were captured and assessed by imaging endogenous fluorescence with a green emission filter at the same wavelength of excitation of 880-900nm. In addition, some samples were stained with FITC-conjugated anti-pan-Cytokeratin

antibody (1:50, Sigma) to visualize carcinoma cells and ductal epithelia. For mouse tissues: *KPCG* mice were imaged without additional staining for carcinoma cells, as ZsGreen1 retains fluorescence post fixation in FFPE samples. However, an anti-RFP (1:100, Abcam) and Alexa-conjugated secondary antibody (Thermo Fisher) were necessary to visualize tdTomato in FFPE *KPCT* tissues. Note, all tdTomato or zsGreen fluorescence is pseudo-colored red in image throughout for consistency of identifying carcinoma cells.

FFPE slides were stained for cytokeratin and RFP following protocols outlined in Chapter 2, with the exception that the following additional primary antibodies were used: 1:50 mouse anti-Cytokeratin Pan-FITC (MilliporeSigma, Human), 1:100 mouse anti-Pan-Keratin (Cell Signaling, Mouse), 1:200 rat anti-mouse CD31 (Dianova, Mouse), 1:400 rabbit anti-CD31/PECAM-1 (Novus Biologicals, Human), 1:400 rabbit anti-RFP (Abcam, Mouse), 1:200 rabbit anti-GFP (Life Technologies, Mouse). Subsequently, slides were washed and incubated for 1h at RT with 1:200 Alexa-fluor secondary antibodies: goat anti-rabbit 488 (Life Technologies), goat anti-rat 568 (Life Technologies) along with 1:500 Draq5 (Biolegend) nuclear stain followed by wash steps and mounting with Prolong Gold (Life Technologies).

**Characterizing collagen content and architecture**

Collagen content and prevalence of TACS was quantified by assessing multiple random fields of view on several slides from different *KPCT*, *KPCG*, or human samples. Images are representative of the various stages of disease involution, from normal/normal adjacent, to PanIN, to both well- and poorly differentiated PDA.

These determinations were made by taking into account pathology assessment and H&E staining to assess morphology and staining patterns. After grading, SHG images were analyzed via a custom MATLAB code which dynamically thresholds images to maintain collagen positive pixels in a binary image, which then served as a metric of fibrous collagen content. Presence of TACS-2 and -3 was assessed using CurveAlign (LOCI), an open-access program which extracts information about fiber orientation and distribution with respect to user defined boundaries (in this case, ductal boundaries) [164]. To quantitate TACS-2 and -3 frequency, millimeter-scale regions of the human samples were imaged using LSMPM/SHG, reconstructed, and used to determine the total number of ducts, as well as the number of ducts positive for TACS-2 and -3 signatures.

**Analysis of cell extrusion *in vivo***

For analysis of cell extrusion, unbiased images of CAN, PanIN and differentiated PDA regions (17-54 fields of view/group) were obtained from pancreatic tumor sections (6-13/group) from different *KPCT* or *KPCG* mice (7-9 mice/group). Within each field of view (300μmX300μm or 600μmX600μm, the number of ductal structures, the percentage with organized periductal collagen (either TACS-2 or TACS-3) and the total number of extrusion events were calculated. An extrusion event was defined as single (or dividing) disseminated cell in the periductal stroma (fully extruded) or a single or pair of cells protruding out from the smooth boundary of a duct (partially extruded). The association of partially extruded cells with TACS-2 or TACS-3 positive areas or that of fully extruded cells with aligned collagen in

the stroma was determined by visual inspection. Morphometric analysis of disseminated cells was performed manually in Fiji, including only single cells fully extruded into the stroma for the analysis.

**Engineering microtissues to analyze cell extrusion and invasion**

Matrigel microtissues approximately 150-200μm in diameter were fabricated modifying previously established protocols [165, 166]. Matrigel (Corning) was thawed on ice overnight and diluted to a concentration of 6 mg/mL with Dulbecco's phosphate-buffered saline (DPBS). At 4°C, the Matrigel solution was partitioned into droplets using a flow-focusing polydimethylsiloxane (PDMS) (Dow Corning) microfluidic device. The continuous phase from the droplet generation (FC-40 with 2% 008-FluoroSurfactant, Ran Biotechnologies), was collected with the droplets in a low retention Eppendorf tube and polymerized for 30 minutes at 37°C. The oil phase was removed and the Matrigel droplets were resuspended in 1x DPBS with a manual micropipette.

Droplets were then moved to agarose microwells, fabricated following previously established protocols [166]. Briefly, polystyrene multi-well plates were coated with 2% agarose and dehydrated in a sterile laminar flow hood overnight. PDMS stamps with 300 μm diameter posts were plasma treated for 2 minutes to produce a hydrophilic surface and sterilized with boiling water. Agarose solution was pipetted into each well and the hydrophilic PDMS stamp placed immediately onto the molten agarose. After cooling for 5 minutes, stamps were removed gently from the polymerized agarose and hydrated with 1 x DPBS. Wells were washed with

appropriate culturing media prior to adding microtissues with a manual micropipette.

Once inside the microwells, droplets were coated with primary *KPCT* or *KPCG* cells at a concentration of 100,000 cells/well. These microtissues were cultured in complete DMEM for 7 days to allow cells to adhere to the outside of the droplets and form luminal structures. Droplets were then treated daily with either 1μM FAK inhibitor VS-4718, or with vehicle control (DMSO) for three days, after which they were embedded in 4mg/mL 3D collagen-I gels (Corning), with continued inhibitor or DMSO treatment. Briefly, collagen gels were generated by mixing collagen-1 with an equal volume of 100mM HEPES buffer in 2X DPBS, as previously described [163, 167, 168]. Droplets were added to this neutralized solution, which was then aliquoted out in 475uL increments into a 12-well culture plate and allowed to polymerize for 30 minutes at room temperature. Constructs were moved to 37°C for 4 hours before overlaying media. Embedded droplets were imaged using LSMPM/SHG imaging over days 0-4 days post-embedding. Invasion events were quantified by counting the number of cells protruding from luminal structures. Laminin staining was performed with 1:100 anti-laminin Ab (ThermoFisher) and 1:200 Alexa-fluor secondary antibody as described in the “Staining and imaging of archival tissues” section. Vehicle and FAK inhibitor treated droplets embedded in collagen gels were stained to assess cleaved caspase-3 and phospho-FAK tyrosine 925 by fixing microtissue-embedded matrices with 0.04% paraformaldehyde for 30 minutes, blocking with 10% goat serum in 0.3% Triton-X

for 4 hours, and incubating with primary anti-CC3 (1:100*, CST) or primary anti-pFAK antibody (1:50*, Santa Cruz) at 4° overnight. Gels were washed for at least 2 hours before adding Hoescht (1:10000*) and Alexa-conjugated secondary antibody at 1:200* for 2 hours. Gels again washed for >1 hour before imaging.

*Note: Due to gel volume (~475uL), a 100uL antibody solution contained antibody to be diluted at a final concentration in 575uL total. All steps require higher volumes, incubations, and wash steps given the nature of collagen gels and the time needed to perfuse 3D samples.

**Statistical analysis**

Multiple groups were compared by ANOVA, followed by the Tukey posthoc analysis, or the non-parametric Kruskal-Wallis test with Dunn's post-hoc testing, as dictated by the size and distribution of the data. Similarly, 2-way ANOVA with Sidak's multiple comparison test was used to compare multiple groups across different conditions. The non-parametric Mann Whitney test or Student's t test was employed for testing null hypotheses between two groups. Number of data points for each experiment, the specific statistical tests, and significance levels (p-value <0.05 was considered significant) are noted in the figure text.

## Results

**Characterizing collagen deposition and architecture in PDA.** To characterize the deposition and architecture of fibrillar collagen with disease progression, we utilized SHG imaging for label-free detection of collagen from live and archival murine and human tissue samples (**Supplemental Figure S3.1**). Multiple ~1mm$^{2,}$

patient samples from a tissue microarray (complete with tumor staging and grading information) were imaged using LSMPM/SHG to assess both fibrillar collagen and endogenous autofluorescence of surrounding tissue, allowing us to map the localization of fibers with respect to tissue architecture. In normal pancreata, little collagen was observed, largely concentrated around the few ducts interspersed in tissue otherwise dominated by acinar cells (**Supplemental Figure S3.1A, E**; note no to low collagen surrounds acinar cells (see magnified region #) in contrast to robust collagen surrounding ductal structures (see magnified region ##)). Notably, cancer-adjacent normal (CAN) regions showed elevated levels of collagen around ductal structures and in some regions between acinar clusters (**Supplemental Figure S3.1B, E**; note acinar regions can possess both collagen (main image) or no collagen regions (see magnified region #)), suggesting regional activation of a fibroinflammatory stromal response in CAN tissue, consistent with the intimate link between fibroblast activity and collagen deposition in PDA development [169, 170]. This may contribute to epithelial dysfunction in adjacent regions (e.g. acinar dropout, ductal hyperplasia, or ADM) and/or prime adjacent regions for invasion. Moreover, consistent with the desmoplastic response associated with PDA, as expected, robust fibrous collagen was ubiquitous in the periductal areas around PanIN lesions, (**Supplemental Figure S3.1C, E**). Elevated collagen remained pervasive throughout disease progression to PDA (**Supplemental Figure S3.1D, E**).

To complement analyses from human patient samples, we turned to *KPCT/G* mice and performed similar analyses of the localization and distribution of collagen

(**Supplemental Figure S3.1F-J**). Consistent with the human data, normal murine tissues possess minimal stromal collagen while CAN regions possess elevated collagen around ducts (**Supplemental Figure S3.1G, J**). Likewise, histologically "pre-invasive" PanIN regions exhibited robust periductal collagen deposition around majority (>95%) of ductal structures (**Supplemental Figure S3.1H, J**). Taken together, data from human and murine samples demonstrate biased collagen localization around ductal structures in normal pancreata, elevated collagen levels in adjacent normal regions, striking collagen surrounding early PanIN lesions, and robust accumulation in PDA.

Since elevated collagen levels in breast carcinomas are organized into specific architectures like TACS-3 which guide local invasion ([107, 113, 162]; **Figure 1.7**), and both TACS-3 architectures [27, 108, 153] and early invasion [135] have been observed in PDA, we hypothesized these architectures may also be prevalent in very early (histologically "pre-invasive") pancreatic cancer and play a key role in early invasion. This prompted us to characterize collagen organization in early disease from *KPC* mice. Analysis of collagen architectures in the periductal space demonstrates ducts are TACS-2 positive (**Supplemental Figure S3.1F-I**). Furthermore, analysis of TACS-2-positive ducts (**Figure 3.1**) from early disease in ~1.5 month old mice (preceding frank tumor formation) indicates many of the ducts are also TACS-3 positive (**Figure 3.1A** and **3.1D**), highlighting collagen surrounding PanIN lesions possess the architecture to facilitate invasion of pancreas epithelia [108]. We note both TACS-2 and TACS-3 architectures also

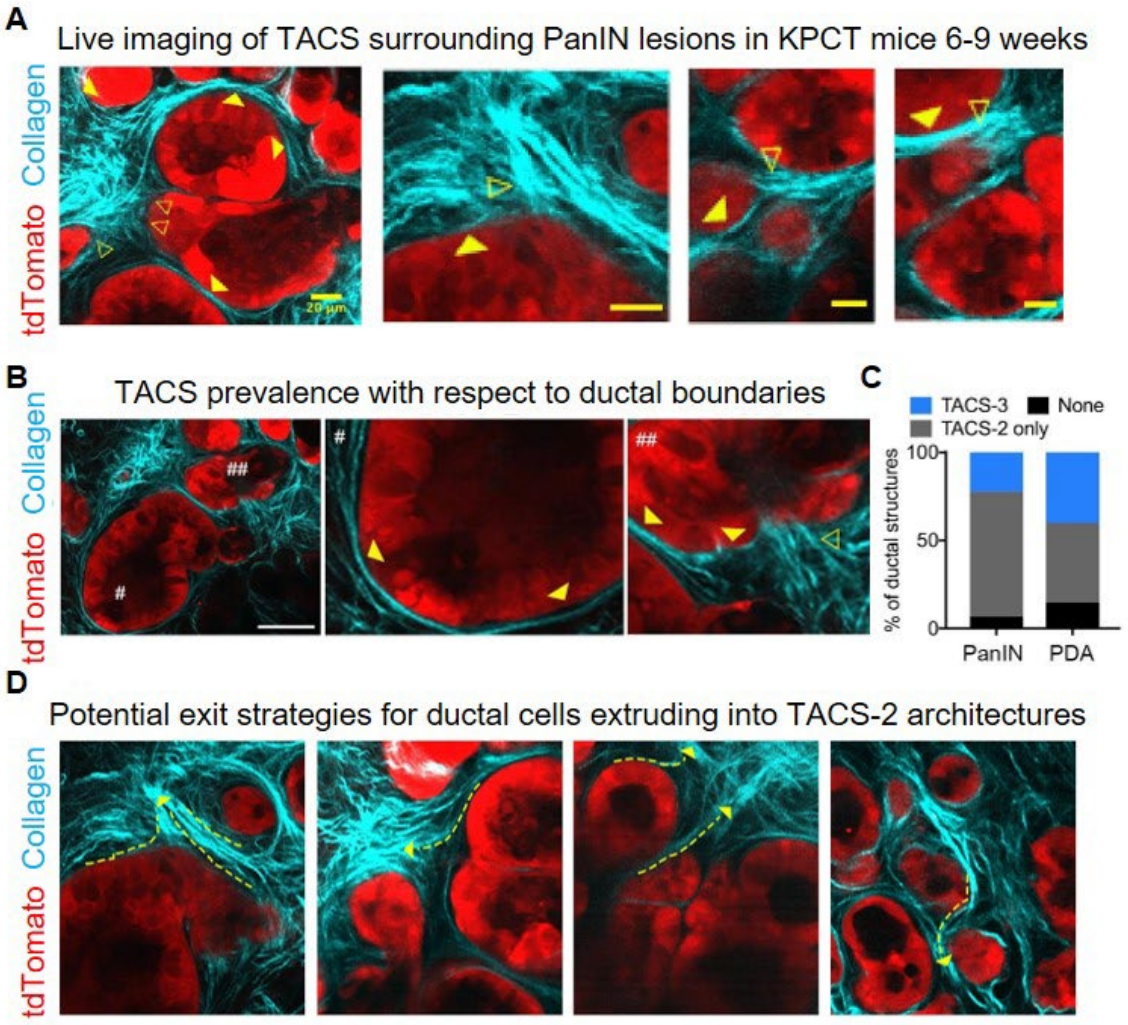


**Figure 3.1 TACS are present around early murine PanIN lesions. A)** Young KPCT mice age 6-9 weeks exhibit TACS-2 (filled arrow head) and TACS-3 architectures (arrow head outline). **B)** TACS-2 (filled arrow head) and TACS-3 (arrow head outline) architectures are prevalent with respect to ductal boundaries and may be present as TACS-2 only (duct #) or as both TACS-2 and TACS-3 (duct ##). **C)** Quantification of TACS-2 and TACS-3 prevalence in murine PanIN and PDA tissue. Majority of ductal structures display TACS, with TACS-2 architectures being more predominant in early disease and TACS-3 architectures gaining prevalence with progression to PDA. **D)** Examples of potential epithelial exit strategies via TACS-2 architectures around ducts (proposed paths depicted with dashed arrows).

exist in well-differentiated PDA regions (**Supplemental Figure S3.1I (#)**), suggesting association of aligned collagen and ductal structures is retained even

with advanced disease. We note frequency of architectures is not significantly different between early and mature disease (**Figure 3.1C**).

In agreement with murine PDA data, both TACS-2 and -3 are found surrounding ductal structures in human pancreatic cancer. TACS-2 is again robustly observed around the vast majority of ductal structures in early and well-differentiated PDA regions (**Supplemental Figure S3.1C, D**). Frequently, TACS-3 is observed locally, often associated with invaginations and regions of irregular ductal boundaries (**Supplemental Figure S3.1K-M**). Moreover, similar to findings in *KPC* mice, quantitative analysis of fiber orientations using a Curvelet Transform of the SHG signal demonstrates TACS-2 or TACS-3 periductal collagen organization (**Supplemental Figure S3.1L**). Notably, in human samples with Stage-I to Stage-IV disease, the presence of TACS architectures was not limited to a particular disease stage, with no significant association between Stage and either the presence of TACS, or TACS type. (**Supplemental Figure S3.1M**). A substantial proportion (~40%) of ductal structures in Stage-I patients already present with TACS-3 (**Supplemental Figure S3.1K**), demonstrating invasion-conducive TACS are present at early stages and remain prevalent through advanced PDA. Early emergence of TACS in both human and mouse samples thus motivated us to further evaluate the influence of collagen alignment on early dissemination of pancreatic carcinoma cells.

**Single cell dissemination along local periductal collagen architectures.** Rhim and colleagues [135] demonstrated invasive dissemination begins prior to

detection of histologically malignant disease and frank tumor formation, resulting in single cells in the tumor stroma and DCCs in the blood of 8-week old *KPC* mice [135]. This is strikingly consistent with our observed timeline of collagen deposition and establishment of TACS architectures, leading us to investigate whether these collagen patterns enable early dissemination. Basal extrusion has been described in normal [171] as well as malignant [172, 173] ductal development and maintenance, and should conceptually precede stromal dissemination from preinvasive lesions. Therefore, we performed combined LSMPM/SHG imaging over multiple regions in several pancreatic tumor sections from *KPCT* and *KPCG* mice. Using ZsGreen1 or tdTomato to identify carcinoma cells (from *KPCG* and *KPCT* mice, respectively), we identified varying stages of extrusion associated with distinct collagen patterns. Partially disseminated cells were found extensively around ductal structures in PanIN lesions and well-differentiated PDA and were, perhaps surprisingly, associated with both TACS-2-like structures and TACS-3 (**Supplemental Figure 3.2A, B**). Strikingly, these partially disseminated cells at the ductal boundary, while still attached to the main duct, were aligned in the direction of local collagen organization (**Figure 3.2A, 3.2B, and 3.2D**) indicating contact guidance [108, 174]. For PanIN lesions, ~53% of the partially extruded cells on average were parallel (TACS-2) and about 28% perpendicular to the ductal boundary (TACS-3) (**Supplemental Figure S3.2C**).

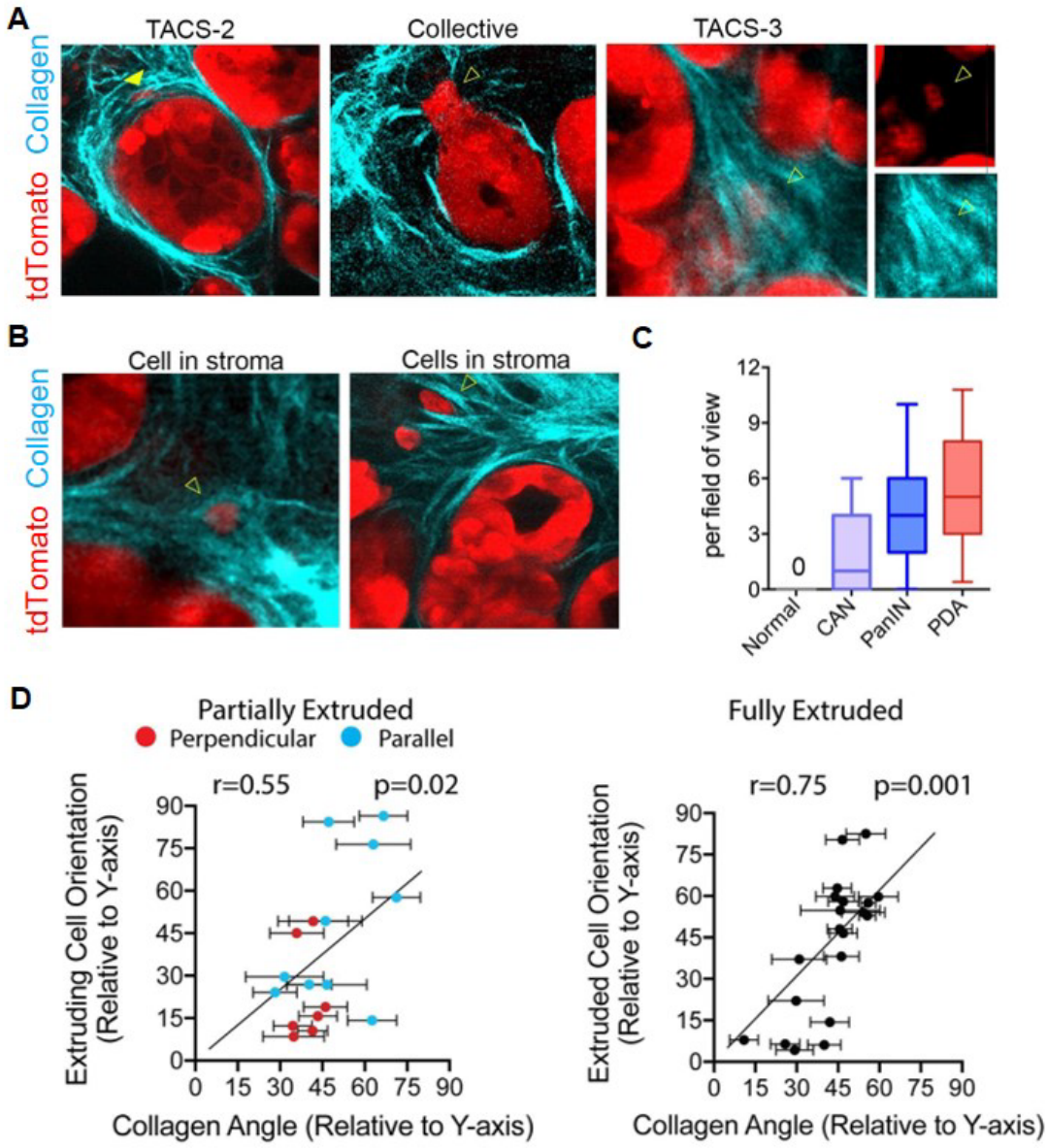


**Figure 3.2 TACS facilitate extrusion around early murine PanIN lesions.** **A)** Examples of ductal epithelial cells invading into TACS in young KPCT mice age 6-9 weeks. Single extruded cells (filled arrow head) and collective group extrusion events (arrow head outline) can be observed into TACS-2 architectures (middle) and TACS-3 (right). **B)** Single, fully extruded cells can be observed interacting with collagen fibers in the stroma of young KPCT mice. **C)** Quantification of the number of extrusion evens per field of view in normal, cancer adjacent normal, PanIN and PDA, and shows an increase in extrusion with disease stage. **D)** Quantification of extrusion into TACS showing both partially (left) and fully extruded cells orient themselves consistent with collagen angle.

This demonstrates pancreatic epithelia can enter less constrained TACS-2 architectures observed in PDA, and likely undergo directed motility along the collagen around the ductal structure (in contrast with motility associated with the more tight TACS-2 in breast tissue). In contrast to early disease, partially extruded cells were equally likely to be on TACS-2 or TACS-3 architectures in advanced well-differentiated disease (**Supplemental Figure 3.2D**). This difference is likely the result of the increased frequency of TACS-3$^{+}$ ductal structures in more advanced disease as compared to early PanIN lesions (**Figure 3.1C** and **Supplemental Figure S3.1M).** Importantly, similar partial dissemination associated with periductal collagen was observed in well-differentiated ductal regions of human PDA sections based on assessment of pan-cytokeratin+ cells (**Supplemental Figure S3.2E**). These partially delaminated cells likely represent the early stages of extrusion and their alignment with the surrounding collagen is indicative of the close association between the ductal epithelium and periductal collagen during this process. In addition to partial extrusion, we observed an abundance of fully extruded, invasive cells in the periductal space of PanIN lesions and well-differentiated PDA (**Supplemental Figure S3.2F-H**, **Figure 3.2C** and **3.2D**), consistent with previous reports identifying carcinoma cells in the stroma during early disease [135, 175]. To confirm these findings, we imaged live pancreata from *KPCT* mice with LSMPM/SHG microscopy, which allows for z-stack imaging around dispersed cells to confirm the presence of extruded invasive cells (**Figure 3.2A** and **3.2B**).

Consistent with findings in fixed samples, extruded cells were identified with the majority aligned along TACS (**Figure 3.2A** and **3.2B**). Moreover, TACS-2 regions often connected to an adjacent TACS-3 region, providing a conduit to migrate away from the duct, while following the ECM alignment into the stroma (**Figure 3.1D**). Phenotypic analysis of fully extruded single cells in the periductal space—which make up the majority of extrusion events recorded (**Supplemental Figure S3.2H**)—highlighted two distinct morphologies of invading cells. While the majority (~70%) of the cells are elongated and aligned to the orientation of the periductal collagen (**Supplemental Figure S3.2F**), a distinct proportion of more rounded, single cells also exist along collagen in the stroma (**Supplemental Figure S3.2G**). This is further supported by morphological analysis revealing a large range of aspect ratios (AR) and small cell diameters for fully extruded cells (**Supplemental Figure S3.2I, J**). A significant proportion of cells (~30%) displayed an aspect ratio of less than 1.5, likely representative of a distinct population from the elongated, more phenotypically mesenchymal-like single cells. These observations are consistent with previous findings that phenotypically heterogenous cancer cells with significant plasticity exist in breast carcinoma and PDA and undergo 3D migration by contact guidance [108, 135, 163, 176, 177]. Moreover, these two phenotypes can be observed in fully extruded cells in human patient samples, often existing in the same local region (**Supplemental Figure S3.2K**), suggesting phenotypically distinct contact-guided subpopulations are capable of invasion leading to metastasis in PDA. However, more extensive genetic and functional

profiling would be necessary to determine the significance of and extent to which these two populations are distinct.

In contrast to normal tissues where we did not observe any basal extrusions in either murine or human pancreata (**Figure 3.2C**), extrusion events were present in CAN regions adjacent to disease in murine and human tissue, albeit at a lower frequency than observed with PanINs (**Supplemental Figure S3.2L, M; Figure 3.2C**). It is striking that even in CAN regions, which have significantly lower collagen content than PanIN lesions, disseminated cells were almost always associated with regions of fibrous collagen (**Supplemental Figure S3.2L, M**). This suggests that the fibro-inflammatory response occurring in activated tissue adjacent to disease may aid the extrusion process by priming adjacent stroma to support disease spread. Therefore, we explored TACS architectures in pancreatitis. Importantly, pancreatitis can display a PDA-like desmoplastic response with an accumulation of straight and thick collagen fibers [153]. Analysis of samples from 6 human patients with chronic pancreatitis revealed an abundance of TACS-2 and TACS-3 associated with ductal structures (analysis from 8-33 fields of view from two biopsies per patient; **Supplemental Figure S3.2N, O**). Consistent with our findings in pancreas cancer, approximately 32-93% of ductal structures were TACS-2 positive and ~28-62% were positive for both TACS-2 and TACS-3 (similar to pancreatic cancer, ducts that are TACS-3+ are also TACS-2+ in different regions of the duct; **Supplemental Figure S3.2O**). Remarkably, every pancreatitis patient sample presented with ducts that were TACS-3 positive.

Extrusion events were observed in CP, although infrequently relative to findings in PanIN lesions and well-differentiated PDA, as expected. These data indicate that fibroinflammatory diseases that may precede PDA, such as pancreatitis, can result in stromal ECM architectures primed to facilitate disease spread from the earliest onset of disease. Interestingly, in **Supplemental Figure S3.3**, both TACS-2 (arrow head) and TACS-3 (arrow head outline) could be found near acinar clusters (a) in an otherwise normal region in young *KPCT* mice, although the frequency and functionality of this was not investigated further.

**Dynamics of single cell extrusion and contact guided migration in stromal collagen.** Given the role periductal collagen plays in facilitating basal cellular extrusion, we speculated TACS located distal to ductal structures also influences cancer cell dissemination through the stroma. Indeed, fully extruded cells in both murine and human samples were found to be colocalized with aligned collagen (**Supplemental Figure S3.2F-H, S3.2K; Figure 3.2A, 3.2B, 3.2D**), suggesting that TACS not only aid in the dispersal of these cells from the epithelium during basal extrusions, but also guide the extruded cells as they invade through the stroma. Indeed, we have previously demonstrated that carcinoma cells, including those of the pancreas, are strongly directed to migrate along aligned ECM via contact guidance with minimal motility lateral to ECM alignment [108, 162, 163, 174, 178].

In line with our conclusions that early extrusion events leading to invasive cells in the stroma contribute to early metastatic spread we note that reports indicate that PDA carcinoma cells can be present in circulation during histologically pre-invasive

disease [135] and that in other desmoplastic systems such as in breast carcinoma, pioneer metastatic cells utilize bundles of aligned collagen as highways to escape towards blood vessels [106], often further guided by macrophages [179] in the tumor stroma. Therefore, we visualized the localization of TACS and extruded cells with respect to $CD31^+$ blood vessels in archival tissue samples. Carcinoma cells in the stroma were observed in close association with blood vessels in the stroma (not quantified, **Figure 3.3; Supplemental Figure S3.2**).

In *KPC* mice, extruded single cells were present on aligned collagen fibers leading to open blood vessels (which are less frequent relative to the larger fraction of collapsed vessels in PDA, [13, 27, 180]) in both PanIN lesions as well as more mature well-differentiated disease (**Figure 3.3A; Supplemental Figure S3.2A**). Importantly, we confirmed these findings in human tissue samples using pan-cytokeratin to mark cancer cells (**Figure 3.3B**). Again, aligned collagen fiber tracks, punctuated with single or streams of multiple carcinoma cells, were observed leading to $CD31^+$ blood vessels (**Figure 3.3B; Supplemental Figure 3.2B**). It is important to note that while a large percentage (~75%) of blood vessels in mature PDA are collapsed and non-perfused [27, 180], those in the early stages of the disease have a much higher likelihood of being open [13] and thereby likely provide a more clear passage for extruding cells to escape and enter the bloodstream.

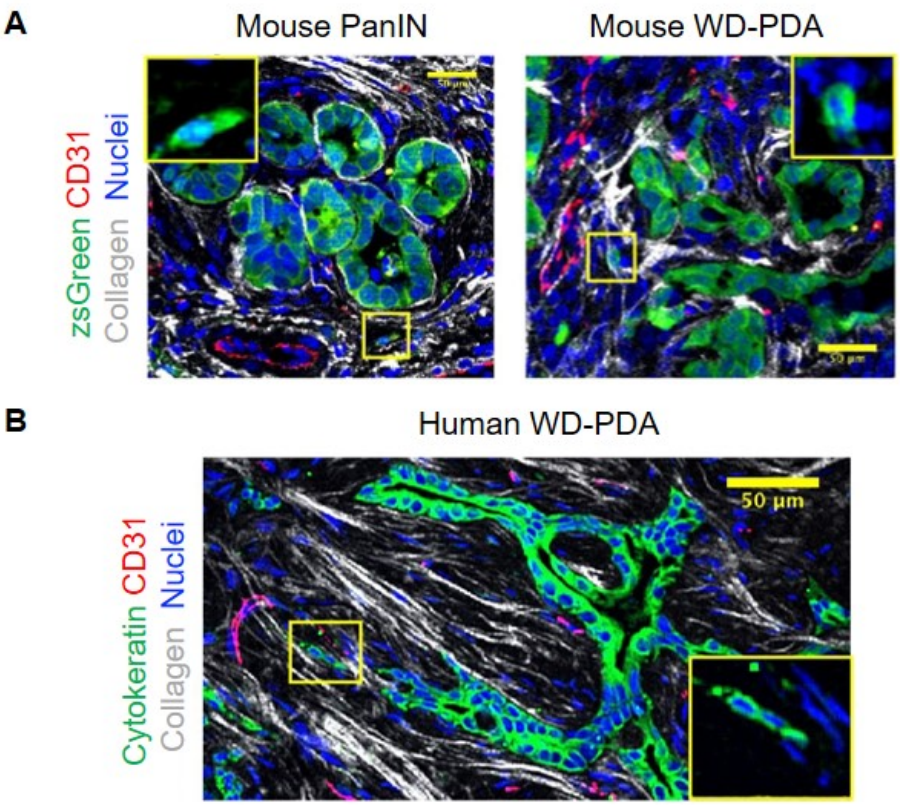


**Figure 3.3 Extruded carcinoma cells are observed migrating in collagen tracts oriented toward CD31+ blood vessels. A)** KPCG epithelial cells extruded into collagen can be seen migrating along collagen fibers oriented toward CD31+ vasculature in both early disease (PanIN) and late stage well-differentiated PDA. **B)** Human patient biopsies also exhibit extruded cells migrating in stromal collagen toward vasculature.

Taken together, these data strongly suggest early extrusion and invasion along organized collagen fibers plays a direct role in early and extensive metastasis observed in PDA. However, while the intra- and intercellular dynamics during basal cell extrusion from ducts has been explored [172, 173, 181], how the ECM affects this process has not, prompting us to delve into biophysical and molecular mechanisms.

**FAK-dependent mechanotransduction enables collagen-guided cell extrusion and invasion *in vitro*.** The data presented thus far point to periductal collagen architectures as an external driver of tumor cell dissemination. However, we suspect cell-intrinsic processes are also a critical player in directly epithelial cell dissemination from ductal structures in PDA. This, along with our understanding of single cell contact guidance [108], prompted us to explore potential molecular mechanisms underlying epithelial cell response to TACS via a multicellular approach. A cell at the interface of ductal epithelia and stromal ECM is presented with multiple, counteracting cues to either remain in its cohesive state in the epithelium or break away from its native structure and follow ECM architecture. To dissect the process of invasion and dissemination from ductal-like structures, we utilized novel microfluidic technology to generate primary PDA cell-derived organoids. This high throughput system allows us to selectively observe tumor cell behavior with retention of key cellular and ECM components found in pancreas pathology, but allows for real time interpretation of bulk and single tumor cell behavior in response to ECM, and biochemical perturbation of these processes. Organoids were generated following the schematic outlined in **Figure 3.4**. As described in the "Experimental Procedures" section of this Chapter, Matrigel droplets were generated via an oil-aqueous interface using a microfluidic flow device, coated with primary *KPCT* or *KPCG* cells, and seeded in individual agarose microwells for isolated culture. Note cells remain organized in a ring around Matrigel droplets with exceedingly rare invasion into the droplet center. These

droplets are closely mimetic of ductal structures in PanIN lesions and PDA, and resemble ductal cross-sections, as evidenced by 3D imaging (**Figure 3.4B**).

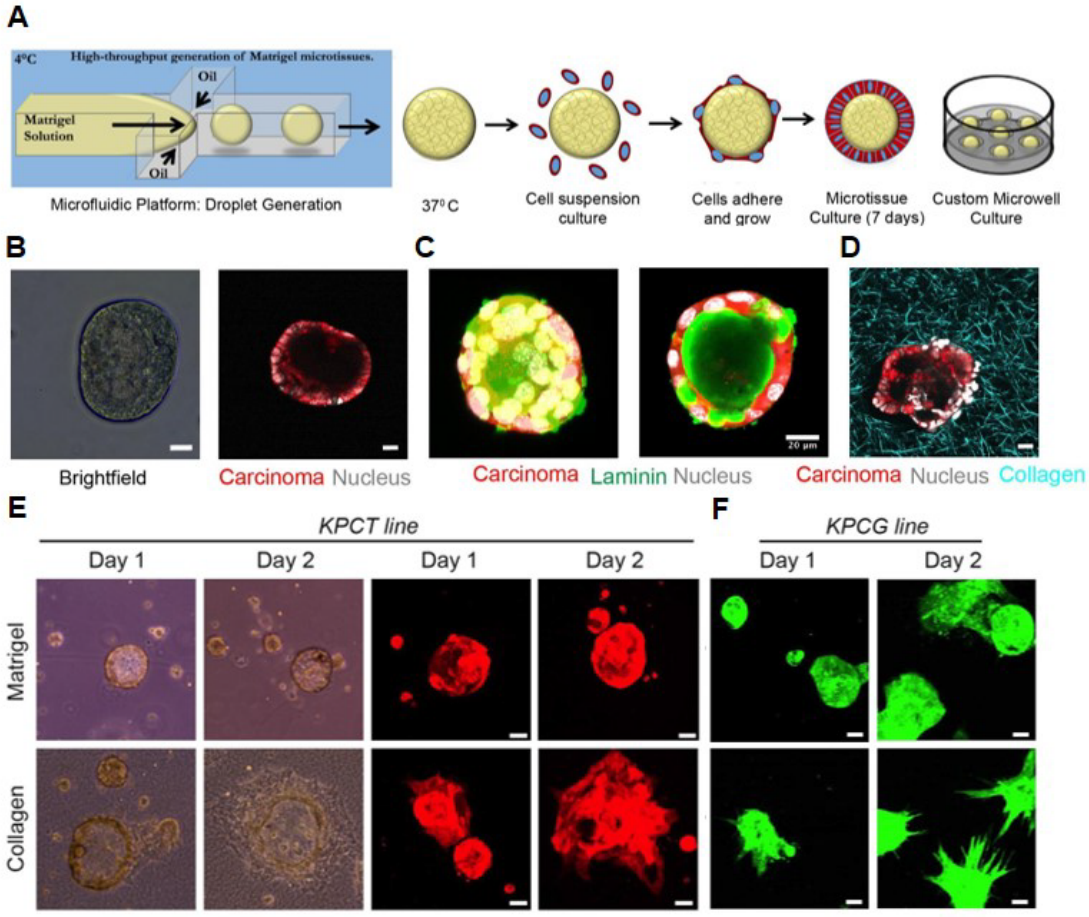


**Figure 3.4 3D pancreatic microtissue fabrication and characterization. A)** Schematic of microtissue fabrication—droplets are generated via microfluidic devices interfacing oil with Matrigel which can then be coated with primary pancreas cancer cells to generate ductal structures reminiscent of those found in PDA. Characterization of ductal structures with brightfield and multiphoton microscopy to assess morphology **(B)**, laminin distribution **(C)**, nuclear organization, and phenotype in 3D collagen gels **(D)**. **E)** *KPCT* microtissues exhibit robust epithelial, noninvasive phenotypes in 3D basement membrane-like environments compared to in 3D collagen environments, suggesting collagen is necessary for invasion *in vitro*. **F)** Microtissues formed using a more invasive *KPCG*-derived primary line also exhibits a robustly invasive phenotype in collagen matrices compared to a rounded, less invasive morphology in Matrigel.

These microtissues were cultured in individual agarose microwells to allow them to evolve into robust epithelial organoids over several days after which they still retain basement membrane (**Figure 3.4C**, Laminin) and luminal structure. Organoids were subsequently embedded in collagen matrices where the interaction of individual organoids with the surrounding ECM could be studied (**Figure 3.4D**, Collagen). Interestingly, in characterizing microtissues, we noted primary PDA *KPCG* or *KPCT* organoids display strikingly different invasion patterns in 3D collagen matrices, which possess fibrous collagen architectures, compared to in 3D Matrigel, which is more representative of basement membrane. Droplets in Matrigel displayed limited protrusion and invasion into the matrix in both a less (*KPCT*) and more (KPCG) invasive primary line, and moreover largely retained their ductal morphology (**Figure 3.4E** and **3.4F**). In contrast, droplets embedded in collagen in **Figure 3.4E** and **3.4F** exhibit extrusions highly reminiscent of ductal outgrowths and collective and single cell dissemination associated with TACS-3 observed in murine and human PDA samples (**Supplemental Figure S3.1** and **S3.2; Figure 3.2A** and **3.2B**). Moreover, within 24 hours of embedding, both TACS-2 and TACS-3 architectures could be identified surrounding organoids, depicted in **Figure 3.5A.** These data indicate that our novel *in vitro* system can recapitulate key features of the extrusion to invasion process and provides a high throughput controllable platform to investigate the molecular mechanisms guiding epithelial extrusion in PDA.

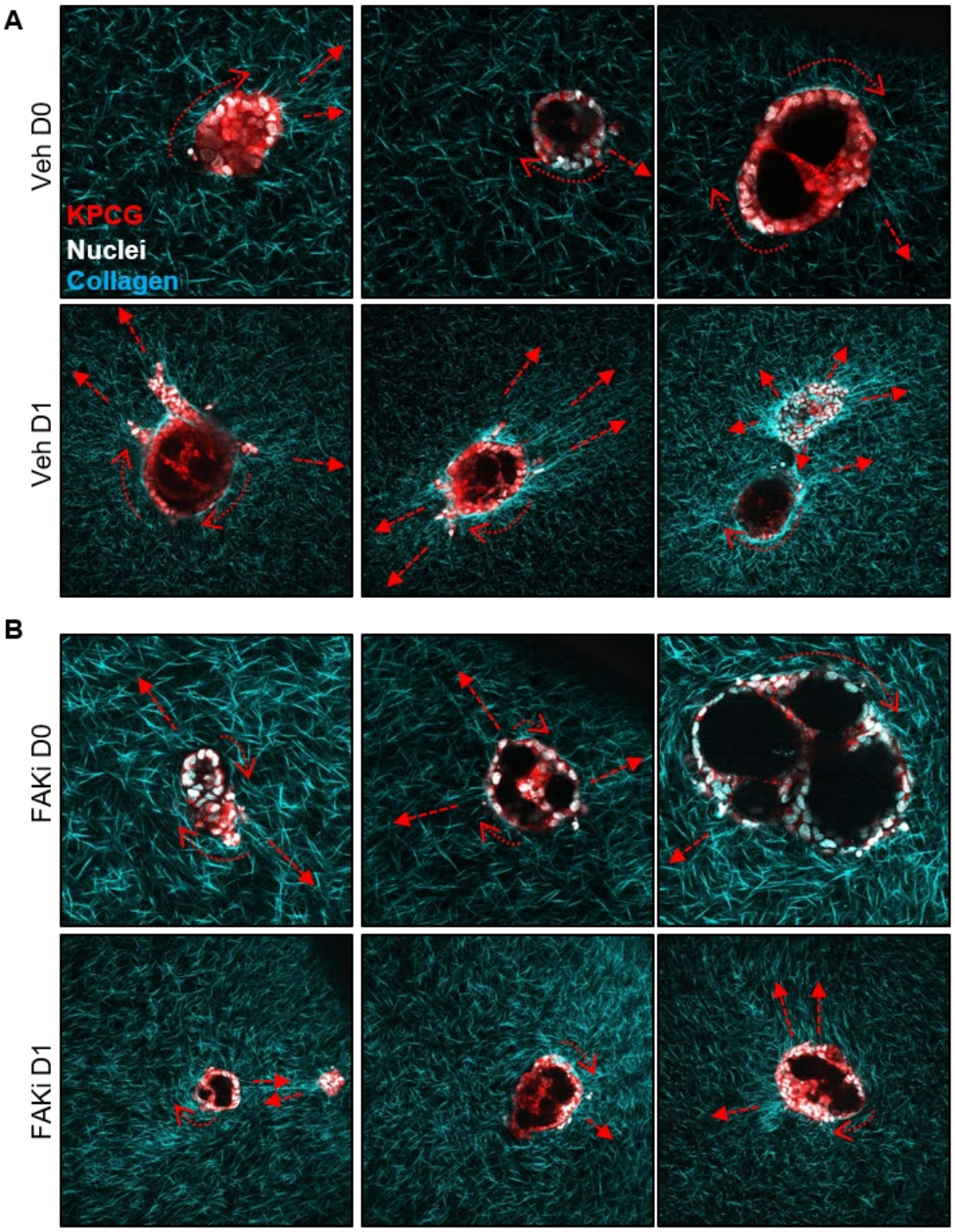


**Figure 3.5 Microtissues develop TACS *in vitro* within 24 hours of seeding.** LSMPM/SHG images of primary KPCG tumor cell droplets (pseudocolored red) seeded in collagen gels at days 0 and 1 with vehicle treatment develop collagen architectures TACS2 (curved, dotted arrows) and TACS3 (straight, dashed arrows) mimicking stromal TACS found *in vivo*. Visualization of TACS in the presence of DMSO vehicle control **(A)** and FAK inhibitor VS-4718 **(B).**

Given the apparent inability of cells to invade into Matrigel, yet clearly robust invade into collagen (**Figure 3.4E** and **3.4F**), we sought to use this microtissue system to explore potential mechanisms underpinning this modulation of extrusion. The intercellular force generation machinery and the molecular linkages between focal adhesions, myosin and F-actin, which are key mediators of contact guidance [108, 182, 183], are likely to be important for extrusion into collagen matrices. Consistent with this hypothesis, increased matrix density and stiffness promote ECM alignment and mammary cell invasion into 3D matrices through a Focal Adhesion Kinase (FAK)-ERK signaling axis, where inhibition of FAK function by expression of dominant-negative FRNK reverts invasive phenotype [103]. Moreover, expression of both total and phosphorylated FAK in PDA carcinoma cells is well established in the literature [31, 157, 184, 185] and a recent study by DeNardo and colleagues demonstrated targeting FAK in PDA not only augments immunotherapy efficacy but also decreases the number of single PDA cells observed in the periductal space [31]. This evidence brought us to explore whether FAK signaling promotes cell extrusion and subsequent invasion into aligned ECM. To test the impact of FAK inhibition *in vitro*, we turned to our embedded microtissue system. Consistent with our hypothesis, FAKi dramatically reduced cell extrusion, to the extent that very little single cell extrusion was observed at Day 1 in the FAKi group versus robust extrusion in the vehicle control group (**Figure 3.5B, 3.6B and 3.6C**). This behavior was maintained through day 3, where extrusion and invasion were profoundly limited by FAK inhibition compared to controls, which exhibit complete dissemination by day 3 (**Figure 3.6A**).

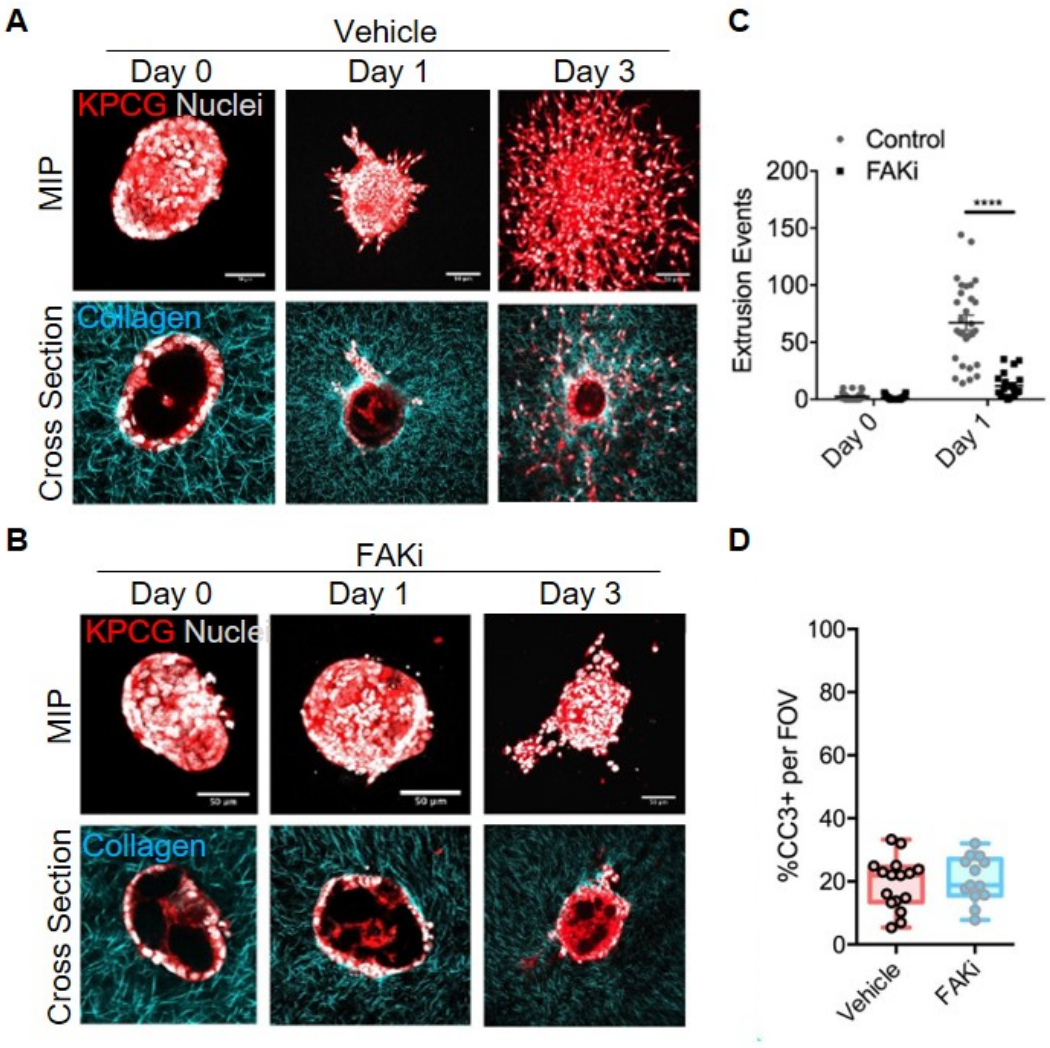


**Figure 3.6 FAK inhibition abrogates collagen fiber guided PDA cell extrusion *in vitro.*** Comparison of primary tumor cell invasion at days 0, 1, and 3 with vehicle treatment **(A)** and with FAK inhibitor VS-4718 **(B)**. Primary KPCG tumor cell microtissues reminiscent of pancreas ducts (pseudocolored red) embedded in collagen gels and imaged using LSMPM/SHG to assess behavior. Max intensity projections (top rows of **A, B**) and cross-sectional images (bottom rows of **A, B**) depict vastly attenuated invasion in FAKi treated samples compared to control, quantified in **(C)** (i n=20-30 droplets per condition from n=2 experiments, data are mean +/- SEM; ****p<0.0001 by ordinary 2-way ANOVA and Sidak's multiple comparison test).This decrease in invasion could not be attributed increased cell death with FAK inhibition, assessed via cleaved caspase-3 (CC3) expression **(D),** with no significant differences in apoptosis observed.

However, we note that in pancreatic carcinoma cells lacking $S1P_2$ receptor, FAK has also been suggested to regulate apoptosis associated with basal extrusions in monolayer culture [173]. We therefore evaluated apoptosis levels to determine if our observed decreases in extrusion and invasion under FAKi could be due, either entirely or in part, to apoptosis. In primary, collagen-embedded microtissue cultures treated with FAKi or vehicle control, analysis of cleaved caspase-3 (CC3) revealed no differences in apoptosis (**Figure 3.6D**).

Interestingly, concomitant with the decrease in extrusion, we did not observe a reduction in organized collagen, especially TACS-3-like arrangements which were present around the ductal structures in both control and FAKi groups (**Figure 3.5B** and **3.6B**), suggesting that even in the presence of TACS-3-like architectures, inhibition of FAK profoundly reduces the ability of cells to extrude and then invade along aligned ECM. We do however observe limited collective invasions in the FAKi group at later time points, but with severely impaired single cell invasion (**Figure 3.6B**, Day 3), which is consistent with cell proliferation and general motility-related quasi-ballistic invasion into aligned ECM resulting from cell crowding [168]. Thus, our data suggest FAKi cells still retain limited ability to outgrow from well-defined ductal structures but disrupting the key signaling node of focal adhesion force transmission and contact guidance by targeting FAK renders single cell invasion inefficient.

**FAK inhibition abrogates single cell extrusion and metastasis in PDA.** Previous work demonstrated FAK and pFAK are expressed throughout PanIN lesions, frank PDA, and invasive carcinoma cells in the stroma [31, 157, 184, 185],

consistent with our finding of continuous pFAK expression throughout PanIN lesions (**Figure 3.7**), and FAKi leads to a decrease in the number of invasive PDA cells observed in the periductal space [31].

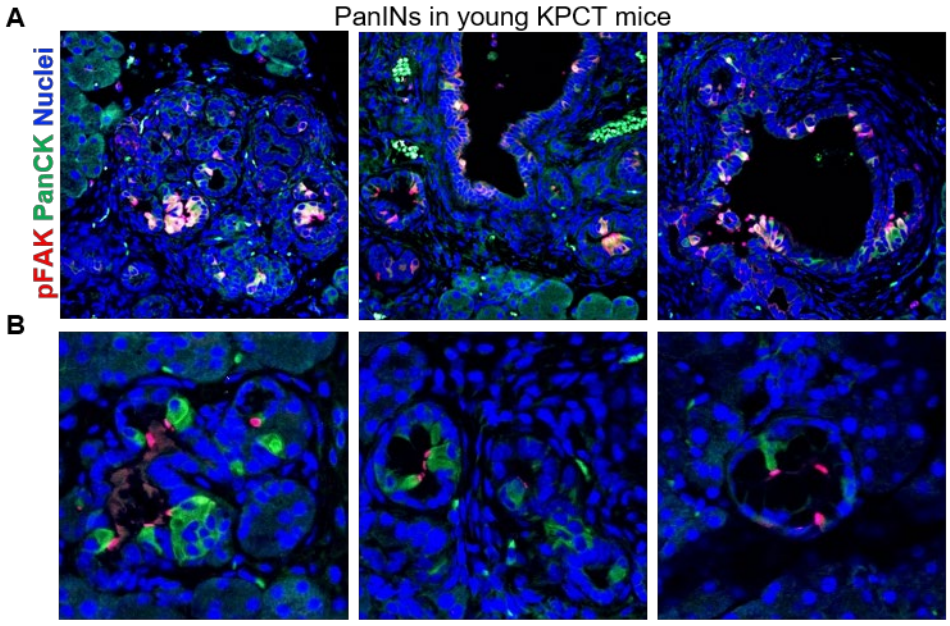


**Figure 3.7 Early PanIN lesions express pFAK Y925. A)** Ductal epithelia in young KPCT mice (6-9 weeks) express phospho-FAK Y925 and epithelial marker pan-Cytokeratin in PanIN lesions. **B)** Magnified images highlighting pFAK Y925 and pan-Cytokeratin patterns in ductal epithelia in otherwise normal pancreas tissue.

We therefore analyzed the PDA FFPE sections from Vehicle vs. FAKi groups described in Chapter 2 and obtained from Jiang et al. to interrogate cell extrusion and invasion in the context of collagen fiber organization to test our hypothesis that FAK influences early dissemination *in vivo*. Consistent with the general abrogation of fibrosis, FAK inhibition led to a decrease in fibrillar collagen in both early (1.5 month group) and end stage *KPC* mice (**Figure 3.8A** and **3.8B**) with a very modest, yet significant, decrease in TACS-2 architectures and a modest, not significant, trend of less TACS-3 architectures (**Figure 3.8C**).

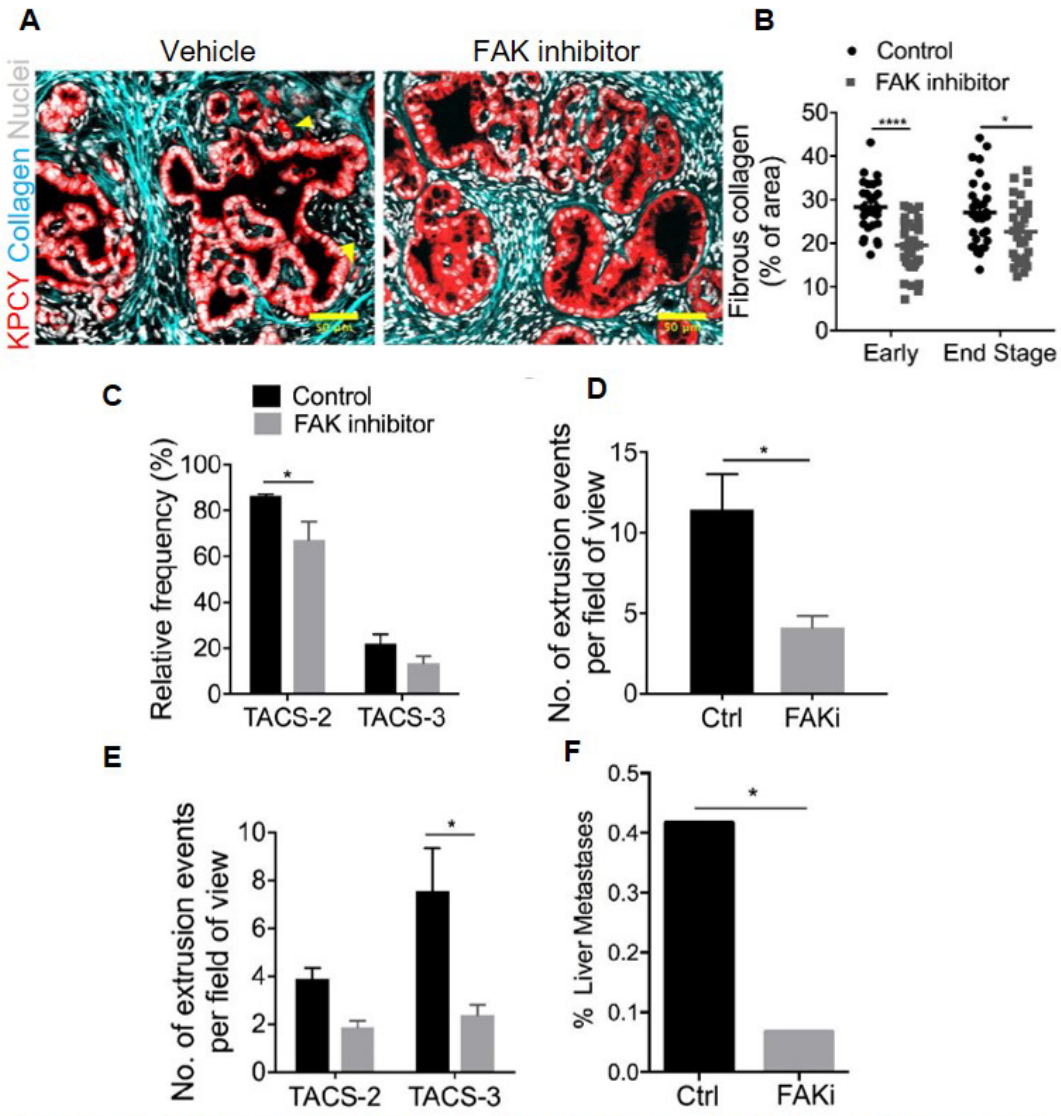


**Figure 3.8 Targeting FAK *in vivo* decreases TACS, extrusion and metastasis. A)** *KPCY* sections (pseudocolored red) from mice treated with vehicle control or FAK inhibitor showing reduced collagen deposition around pronounced ductal boundaries with a decrease in extrusion. Arrow heads indicate single cell extrusion events in the control sample. **B)** Quantification of collagen content in *KPCY* mice shows a reduction in fibrous collagen in both early (1.5 month) and end stage mice treated with VS-4718. Moreover, FAK inhibition reduced TACS-like architectures in *KPCY* mice **(C)**. **D)** Quantification of extrusion events with FAK inhibition compared to mice treated with vehicle control. **E)** Extrusion events for control and FAK inhibited groups quantified as a function of TACS-2 or TACS-3-architectures showing a decrease in extrusion in TACS3 regions. **F)** Frequency of liver metastasis in control and FAKi treated mice showing reduction in metastases with FAK inhibitor treatment (samples from *Jiang et. al)*. ****p<0.0001, *p<0.05 by 2-way ANOVA and Sidak's multiple comparison test for (c, d, f) per group, *p<0.05 for (e) by t-test, *p<0.05 by Fisher's exact test for (g); Scale bars = 50 μm.

Thus, while collagen levels are reduced, likely by attenuation of FAK-dependent mechanotransduction in myofibroblasts that regulates the fibroinflammatory response in PDA [31, 157, 186], TACS architectures are still present around majority of ductal structures (**Figure 3.8B** and **3.8C**). As such, we can evaluate cell-intrinsic FAK signaling in response to in place cell-extrinsic collagen architectures. In agreement with our hypothesis and *in vitro* data, there was a significant decrease in the frequency of single cell extrusions following inhibition of FAK (**Figure 3.8D**). We also observed smoother and more organized ductal morphology in FAKi-treated mice, indicative of a less advanced or more limited progression of disease (**Figure 3.8A**). Interestingly, the number of extrusions associated with both TACS-2 and TACS-3 showed decreasing trends following FAK inhibition. However, the difference was significant and much more pronounced for TACS-3 associated extrusions (**Figure 3.8E**), consistent with our *in vitro* findings and suggestive that TACS-3-mediated extrusions and invasion may be more FAK-dependent. This is critical since collective data suggest that for robust dissemination of extruded cells invading through periductal TACS-2 architectures ultimately rely on TACS-3 architectures to serve as an exit point from the duct-adjacent space and that decreased extrusion and invasion would limit metastatic burden. Indeed, *KPC* mice undergoing FAKi treatment from the same cohort showed decreased metastasis to the liver ([31]; **Figure 3.8F**), consistent with the conclusion that FAK-dependent single cell extrusion and subsequent invasion through the stroma promotes metastasis. Overall, these data implicate FAK as a key mechanotransduction node during the response to established

TACS-3 aligned collagen and the subsequent invasion in PDA leading to enhanced metastatic dissemination. Thus, early dissemination and therefore early metastasis in PDA is driven, at least in part, by both the local organization of periductal collagen and focal adhesion-dependent recognition of these ECM patterns by carcinoma cells.

## Conclusions

This chapter presents advancement in the understanding of how desmoplastic collagen drives dissemination in PDA by considering the epithelial compartment specifically. We utilize LSMPM/SHG to visualize and quantify collagen deposition and architecture across PDA progression and establish critical links between the periductal collagen organization and early invasion in mouse and human PDA. Moreover, we translate the canonical understanding of TACS from their established patterns and role in breast cancer to pancreatic disease (**Figure 3.9**). Both TACS-2 and TACS-3 manifest with largely straighten collagen fibers in PDA, albeit often with a looser organization for TACS-2 than observed in mammary carcinomas. As we observe TACS-2 architecture connecting to TACS-3 regions, we speculate that carcinoma cells extruded into TACS-2 regions migrate along collagen around ducts until encountering a TACS-3 exit point or do not easily leave the periductual space since migration perpendicular to dense collagen is profoundly less efficient and in many cases rare [108, 156, 162, 163, 168].

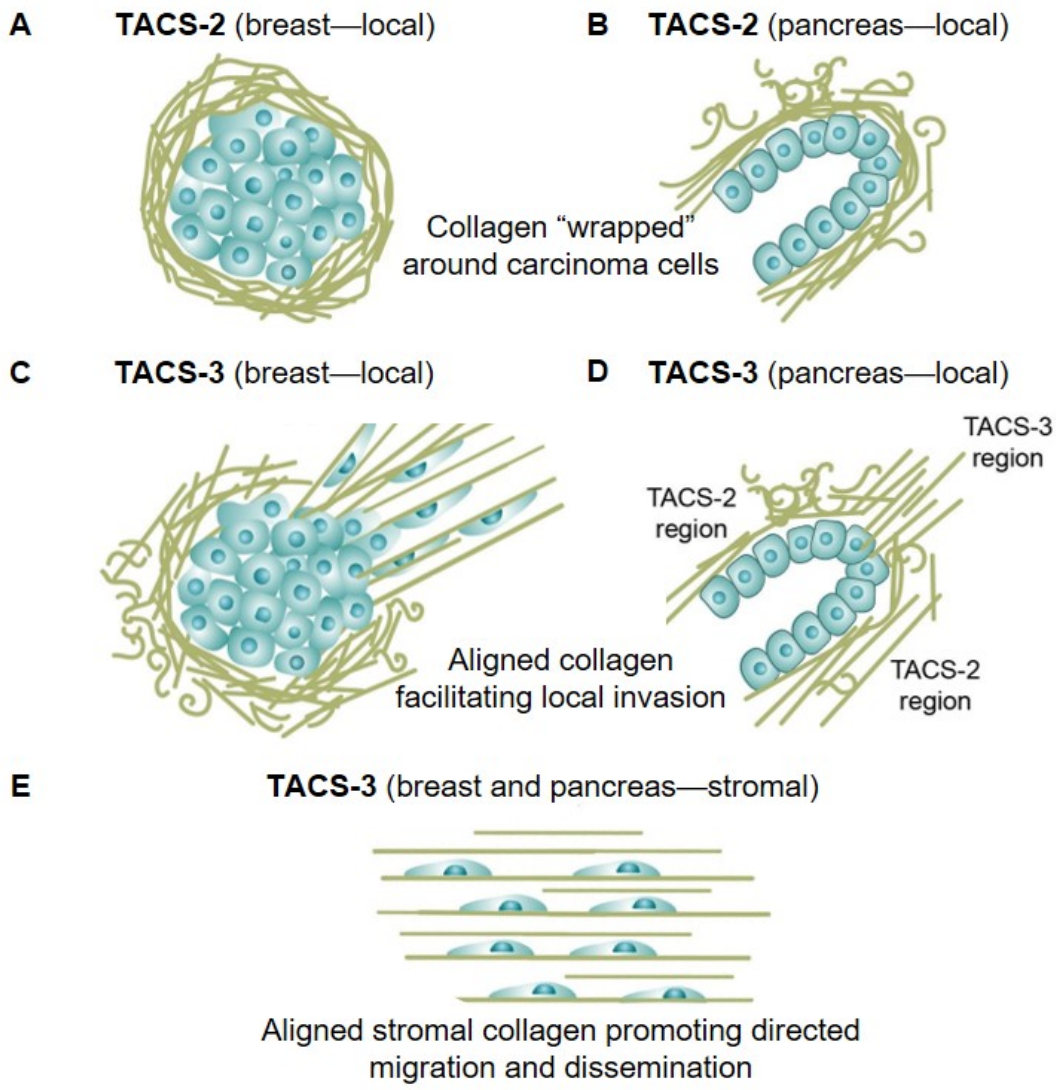


**Figure 3.9 (Re)defining Tumor-Associated Collagen Signatures.** Schematics of collagen signatures in the breast, and our findings of how these signatures translate to the pancreas. **A)** Classical TACS-2 signatures originally identified in the breast, oriented parallel/circumferentially around tumor cells. **B)** Translation of TACS-2 signatures to the pancreas, oriented parallel/circumferentially around ductal structures. **C)** Classical TACS-3 signatures originally identified in the breast, oriented perpendicular to carcinoma cells and facilitating local invasion into collagen tracts. **D)** Translation of TACS-3 signatures to the pancreas, oriented perpendicular to ductal structures and facilitating local invasion into collagen tracts. **E)** TACS-3 signatures in the stroma in both breast and pancreas tumors, oriented parallel to one another and promoting directed cell migration.

Furthermore, we observed cell extrusions in cancer-adjacent normal sections showing signs of inflammation and collagen deposition, supporting the notion from Chapter 2 that normal—or in this case, normal adjacent—tissue is pre-primed to support disease infiltration and the progression to metastasis. Importantly, our findings suggest this is likely the case for fibrotic diseases like pancreatitis. Notably, we found ample evidence of fibrotic collagen in the form of TACS-2 and TACS-3 in human pancreatitis, but with minimal extrusion (**Supplemental Figure 3.2**), suggesting that TACS alone may be insufficient sufficient for robust cell extrusion in untransformed cells. Therefore, the risk factor posed by chronic pancreatitis for malignant transformation may at least, in part, be attributed to the generation of the "ECM phenotype" as a priming microenvironment for PDA to arise and disseminate from early stages. Thus therapeutic strategies to resolve fibroinflammation, such as stroma-targeting antifibrotic therapies [13, 187], may be beneficial in disrupting ECM architectures conducive to disease spread, thus impeding development of early DCCs in patients who later develop PDA.

# 4. MACROPHAGES PHYSICALLY INTERACT WITH DUCTAL EPITHELIA *IN VITRO* AND *IN VIVO*

## Summary

In this chapter, we explore the interplay between data presented in Chapters 2 and 3. How do macrophages, tumor cells, and collagen interact to facilitate tumor cell invasion, adhesion, and migration within collagen matrices and fibrotic disease? We further establish a set of procedures to perform live-imaging of macrophage-epithelial-collagen interactions both *ex vivo* in live slice cultures and *in vitro* in embedded microtissue cocultures.

## Introduction

While the role of macrophages in metastasis has long been appreciated, a new mechanism is emerging: physical contact. Evidence from the Condeelis group demonstrated macrophages enhanced tumor cell invasion upon physical contact, causing tumor cells to develop invasive protrusions, called “invadapodia,” capable of degrading the ECM. The formation of these invasive “feet” was promoted via induction of RhoA activity and subsequent changes in the actin cytoskeleton. This observation was dependent on physical contact and was observed in both mouse orthotopic and human tumor samples [188].

Interestingly, several studies have observed the presence of circulating hybrid cells (CHCs) in mouse autochthonous tumor models, which appear to be the result of fusion between epithelial and immune cells and are distinct from circulating cancer

cells in proximity to immune cells. Studies have confirmed these hybrid cells in patient blood samples in numerous cancers including those of the pancreas [53, 83-85]. CHCs display characteristics of both epithelial cancer cells and macrophages and are speculated to be the product of physical cell-cell fusion between the two cell types resulting in hybrid cells which are bestowed with both the enhanced migratory capacity of epithelial carcinoma cells as well as the immune privilege experienced by macrophages. Thus, CHCs have higher metastatic potential and "stealth" compared to epithelial CTCs [53, 82]. CHCs have been observed in PDA in both human and mouse blood samples, and have been speculated to form "stealth" metastases which form before and/or in parallel with respect to primary pancreas tumors [53]; it is likely CHCs contribute to the early spreading and metastasis which gives PDA its gruesome outcome. Given this literature, we sought to better characterize interactions between carcinoma cells and macrophages in real time to observe how macrophages influence carcinoma cell invasion, and how they may be physically interacting with tumor cells in 3D systems. Moreover, exploration of how macrophages may regulate epithelial cell invasion in early disease and in pancreatitis is severely lacking.

## Experimental Procedures

### Microtissue coculture system

*KPCG/T* microtissues were generate and embedded in 3mg/mL collagen matrices consistent with protocols in Chapter 3. Primary macrophages isolated and differentiated following procedures outlined in Chapter 2 were stained with

CellTracker™ Green CMFDA dye consistent with protocol in Chapter 2 for CellTracker™ Red CMTPX and added to neutralized, polymerizing collagen/HEPES/media/microtissue slurry. Matrices were polymerized for 15 minutes at room temperature, and at least 3 hours at 37° to allow collagen crosslinking and gel polymerization before adding complete media (DMEM recipe in Chapter 2). Prior to imaging, gels were overlaid with Leibovitz L-15 media (Thermo Fischer, Cat# 11415064) with 10% FBS (Fisher, Cat# SH3007103), 1X Antibiotic-antimycotic (Thermo Fisher, Cat#15240062), 2mM L-glutamine (Life Technologies, Cat# 25030081), 25mg/mL plasmocin (Invivogen, Cat# ant-mpt). And imaged using LSMPM/SHG in 5-10 minute increments.

**Immunofluorescence**

Chronic pancreatitis biopsies were obtained and stained according to procedures outlined in Chapters 1 and 2.

**Live labeling and imaging**

Tissues were harvested in filter sterilized isolation solution made with complete DMEM (Chapter 2) supplemented with with 1x DNase1 and 100ug/mL soybean trypsin inhibitor. Live tissue was assessed for stiffness and integrity before deciding whether to slice with vibrotome sectioning with stiffer tissues or to move forward with endogenous labeling with softer. Because normal pancreas is 1) incredibly pliable and 2) self-digestive, working quickly with minimal handling and with the addition of other tissue inhibitors is recommended for any time frame of live imaging. In general, we recommend working with sections or pieces that are as flat as possible, and employing tissue anchors to physically constrain tissues in

place for more uniform staining. High levels of antibody will be necessary for adequate surface staining and visualization, and staining is easier in live tumor sections with more flat surfaces and more thin, even cross sections for uniform distribution of antibody and for limiting surface area of tissue out of focus. Staining was performed using FITC-conjugated anti-CD11b antibody (eBioscience Cat# 11-0112-41) at dilutions dependent on tissue density and size. More antibody will be necessary for more fibrous tissues.

## Results

**Macrophages increase primary tumor cell invasion from microtissues embedded in 3D collagen gels.** Given the role macrophages play in tumor cell dissemination, and the role collagen and FAK signaling evidently play in both macrophage phenotype and epithelial invasion, we sought to examine the interplay of these three components in real time. Microtissues described in Chapter 3 were generated using *KPCT/G* primary tumor cells, cultured for 7 days, and then embedded with primary BMDMs to observe how BMDMs influence extrusion into collagen matrices. We observed a general increase in extrusion when microtissues were cultured with BMDMs as compared to without (**Figure 4.1A** and **4.1C**). Interestingly, the addition of primary *KPC* tumor-derived pancreatic stellate cells did not induce the same type of invasion, promoting more of a generalized, group "pushing" rather than sharp single cell protrusions (**Figure 4.1C**). Most surprisingly, we noticed a rare but reproducible physical interaction occurring between

macrophages and tumor cells at the base of extruding tumor cells in both *KPCG* microtissues, which exhibit more invasive behavior (**Figure 4.1A**, top), and with

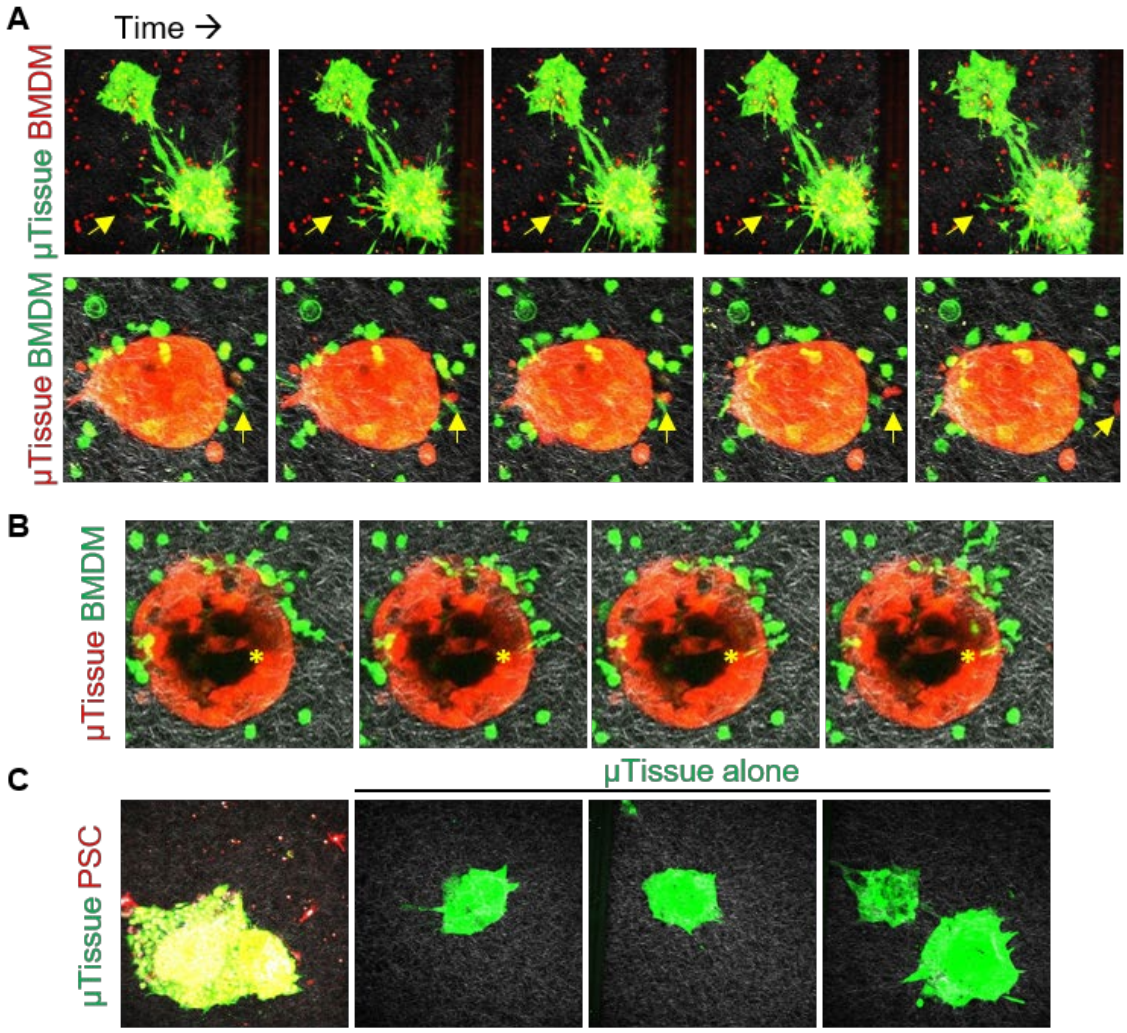


**Figure 4.1 Macrophages increase tumor cell invasion in novel 3D microtissue cocultures. A)** Microtissue primary droplets with *KPCG* (top, more invasive) and *KPCT* (bottom, less invasive) cocultured with primary BMDMs. Arrows show macrophages physically interacting with tumor cells before single tumor cell breaks away. **B)** *KPCT* microtissue highlight macrophages probing along collagen fibers and into microtissue (asterisk). **C)** Microtissue controls (*KPCG*) with addition of primary pancreatic stellate cells (PSC) and without addition of any other stromal cells. Qualitative assessment of *KPCG* microtissues in **(A)** and **(C)** show macrophages strikingly enhance invasion after 24 hours.

*KPCT* microtissues, which exhibit less invasive behavior (**Figure 4.1A**, bottom). Arrows represent physical interaction at extrusion points. While we anticipated observing an increase in the invasive potential of carcinoma cells, we did not anticipate observing any direct physical interactions between carcinoma cells and macrophages, especially at the base of the cell rather than at the leading, protrusive front. Other surprising interactions were observed as well, including macrophages extending protrusions of their own along aligned collagen fibers and through duct-like structures toward the center of the microtissue (**Figure 4.1B**, asterisk), and appeared to be probing the space. To further investigate these physical interactions, we moved to human CP FFPE biopsies.

**Macrophages preferentially colocalize with stromal ducts and PanINs in human chronic pancreatitis.** Physical contact between macrophages and primary *KPCT/G* microtissues in our *in vitro* coculture system was surprising, so we sought to better characterize the association between macrophages and ductal structures in chronic human pancreatitis. Images were graded based on the following requirements: regions containing no ducts and little to no collagen were used to assess macrophage number in “normal” fields of view (**Figure 4.2A**). Images containing one or more ducts (**Figure 4.2B**, arrow head), abnormally high PanCK levels with abnormal staining patterns (**Figure 4.2B**, arrows), and/or stromal interlobular and intralobular collagen (**Figure 4.2B**, asterisk) were used to assess macrophage levels in the “Duct/Stroma” group.

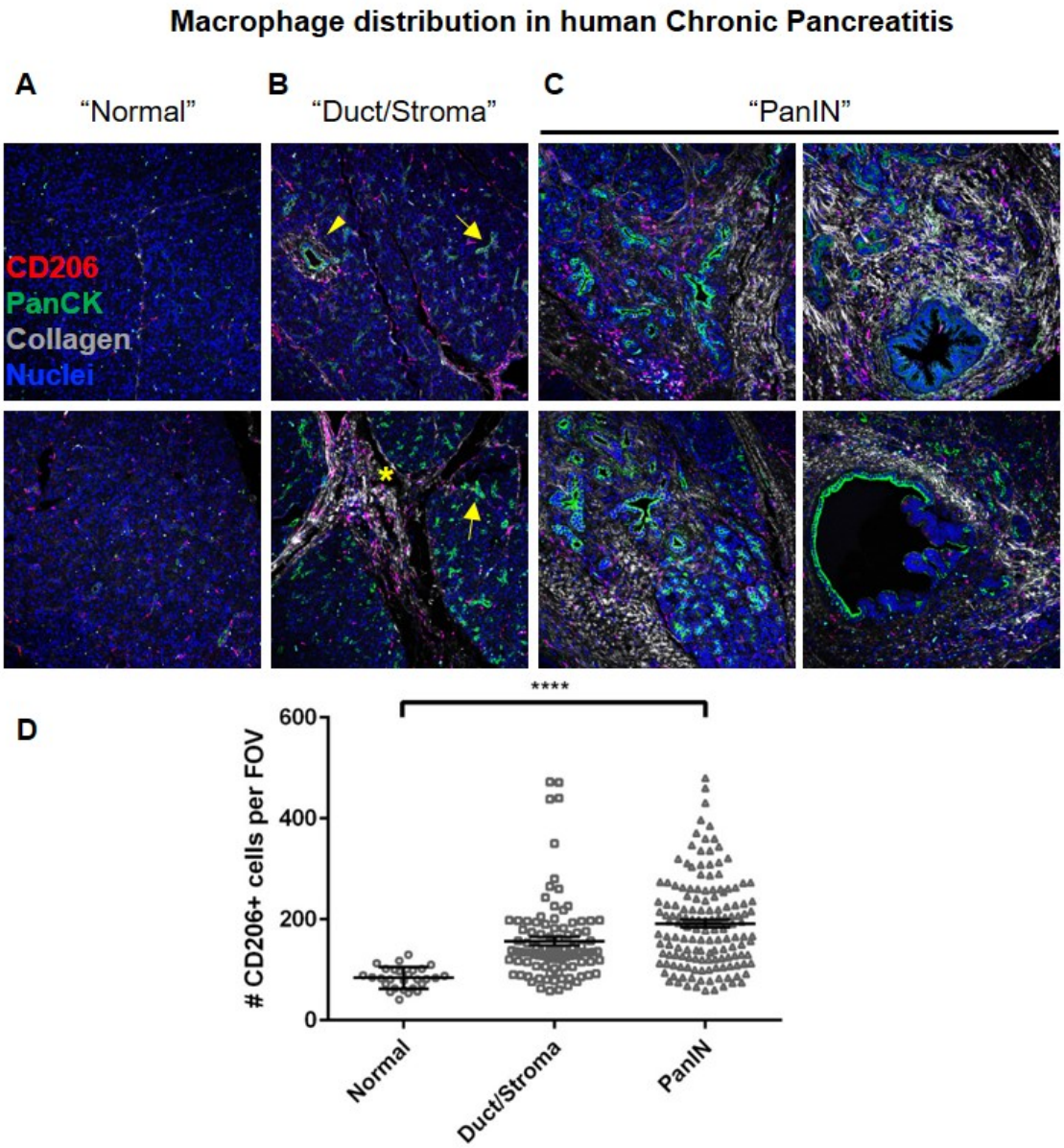


**Figure 4.2 Macrophages preferentially colocalize with stromal ducts and fibrosis in human chronic pancreatitis. A)** Quantification of macrophage accumulation with respect to ducts in hCP. **B)** through **D)** Representative images depicting how samples were graded in terms of ductal and stromal appearance. Fields of view were graded as "Normal," defined by no presence of ducts with little to no collagen per field of view **(B)**, as "Duct/Stroma" for fields of view with any ductal presence (arrow head), abnormal levels or patterns of PanCK (arrows) and/or intra-/interlobular collagen (asterisk) **(C)**, or as "PanIN" for fields of view with an abundance of abnormal ducts as marked by PanCK expression, and/or evident PanIN/PanIN-like lesions **(D).** ($p<0.0001$, one-way ANOVA).

Fields of view in the “PanIN” group were graded based on an abundance of abnormal ducts, acinar drop out, high PanCK expression, and the presence of PanIN/PanIN like lesions (**Figure 4.2C**). These three groups were then used to quantify abundance of CD206+ cells in human biopsies (**Figure 4.2D**). We found a significant increase in macrophages in regions with even 1 duct compared to normal, with even more robust enrichment in regions with PanIN/PanIN-like lesions ($p<0.0001$, one-way ANOVA). This localization was anticipated as collagen also accumulates around ducts, and Chapter 2 establishes colocalization of macrophages and stromal collagen. However, the association of macrophages with PanINs has been shown in PDA, but to our knowledge has not been described in human CP.

**Macrophages physically contact ductal epithelia in human chronic pancreatitis.** Data observed in **Figure 4.1** prompted us to use hCP samples to assess whether physical contact between ductal epithelia and macrophages occurs in the fibrotic pancreas. Indeed, in Figure 4.3, CD206+ macrophages were observed not only in close proximity to ductal structures, but could even be found within ductal structures making direct physical contact with PanCK+ epithelium (**Figure 4.3A**). Instances of macrophages extending protrusions in between ductal cells (**Figure 4.3B,** arrow heads) were also observed, although a rare occurrence, but this rarity is consistent with findings in our *in vitro* microtissue cocultures where physical regulation of invasion was not abundantly common. Regardless, these images highlight the possibility of fusion between macrophages and ductal

epithelial cells given their consistent close proximity to one another in pancreatitis and suggest this may be one mechanism by which epithelial cells disseminate so early in disease.

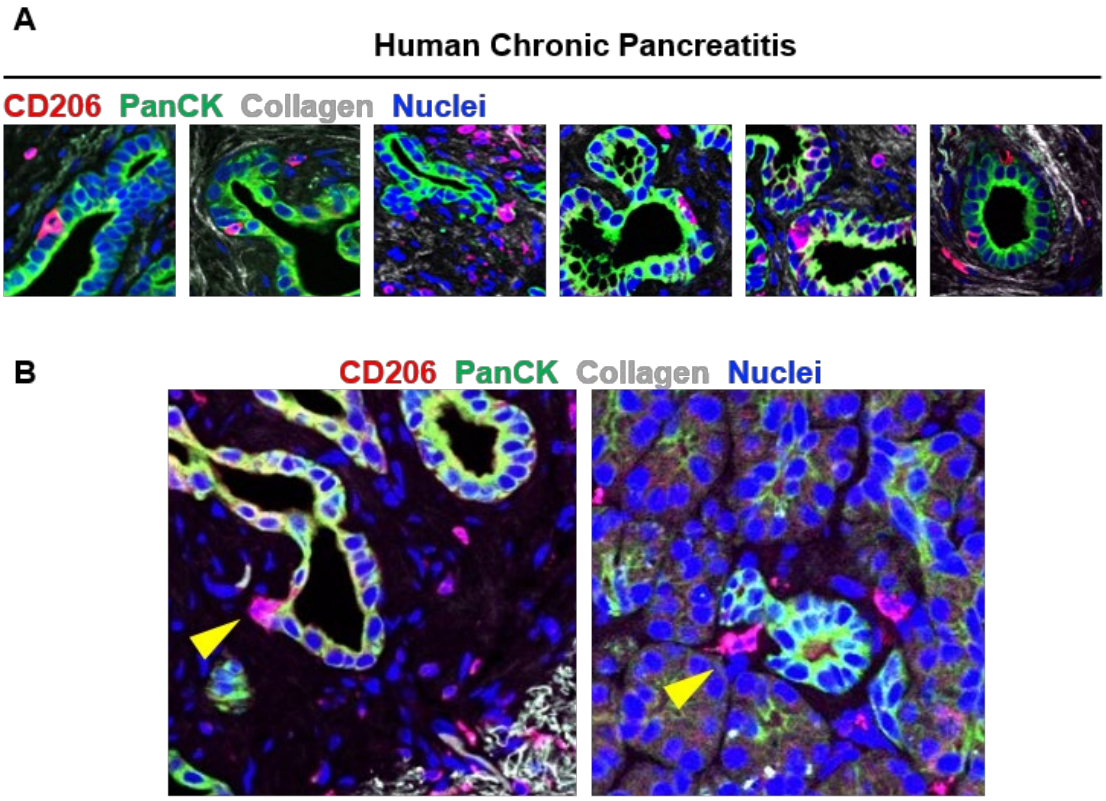


**Figure 4.3 Macrophages physically contact ductal epithelia in human chronic pancreatitis. A)** Images showing macrophages making physical contact with ductal epithelia in human chronic pancreatitis biopsies, and, rarely, even extending protrusions in between ductal cells (arrow heads) **(B)**, an interaction similar to what was observed in *in vitro* microtissue cocultures in **Figure 4.1.**

**Dual pan-Cytokeratin+ CD206+ single cells are present in human chronic pancreatitis.** In the literature, circulating cells displaying both immune markers and epithelial markers have been identified and termed “circulating hybrid cells” (CHCs). To investigate the potential existence of fused “hybrid cells” in CP,

biopsies were imaged using LSMPM/SHG to locate CD206+ macrophages also displaying epithelial marker pan-cytokeratin. Interestingly, dual positive cells were indeed present in CP biopsies as marked by their co-expression of CD206 and PanCK (**Figure 4.4A,** arrow heads). To ensure this staining was not an artifact of signal bleed through or autofluorescence, we imaged autofluorescence in biopsies as well (**Figure 4.4B**) and note that this staining pattern could not be attributed to autofluorescence. Enlarged images of hybrid cells show distinct, colocalized patterns of CD206 and PanCK (**Figures 4.4C** and **4.4D**), and exhibit single nuclei suggesting these hybrid cells are truly one single cell rather than two cells with overlapping signal (**Figure 4.4E**), although the possibility this is a phagocytic macrophage which recently engulfed an epithelial cell cannot be ruled out and would require further investigation.

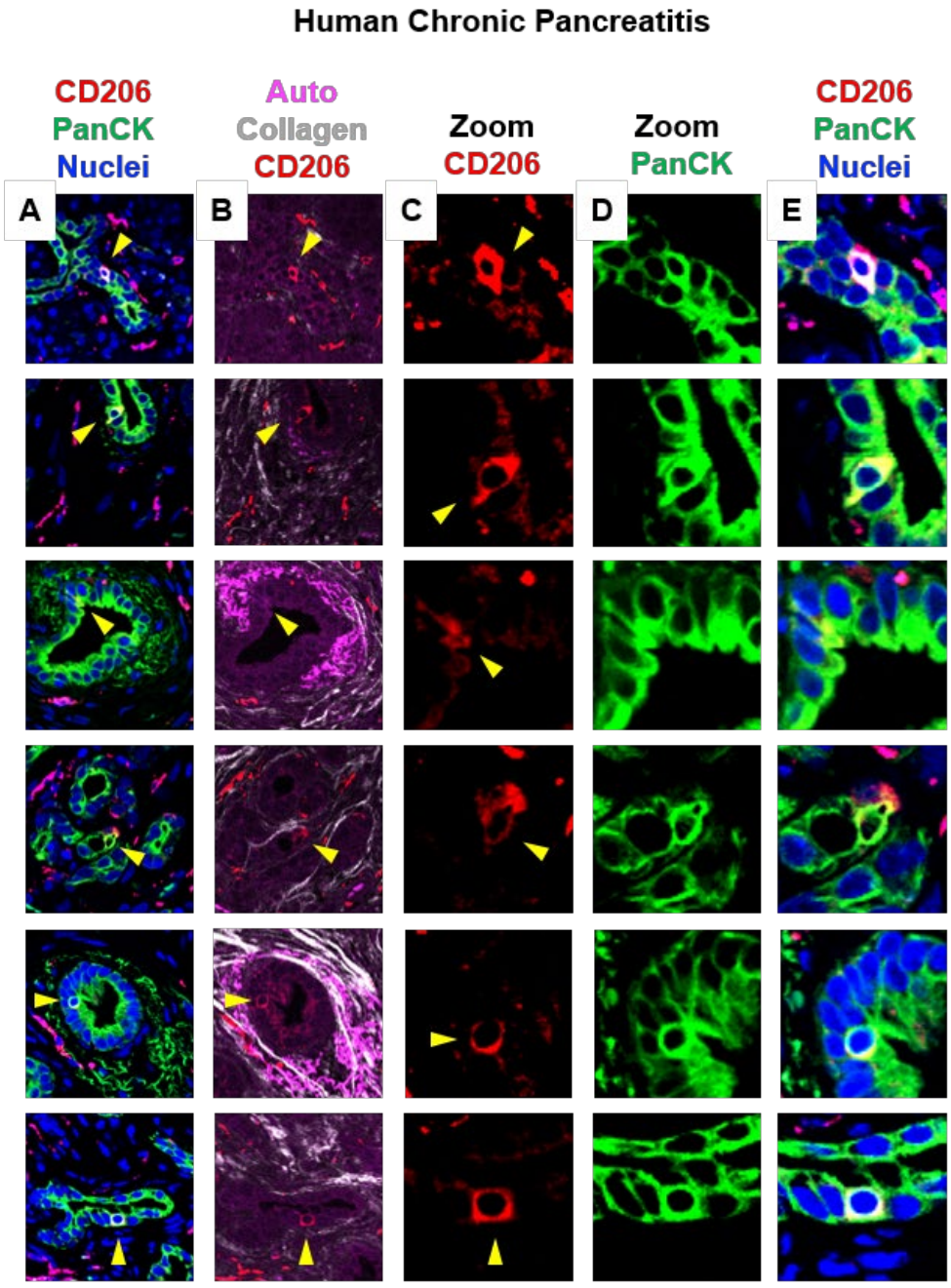


**Figure 4.4 Dual pan-Cytokeratin+ CD206+ single cells are present in human chronic pancreatitis.** Human chronic pancreatitis biopsies showing presence of what appear to be single cells with a single nuclei positive for both epithelial, ductal marker PanCK and macrophage marker CD206 (arrow heads), suggesting existence of CHCs in human pancreatitis. **A)** Ducts with double positive cells (arrow heads) could not be explained by autofluorescence shown in **(B)**. Enlarged insets of cells of interest show distinct cell surface patterns of both CD206 **(C)**, and pan-cytokeratin **(D)**, shown merged and colocalized in **(E)**.

**Endogenous macrophages can be labeled and live imaged *ex vivo* in live pancreas tissue.** As a complimentary and parallel approach to the microtissue experiments outlined here, as well as to the seeding of exogenous macrophage approach presented in Chapter 2, we have also developed a protocol to stain live CD11b+ macrophages in the pancreas (**Figure 4.5**). This approach could be applied to answer many unanswered questions discussed in more detail below.

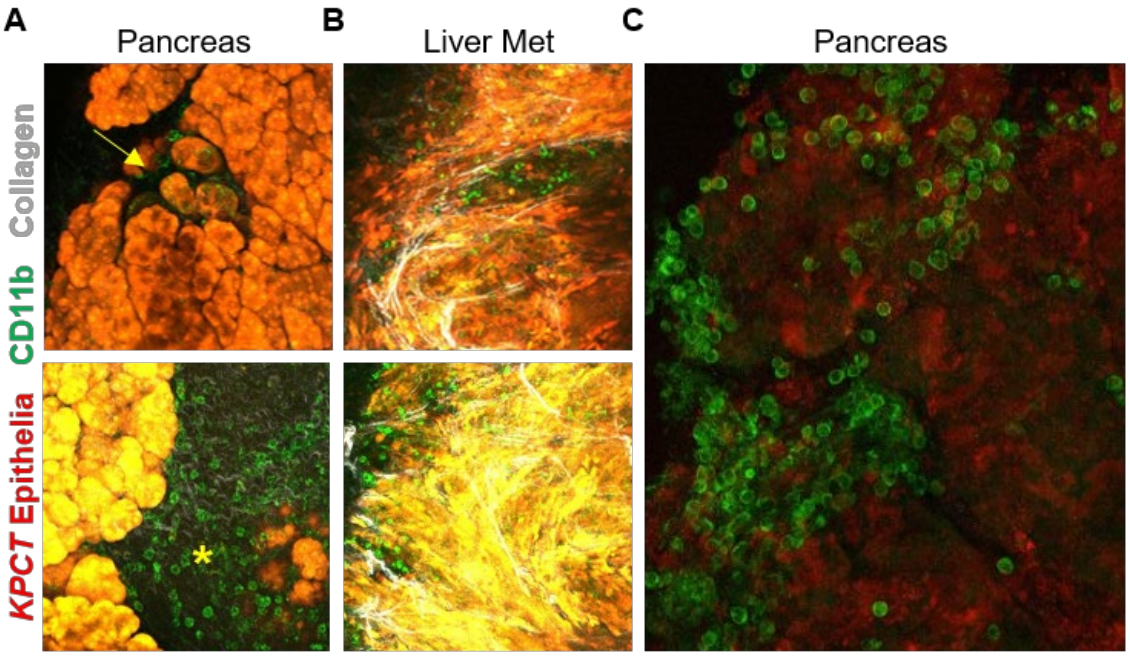


**Figure 4.5 Experimental approaches to elucidate physical mechanisms *in vivo*. A)** *KPCT* pancreas tissue demonstrating live imaging of endogenous CD11b+ macrophages labeled with primary FITC-conjugated antibody near a duct (arrow, top), and within intralobular collagen (asterisk, bottom). **B)** Live imaging of a metastatic site in the liver of the mouse in **(A)**. **C)** Protocol optimization to increase pancreas viability over imaging time and decrease background fluorescence from FITC-conjugated antibody shows clear membrane staining of CD11b on macrophages in the pancreas.

## Future Directions

Overall, this chapter presents around a central theme of combining conclusions from Chapters 2 and 3 regarding how collagen impacts both myeloid and epithelial

compartments and culminates to exacerbate disease severity via FAK—but how the myeloid and epithelial compartments interact in fibrous environments is poorly explored in real time. Preliminary conclusions from this section are 1) macrophages make physical contact with epithelial cells in microtissues and in human CP and 2) CD206/PanCK double positive cells can be observed in human CP biopsies. We also present a set of *in vitro* and *ex vivo* procedures which could be used in conjunction with LSMPM/SHG across different tissue culture platforms to help elucidate the mechanisms underlying macrophage facilitation of epithelial dissemination (see **Figure 4.5**). We have categorized future directions into three areas of interest:

1. Characterizing macrophage migration. In general, there is little known about macrophage migration, in 2D, 3D gels, and in live tissues (**Figure 4.1** and **4.5**). Further, little is known about how macrophage migration changes across the spectrum of macrophage behavior. Both the microtissue coculture system and endogenous labeling offer potential to characterize macrophage behavior in varied environments, i.e., with addition of other ECM components to *in vitro* cultures, or compared across tumor sections high versus low collagen density. Moreover, comparison of migration of macrophages at ectopic sites (**Figure 4.5A** and **4.5B**), either before or after colonization—tumors preferentially home to similar ectopic sites across patients reproducibly, and given the role of macrophages in priming pre-metastatic sites, it is possible there are inherent cues in the stroma of ectopic sites directing macrophages to settle in.

2. Observing physical macrophage-epithelial contact *ex vivo*. These observations could similarly be made utilizing tumor slices and endogenous labeling of macrophages and would allow for addition of STTs like collagenase to see if this abrogates physical contact. This system would also allow for potential to identify CHCs and fusion events, especially in the case of using *KPCT/G* models. Identifying fluorescent pancreas-derived epithelia dual positive for immune markers in either live primary or secondary tissue would help to strengthen this needle-in-a-haystack observation.
3. Validate presence of CHCs. Given the phagocytic ability of macrophages, it is possible the observed “CHCs” may appear as double positive single cells as an artifact of macrophages consuming and breaking down epithelial cells. To further characterize this population to more definitively define them as true fusion events, multiple experiments should be employed. In vitro, live cell imaging of co-cultures could be used to track the merging of cytoplasmic, nuclear, and cell surface components to verify whether this event is truly fusion of two distinct cells. *Ex vivo*, slices could be employed to more closely mimic the factors present in the TME likely influencing fusion. In mouse models and in human samples, blood should be collected and to assess the presence and prevalence of CHCs, and to further profile at a single-cell level the co-expression of multiple immune and epithelial markers simultaneously.
4. Comparing tumor cell invasion from microtissues in varied microTMEs. It would be interesting to culture microtissues with varied ECM composition and stiffness—both internally via stiffer Matrigel concentrations at the core or

externally via increased collagen matrix concentrations—or to coculture with other stromal cells like fibroblasts to see if physical contact and enhancement of invasion is observed with other cell types or is specific to macrophages. One could even envision this system allow for addition of other immune cells like T cells to, as a lofty idea, serve as a screening tool for personalized therapeutics.

Experimental procedures and observations presented in this chapter offer an opportunity to explore both sides of one coin. Given the evident role of collagen in directing both macrophage and tumor cell dissemination, it would be of great use to have systems which would allow for perturbation and observation of these two arms together, especially in more reductionist systems that mimic *in vivo* microenvironments, but with more tunability and with more opportunity to screen inhibitors, perform genetic knock outs, etc. While not “reductionist,” it is also likely of great importance to understand macrophage migration in early stages of disease, especially given this entire dissertation focuses primarily on early stromal priming in PDA. But more optimization of endogenous labeling and maintenance of normal pancreas tissue integrity is necessary for these studies to be properly conducted.

# 5. DISCUSSION AND FUTURE DIRECTIONS

The work presented in this dissertation points to a critical relationship between collagen, macrophages and disseminating epithelial cells which act in concert to exacerbate PDA progression and serve to prime the microenvironment to support cancer before disease involution. Moreover, these studies collectively point to an urgent need to better understand how ECM architectures influence cancer progression in PDA, as well as how this role of ECM—and potential strategies to dismantle it—can be translated to other solid tumors. TACS and ECM landscapes clearly develop to aid and abet cancer cells from very early stages of progression in a FAK dependent manner. Further, the prevalence of both TACS and suppressive myeloid cells localized to collagen in early pancreatitis may serve as a novel biomarker to assist in pathological assessment, informing treatment steps for patients with histologically and architecturally conspicuous biopsies.

**Perturb cytoskeletal dynamics and the cell shape-cell phenotype axis.** *In vitro*, nanopatterned substrates and other culture systems like novel aligned 3D collagen matrices offer the chance to glean more information regarding how alignment and cell shape influence intracellular changes in gene expression, protein localization, and cell function and response. Utilization of these systems combined with inhibitors or genetic manipulation via shRNAs or lentiviral delivery of targeted CRISPR/Cas9 could help clarify mechanisms underlying signal transduction from the extracellular to the intracellular space.

**Consider architectures of and contributions by other ECMs.** Overall, there is an evident need for a better understanding of how extracellular matrix composition, content, and architecture influence pancreas cancer progression from its earliest stages, even preceding disease onset. For example, there is a fundamental lack in understanding of whether extracellular matrix components like collagen, hyaluronic acid, fibrin, and laminin have differential, additive, compensatory, or conflicting roles in promoting pancreas cancer progression and immune cell phenotype. Moreover, our understanding of ECM architectures outside of collagen is wholly lacking—do other matrix components undergo remodeling toward architectures which would enhance tumor cell dissemination, immune suppression, or other processes crucial to cancer progression? Given the structure of collagen fibrils in patient samples is indicative of recurrence and survival in breast cancer, it would be interesting to assess the topography of other ECMs in breast and pancreas cancers to determine whether they also correlate with survival, resistance, etc. thus serving as potential new diagnostic ECM signatures not unlike current genetic signatures used to predict patient outcome and response to therapy. It would be of immense clinical benefit to follow larger patient cohorts for longer periods of time to determine how TACS, as well as the co-prevalence or -absence of other ECMs, may impact outcome in PDA in terms of both general prognosis as well as response to conventional and emerging therapeutic options.

**Elucidate stromal alterations and persistence of changes in other risk factors of PDA.** This dissertation does not take into consideration how other risk

factors for PDA—like diabetes, alcohol consumption, and obesity—may be impacting the fibroinflammatory environment in the pancreas. Therefore, future studies ought to explore the stromal composition of patient pancreas samples from other pancreas pathologies. The data here also beg the question of how stromal changes during resolvable pancreas pathology may persist as “stromal memory,” wherein repetitive exposure to bouts of pancreatitis, trauma, injury, or prolonged exposure to excessive alcohol may leave residual, unresolved architectures capable of later supporting PDA. Parallel to exploration in patient samples, combining *KPCT/G* mice with models of pancreatitis, obesity, and high-alcohol diet would help provide an understanding of how these life-style risk factors may exacerbate one another, and how various treatment schemes may reduce risk.

**Characterize the prevalence and contribution of TACS in the pre-metastatic niche.** While the notion of early dissemination is still emerging and underlying mechanisms still veiled, this idea of tissue priming is foundational to the field of studying pre-metastatic niche formation, wherein secondary sites are prepared by non-neoplastic cells and factors to support disease prior to presentation. The study of TACS prevalence and how TACS influences metastasis at secondary sites is wholly lacking, but if TACS are capable of facilitating EMT and dissemination out of primary tumors and into the vasculature, it would be of no surprise if TACS in secondary sites, formed by activated stromal fibroblasts and macrophages, are capable of facilitating extravasation into secondary sites and MET. Observation of typical ectopic sites through histology, immunofluorescence and LSMPM/SHG may provide surprising information on how these sites are prepared to facilitate

spread before dissemination has occurred and could bolster our lacking understanding of why specific tumor types display preferential spreading to reproducible sites.

**Compare myeloid populations and their response to stromal architectures.** Myeloid cells in the pancreas have been shown to be derived from different sources, from embryonic origin (resident macrophages) and from hematopoetic origin (bone marrow, blood monocytes). While both populations are expanded and play a role in pancreas cancer, DeNardo and colleagues report differential functions of the two populations [152]. Moreover, suppressive tumor-associated neutrophils and myeloid derived suppressor cells are also derived from myeloid lineages [189] and may thus also respond to physical cues. In this dissertation, we observe a more robust response of whole bone marrow as compared to differentiated macrophages, but more experiments should be done to specifically compare the response of myeloid progenitors, circulating monocytes, and mature macrophages to architectural cues.

**Clarify mechanisms of macrophage "re-programming."** Cumulative data *in vitro* and *in vivo* is in conflict as to whether existing, polarized macrophages can "switch," or rather, "slide" on the scale of phenotypes. *In vivo*, it is possible increases in anti-tumor macrophages arise as a result of influx of new macrophages which can be then educated toward anti-tumor behavior. Further study of exactly how therapeutics which have been observed to "re-program," macrophages, like nanoparticles, or CD40/CD11b agonism, should be further characterized *in vitro* and *in vivo* to definitively decide whether we can change

existing macrophage phenotypes, or whether we should focus more on calling in naïve cells and promoting their anti-tumor differentiation. In our study, FAK inhibited mice still possessed CD206+ macrophages. It would be interesting to see if remaining CD206+ cells are functionally distinct from those in vehicle treated samples. Are macrophages in FAK treated samples more susceptible to repolarization and/or less proficient at suppressing T cells? Future studies should seek to combine immunotherapies with FAK inhibitors and assess the utility in these strategies to re-engineer macrophages toward anti-tumor, T-cell supportive phenotypes.

**Determinate STT utility in precursory disease.** Perhaps the most complex but highest priority future direction will be to fully evaluate the utility of using STTs, anti-fibrotics, and anti-inflammatories to pre-invasive inflammation and lesioning. Targeting collagen architectures via STTs, or targeting a cell's ability to sense and respond to these architectures via integrin or FAK inhibition, offers a "two birds one stone" approach to not only hinder cancer cell invasion and metastasis, but also to abrogate the influx and maintenance of immunosuppressive immune cells. Future studies in *KPCT/G* mice, as well as with live patient biopsies *ex vivo* or 3D microtissue cocultures *in vitro*, will assist in determining how FAK inhibition, alone or in combination with other STTs, immunotherapies or chemotherapies impact neoplastic and stromal cell behavior.

It is widely accepted that inflammation precedes, exacerbates, and foreshadows cancer in several contexts, and while this work does not conclusively define a mechanistic connection between pancreatitis, myeloid cells, and dissemination, it

does support a need to further study the connection between precursor inflammation and PDA with the intent of informing new treatment strategies for high-risk, pre-invasive fibrosis. There is a desperate need to explore proactive, preventative treatments in addition to the existing reactive, inadequate regimes. For example, is it possible to aggressively treat pancreatitis with antifibrotic therapeutics as a preventative strategy to abrogate or even slow PDA inception and spread? Further investigation of how anti-inflammatory, antifibrotic, and/or STT administration in early stages of pancreatic inflammation or pancreatitis may prove to help decrease risk and severity of PDA, lend to a better understanding of the link between CP and PDA, and give rise to more reliable screening and treatment methods. For example, further assessment of collagen signatures, perhaps in combination with macrophage prevalence and shape, may assist in stratifying patients and predicting response to various therapeutic strategies. Moreover, we hypothesize this link between precursor fibrosis, collagen architecture, and immune cell function is conserved across other fibroinflammatory diseases, and may play a role in priming other tissues to support solid tumor progression and spreading. Identifying the ways in which mechanical cues influence patient immunity will be key to tilting the scales to favor the patient.

Stroma targeted therapies have assisted in alleviating stromal barriers to treatment of solid tumors, and facilitate processes like anti-tumor immune influx and response, decrease in tumor volume and spreading, and increases in overall response and survival. For instance, we recently demonstrated that Halofuginone

can help normalize CAF behavior to robustly decrease the fibrotic response in PDA while also increasing anti-tumor immunity [13]. Likewise, antifibrotic therapy with Losartan has been shown to decrease fibrous ECM and has gone through promising Phase II trials [190], and multiple early trials with FAK inhibitors are ongoing for PDA (e.g. NCT02758587, NCT04331041, NCT03727880).

In conclusion, therapies to re-engineer and normalize the pancreas microenvironment in both precursory and unresectable, invasive disease will be paramount to extending patient survival for patients with PDA. The work presented here offers up macrophages, collagen, epithelial cells, and FAK as a network of intertwined targets contributing to disease severity in PDA. Strategies to target this network has promise in an ability to limit desmoplasia, immune suppression, and dissemination not only in unresectable, invasive disease, but also in preceding risk-associated fibrosis.

# BIBLIOGRAPHY


1. ACS, *American Cancer Society*. 2014.
2. Sleeman, J. and P.S. Steeg, *Cancer metastasis as a therapeutic target.* Eur J Cancer, 2010. **46**(7): p. 1177-80.
3. Steeg, P.S. and D. Theodorescu, *Metastasis: a therapeutic target for cancer.* Nat Clin Pract Oncol, 2008. **5**(4): p. 206-19.
4. Becker, A.E., et al., *Pancreatic ductal adenocarcinoma: risk factors, screening, and early detection.* World J Gastroenterol, 2014. **20**(32): p. 11182-98.
5. Hruban, R.H., et al., *Precursors to pancreatic cancer.* Gastroenterol Clin North Am, 2007. **36**(4): p. 831-49, vi.
6. Scarlett, C.J., et al., *Precursor lesions in pancreatic cancer: morphological and molecular pathology.* Pathology, 2011. **43**(3): p. 183-200.
7. Iacobuzio-Donahue, C.A., *Genetic evolution of pancreatic cancer: lessons learnt from the pancreatic cancer genome sequencing project.* Gut, 2012. **61**(7): p. 1085-94.
8. Rodríguez Gil, Y., et al., *Molecular Alterations in Pancreatic Cancer: Transfer to the Clinic.* Int J Mol Sci, 2021. **22**(4).
9. Carrière, C., et al., *Acute pancreatitis markedly accelerates pancreatic cancer progression in mice expressing oncogenic Kras.* Biochem Biophys Res Commun, 2009. **382**(3): p. 561-5.
10. Hingorani, S.R., et al., *Trp53R172H and KrasG12D cooperate to promote chromosomal instability and widely metastatic pancreatic ductal adenocarcinoma in mice.* Cancer Cell, 2005. **7**(5): p. 469-83.
11. Feig, C., et al., *The pancreas cancer microenvironment.* Clin Cancer Res, 2012. **18**(16): p. 4266-76.
12. Waghray, M., et al., *Deciphering the role of stroma in pancreatic cancer.* Curr Opin Gastroenterol, 2013. **29**(5): p. 537-43.
13. Elahi-Gedwillo, K.Y., et al., *Antifibrotic Therapy Disrupts Stromal Barriers and Modulates the Immune Landscape in Pancreatic Ductal Adenocarcinoma.* Cancer Res, 2019. **79**(2): p. 372-386.
14. Zhang, Y., H.C. Crawford, and M. Pasca di Magliano, *Epithelial-Stromal Interactions in Pancreatic Cancer.* Annu Rev Physiol, 2019. **81**: p. 211-233.
15. Clark, C.E., et al., *Dynamics of the immune reaction to pancreatic cancer from inception to invasion.* Cancer Res, 2007. **67**(19): p. 9518-27.
16. Masamune, A., et al., *Roles of pancreatic stellate cells in pancreatic inflammation and fibrosis.* Clin Gastroenterol Hepatol, 2009. **7**(11 Suppl): p. S48-54.
17. Salmon, H., et al., *Matrix architecture defines the preferential localization and migration of T cells into the stroma of human lung tumors.* J Clin Invest, 2012. **122**(3): p. 899-910.
18. Schmiechen, Z.C. and I.M. Stromnes, *Mechanisms Governing Immunotherapy Resistance in Pancreatic Ductal Adenocarcinoma.* Front Immunol, 2020. **11**: p. 613815.
19. Stromnes, I.M., et al., *Stromal reengineering to treat pancreas cancer.* Carcinogenesis, 2014. **35**(7): p. 1451-60.
20. Öhlund, D., et al., *Distinct populations of inflammatory fibroblasts and myofibroblasts in pancreatic cancer.* J Exp Med, 2017. **214**(3): p. 579-596.

21. Provenzano, P.P. and S.R. Hingorani, *Hyaluronan, fluid pressure, and stromal resistance in pancreas cancer.* Br J Cancer, 2013. **108**(1): p. 1-8.
22. Stromnes, I.M., et al., *Targeted depletion of an MDSC subset unmasks pancreatic ductal adenocarcinoma to adaptive immunity.* Gut, 2014. **63**(11): p. 1769-81.
23. von Ahrens, D., et al., *The role of stromal cancer-associated fibroblasts in pancreatic cancer.* J Hematol Oncol, 2017. **10**(1): p. 76.
24. Zhang, Y., et al., *Epithelial-Myeloid cell crosstalk regulates acinar cell plasticity and pancreatic remodeling in mice.* Elife, 2017. **6**.
25. Olive, K.P., et al., *Inhibition of Hedgehog signaling enhances delivery of chemotherapy in a mouse model of pancreatic cancer.* Science, 2009. **324**(5933): p. 1457-61.
26. Nywening, T.M., et al., *Targeting both tumour-associated CXCR2.* Gut, 2018. **67**(6): p. 1112-1123.
27. Provenzano, P.P., et al., *Enzymatic targeting of the stroma ablates physical barriers to treatment of pancreatic ductal adenocarcinoma.* Cancer Cell, 2012. **21**(3): p. 418-29.
28. Jiang, B., et al., *Stroma-Targeting Therapy in Pancreatic Cancer: One Coin With Two Sides?* Front Oncol, 2020. **10**: p. 576399.
29. Chen, Y., et al., *Type I collagen deletion in αSMA.* Cancer Cell, 2021. **39**(4): p. 548-565.e6.
30. Özdemir, B.C., et al., *Depletion of Carcinoma-Associated Fibroblasts and Fibrosis Induces Immunosuppression and Accelerates Pancreas Cancer with Reduced Survival.* Cancer Cell, 2015. **28**(6): p. 831-833.
31. Jiang, H., et al., *Targeting focal adhesion kinase renders pancreatic cancers responsive to checkpoint immunotherapy.* Nat Med, 2016. **22**(8): p. 851-60.
32. Jiang, H., et al., *Development of resistance to FAK inhibition in pancreatic cancer is linked to stromal depletion.* Gut, 2020. **69**(1): p. 122-132.
33. Hingorani, S.R., et al., *HALO 202: Randomized Phase II Study of PEGPH20 Plus Nab-Paclitaxel/Gemcitabine Versus Nab-Paclitaxel/Gemcitabine in Patients With Untreated, Metastatic Pancreatic Ductal Adenocarcinoma.* J Clin Oncol, 2018. **36**(4): p. 359-366.
34. Ajina, R. and L.M. Weiner, *T-Cell Immunity in Pancreatic Cancer.* Pancreas, 2020. **49**(8): p. 1014-1023.
35. Anderson, K.G., I.M. Stromnes, and P.D. Greenberg, *Obstacles Posed by the Tumor Microenvironment to T cell Activity: A Case for Synergistic Therapies.* Cancer Cell, 2017. **31**(3): p. 311-325.
36. Hartmann, N., et al., *Prevailing role of contact guidance in intrastromal T-cell trapping in human pancreatic cancer.* Clin Cancer Res, 2014. **20**(13): p. 3422-33.
37. Stromnes, I.M., et al., *Differential Effects of Depleting versus Programming Tumor-Associated Macrophages on Engineered T Cells in Pancreatic Ductal Adenocarcinoma.* Cancer Immunol Res, 2019. **7**(6): p. 977-989.
38. Stromnes, I.M., et al., *T Cells Engineered against a Native Antigen Can Surmount Immunologic and Physical Barriers to Treat Pancreatic Ductal Adenocarcinoma.* Cancer Cell, 2015. **28**(5): p. 638-652.
39. Wynn, T.A., A. Chawla, and J.W. Pollard, *Macrophage biology in development, homeostasis and disease.* Nature, 2013. **496**(7446): p. 445-55.
40. Guerriero, J.L., *Macrophages: Their Untold Story in T Cell Activation and Function.* Int Rev Cell Mol Biol, 2019. **342**: p. 73-93.
41. Watanabe, S., et al., *The role of macrophages in the resolution of inflammation.* J Clin Invest, 2019. **129**(7): p. 2619-2628.

42. Najafi, M., et al., *Macrophage polarity in cancer: A review.* J Cell Biochem, 2019. **120**(3): p. 2756-2765.
43. DeNardo, D.G. and B. Ruffell, *Macrophages as regulators of tumour immunity and immunotherapy.* Nat Rev Immunol, 2019. **19**(6): p. 369-382.
44. Habtezion, A., M. Edderkaoui, and S.J. Pandol, *Macrophages and pancreatic ductal adenocarcinoma.* Cancer Lett, 2016. **381**(1): p. 211-6.
45. Cassetta, L. and J.W. Pollard, *Targeting macrophages: therapeutic approaches in cancer.* Nat Rev Drug Discov, 2018. **17**(12): p. 887-904.
46. Lankadasari, M.B., et al., *TAMing pancreatic cancer: combat with a double edged sword.* Mol Cancer, 2019. **18**(1): p. 48.
47. Salmaninejad, A., et al., *Tumor-associated macrophages: role in cancer development and therapeutic implications.* Cell Oncol (Dordr), 2019. **42**(5): p. 591-608.
48. Maller, O., et al., *Tumour-associated macrophages drive stromal cell-dependent collagen crosslinking and stiffening to promote breast cancer aggression.* Nat Mater, 2020.
49. Jiang, H., S. Hegde, and D.G. DeNardo, *Tumor-associated fibrosis as a regulator of tumor immunity and response to immunotherapy.* Cancer Immunol Immunother, 2017. **66**(8): p. 1037-1048.
50. Allavena, P. and C. Belgiovine, *Tumor-Associated Macrophages*. 2016: Encyclopedia of Immunobiology. p. 493-498.
51. Caux, C., et al., *A Milestone Review on How Macrophages Affect Tumor Growth.* Cancer Res, 2016. **76**(22): p. 6439-6442.
52. Noy, R. and J.W. Pollard, *Tumor-associated macrophages: from mechanisms to therapy.* Immunity, 2014. **41**(1): p. 49-61.
53. Clawson, G.A., et al., *"Stealth dissemination" of macrophage-tumor cell fusions cultured from blood of patients with pancreatic ductal adenocarcinoma.* PLoS One, 2017. **12**(9): p. e0184451.
54. Xiang, X., et al., *Targeting tumor-associated macrophages to synergize tumor immunotherapy.* Signal Transduct Target Ther, 2021. **6**(1): p. 75.
55. Rodriguez, P.C., et al., *L-arginine consumption by macrophages modulates the expression of CD3 zeta chain in T lymphocytes.* J Immunol, 2003. **171**(3): p. 1232-9.
56. Rath, M., et al., *Metabolism via Arginase or Nitric Oxide Synthase: Two Competing Arginine Pathways in Macrophages.* Front Immunol, 2014. **5**: p. 532.
57. Saha, D., R.L. Martuza, and S.D. Rabkin, *Macrophage Polarization Contributes to Glioblastoma Eradication by Combination Immunovirotherapy and Immune Checkpoint Blockade.* Cancer Cell, 2017. **32**(2): p. 253-267.e5.
58. Bayne, L.J., et al., *Tumor-derived granulocyte-macrophage colony-stimulating factor regulates myeloid inflammation and T cell immunity in pancreatic cancer.* Cancer Cell, 2012. **21**(6): p. 822-35.
59. Candido, J.B., et al., *CSF1R.* Cell Rep, 2018. **23**(5): p. 1448-1460.
60. Clark, C.E., G.L. Beatty, and R.H. Vonderheide, *Immunosurveillance of pancreatic adenocarcinoma: insights from genetically engineered mouse models of cancer.* Cancer Lett, 2009. **279**(1): p. 1-7.
61. Cruz, A.F., R. Rohban, and F. Esni, *Macrophages in the pancreas: Villains by circumstances, not necessarily by actions.* Immun Inflamm Dis, 2020.
62. Calderon, B., et al., *The pancreas anatomy conditions the origin and properties of resident macrophages.* J Exp Med, 2015. **212**(10): p. 1497-512.

63. Iurca, I., et al., *Macrophages Interaction and MicroRNA Interplay in the Modulation of Cancer Development and Metastasis.* Front Immunol, 2020. **11**: p. 870.
64. Mitchem, J.B., et al., *Targeting tumor-infiltrating macrophages decreases tumor-initiating cells, relieves immunosuppression, and improves chemotherapeutic responses.* Cancer Res, 2013. **73**(3): p. 1128-41.
65. Panni, R.Z., et al., *Agonism of CD11b reprograms innate immunity to sensitize pancreatic cancer to immunotherapies.* Sci Transl Med, 2019. **11**(499).
66. Steele, C.W., et al., *CXCR2 Inhibition Profoundly Suppresses Metastases and Augments Immunotherapy in Pancreatic Ductal Adenocarcinoma.* Cancer Cell, 2016. **29**(6): p. 832-845.
67. Zhu, Y., et al., *CSF1/CSF1R blockade reprograms tumor-infiltrating macrophages and improves response to T-cell checkpoint immunotherapy in pancreatic cancer models.* Cancer Res, 2014. **74**(18): p. 5057-69.
68. Borgoni, S., et al., *Depletion of tumor-associated macrophages switches the epigenetic profile of pancreatic cancer infiltrating T cells and restores their anti-tumor phenotype.* Oncoimmunology, 2018. **7**(2): p. e1393596.
69. Ries, C.H., et al., *Targeting tumor-associated macrophages with anti-CSF-1R antibody reveals a strategy for cancer therapy.* Cancer Cell, 2014. **25**(6): p. 846-59.
70. Lin, Y., J. Xu, and H. Lan, *Tumor-associated macrophages in tumor metastasis: biological roles and clinical therapeutic applications.* J Hematol Oncol, 2019. **12**(1): p. 76.
71. Sanchez, L.R., et al., *The emerging roles of macrophages in cancer metastasis and response to chemotherapy.* J Leukoc Biol, 2019. **106**(2): p. 259-274.
72. Kaplan, R.N., et al., *VEGFR1-positive haematopoietic bone marrow progenitors initiate the pre-metastatic niche.* Nature, 2005. **438**(7069): p. 820-7.
73. Zhang, W.J., et al., *Tumor-associated macrophages correlate with phenomenon of epithelial-mesenchymal transition and contribute to poor prognosis in triple-negative breast cancer patients.* J Surg Res, 2018. **222**: p. 93-101.
74. Gao, L., et al., *Tumor associated macrophages induce epithelial to mesenchymal transition via the EGFR/ERK1/2 pathway in head and neck squamous cell carcinoma.* Oncol Rep, 2018. **40**(5): p. 2558-2572.
75. Alonso-Nocelo, M., et al., *Matrix stiffness and tumor-associated macrophages modulate epithelial to mesenchymal transition of human adenocarcinoma cells.* Biofabrication, 2018. **10**(3): p. 035004.
76. Gao, L., et al., *CCL2/EGF positive feedback loop between cancer cells and macrophages promotes cell migration and invasion in head and neck squamous cell carcinoma.* Oncotarget, 2016. **7**(52): p. 87037-87051.
77. Zeng, X.Y., et al., *M2-like tumor-associated macrophages-secreted EGF promotes epithelial ovarian cancer metastasis via activating EGFR-ERK signaling and suppressing lncRNA LIMT expression.* Cancer Biol Ther, 2019. **20**(7): p. 956-966.
78. Zhou, K., et al., *Targeting tumor-associated macrophages in the tumor microenvironment.* Oncol Lett, 2020. **20**(5): p. 234.
79. Corliss, B.A., et al., *Macrophages: An Inflammatory Link Between Angiogenesis and Lymphangiogenesis.* Microcirculation, 2016. **23**(2): p. 95-121.
80. Sunderkötter, C., et al., *Macrophages and angiogenesis.* J Leukoc Biol, 1994. **55**(3): p. 410-22.

81. Chen, Q., X.H. Zhang, and J. Massagué, *Macrophage binding to receptor VCAM-1 transmits survival signals in breast cancer cells that invade the lungs.* Cancer Cell, 2011. **20**(4): p. 538-49.
82. Reduzzi, C., et al., *The curious phenomenon of dual-positive circulating cells: Longtime overlooked tumor cells.* Semin Cancer Biol, 2020. **60**: p. 344-350.
83. Sutton, T.L., B.S. Walker, and M.H. Wong, *Circulating Hybrid Cells Join the Fray of Circulating Cellular Biomarkers.* Cell Mol Gastroenterol Hepatol, 2019. **8**(4): p. 595-607.
84. Dietz, M.S., et al., *Relevance of Circulating Hybrid Cells as a Non-Invasive Biomarker for Myriad Solid Tumors.* bioRxiv, 2021: p. 2021.03.11.434896.
85. Gast, C.E., et al., *Cell fusion potentiates tumor heterogeneity and reveals circulating hybrid cells that correlate with stage and survival.* Sci Adv, 2018. **4**(9): p. eaat7828.
86. Qian, B., et al., *A distinct macrophage population mediates metastatic breast cancer cell extravasation, establishment and growth.* PLoS One, 2009. **4**(8): p. e6562.
87. Long, K.B., et al., *IFNγ and CCL2 Cooperate to Redirect Tumor-Infiltrating Monocytes to Degrade Fibrosis and Enhance Chemotherapy Efficacy in Pancreatic Carcinoma.* Cancer Discov, 2016. **6**(4): p. 400-413.
88. Hartley, G.P., et al., *Programmed Cell Death Ligand 1 (PD-L1) Signaling Regulates Macrophage Proliferation and Activation.* Cancer Immunol Res, 2018. **6**(10): p. 1260-1273.
89. Kuang, D.M., et al., *Activated monocytes in peritumoral stroma of hepatocellular carcinoma foster immune privilege and disease progression through PD-L1.* J Exp Med, 2009. **206**(6): p. 1327-37.
90. Gordon, S.R., et al., *PD-1 expression by tumour-associated macrophages inhibits phagocytosis and tumour immunity.* Nature, 2017. **545**(7655): p. 495-499.
91. Chen, S., et al., *Harnessing and Enhancing Macrophage Phagocytosis for Cancer Therapy.* Front Immunol, 2021. **12**: p. 635173.
92. Zhang, F., et al., *Genetic programming of macrophages to perform anti-tumor functions using targeted mRNA nanocarriers.* Nat Commun, 2019. **10**(1): p. 3974.
93. Ramesh, A., et al., *CSF1R- and SHP2-Inhibitor-Loaded Nanoparticles Enhance Cytotoxic Activity and Phagocytosis in Tumor-Associated Macrophages.* Adv Mater, 2019. **31**(51): p. e1904364.
94. Zhang, Y.R., et al., *Nanoparticle-Enabled Dual Modulation of Phagocytic Signals to Improve Macrophage-Mediated Cancer Immunotherapy.* Small, 2020. **16**(46): p. e2004240.
95. Algül, H., et al., *Mechanisms of disease: chronic inflammation and cancer in the pancreas--a potential role for pancreatic stellate cells?* Nat Clin Pract Gastroenterol Hepatol, 2007. **4**(8): p. 454-62.
96. Jin, G., et al., *Molecular Mechanism of Pancreatic Stellate Cells Activation in Chronic Pancreatitis and Pancreatic Cancer.* J Cancer, 2020. **11**(6): p. 1505-1515.
97. Apte, M., R.C. Pirola, and J.S. Wilson, *Pancreatic stellate cell: physiologic role, role in fibrosis and cancer.* Curr Opin Gastroenterol, 2015. **31**(5): p. 416-23.
98. Butcher, D.T., T. Alliston, and V.M. Weaver, *A tense situation: forcing tumour progression.* Nat Rev Cancer, 2009. **9**(2): p. 108-22.
99. Paszek, M.J., et al., *Tensional homeostasis and the malignant phenotype.* Cancer Cell, 2005. **8**(3): p. 241-54.

100. Engler, A.J., et al., *Matrix elasticity directs stem cell lineage specification.* Cell, 2006. **126**(4): p. 677-89.
101. Ayad, N.M.E., S. Kaushik, and V.M. Weaver, *Tissue mechanics, an important regulator of development and disease.* Philos Trans R Soc Lond B Biol Sci, 2019. **374**(1779): p. 20180215.
102. Levental, K.R., et al., *Matrix crosslinking forces tumor progression by enhancing integrin signaling.* Cell, 2009. **139**(5): p. 891-906.
103. Provenzano, P.P., et al., *Matrix density-induced mechanoregulation of breast cell phenotype, signaling and gene expression through a FAK-ERK linkage.* Oncogene, 2009. **28**(49): p. 4326-43.
104. Rice, A.J., et al., *Matrix stiffness induces epithelial-mesenchymal transition and promotes chemoresistance in pancreatic cancer cells.* Oncogenesis, 2017. **6**(7): p. e352.
105. Carey, S.P., et al., *Local extracellular matrix alignment directs cellular protrusion dynamics and migration through Rac1 and FAK.* Integr Biol (Camb), 2016. **8**(8): p. 821-35.
106. Han, W., et al., *Oriented collagen fibers direct tumor cell intravasation.* Proc Natl Acad Sci U S A, 2016. **113**(40): p. 11208-11213.
107. Provenzano, P.P., et al., *Collagen reorganization at the tumor-stromal interface facilitates local invasion.* BMC Med, 2006. **4**(1): p. 38.
108. Ray, A., et al., *Anisotropic forces from spatially constrained focal adhesions mediate contact guidance directed cell migration.* Nat Commun, 2017. **8**: p. 14923.
109. Boyd, N.F., et al., *Mammographic densities and breast cancer risk.* Cancer Epidemiol Biomarkers Prev, 1998. **7**(12): p. 1133-44.
110. Boyd, N.F., et al., *Mammographic densities as a marker of human breast cancer risk and their use in chemoprevention.* Curr Oncol Rep, 2001. **3**(4): p. 314-21.
111. Habel, L.A., et al., *Mammographic density and breast cancer after ductal carcinoma in situ.* J Natl Cancer Inst, 2004. **96**(19): p. 1467-72.
112. McCormack, V.A. and I. dos Santos Silva, *Breast density and parenchymal patterns as markers of breast cancer risk: a meta-analysis.* Cancer Epidemiol Biomarkers Prev, 2006. **15**(6): p. 1159-69.
113. Provenzano, P.P., et al., *Collagen density promotes mammary tumor initiation and progression.* BMC Med, 2008. **6**: p. 11.
114. Ursin, G., et al., *Greatly increased occurrence of breast cancers in areas of mammographically dense tissue.* Breast Cancer Res, 2005. **7**(5): p. R605-8.
115. Conklin, M.W., et al., *Aligned collagen is a prognostic signature for survival in human breast carcinoma.* Am J Pathol, 2011. **178**(3): p. 1221-32.
116. Conklin, M.W., et al., *Collagen Alignment as a Predictor of Recurrence after Ductal Carcinoma.* Cancer Epidemiol Biomarkers Prev, 2018. **27**(2): p. 138-145.
117. Drifka, C.R., et al., *Highly aligned stromal collagen is a negative prognostic factor following pancreatic ductal adenocarcinoma resection.* Oncotarget, 2016. **7**(46): p. 76197-76213.
118. Gill, J.K., et al., *The association of mammographic density with ductal carcinoma in situ of the breast: the Multiethnic Cohort.* Breast Cancer Res, 2006. **8**(3): p. R30.
119. Larsen, A.M.H., et al., *Collagen Density Modulates the Immunosuppressive Functions of Macrophages.* J Immunol, 2020. **205**(5): p. 1461-1472.

120. Tam, W.Y. and C.H. Ma, *Bipolar/rod-shaped microglia are proliferating microglia with distinct M1/M2 phenotypes.* Sci Rep, 2014. **4**: p. 7279.
121. McWhorter, F.Y., et al., *Modulation of macrophage phenotype by cell shape.* Proc Natl Acad Sci U S A, 2013. **110**(43): p. 17253-8.
122. Liu, Y., et al., *Dissonant response of M0/M2 and M1 bone-marrow-derived macrophages to RhoA pathway interference.* Cell Tissue Res, 2016. **366**(3): p. 707-720.
123. Luu, T.U., et al., *Micro- and Nanopatterned Topographical Cues for Regulating Macrophage Cell Shape and Phenotype.* ACS Appl Mater Interfaces, 2015. **7**(51): p. 28665-72.
124. Schwartz, M.A., *Integrins and extracellular matrix in mechanotransduction.* Cold Spring Harb Perspect Biol, 2010. **2**(12): p. a005066.
125. Sulzmaier, F.J., C. Jean, and D.D. Schlaepfer, *FAK in cancer: mechanistic findings and clinical applications.* Nat Rev Cancer, 2014. **14**(9): p. 598-610.
126. Schaller, M.D., *Cellular functions of FAK kinases: insight into molecular mechanisms and novel functions.* J Cell Sci, 2010. **123**(Pt 7): p. 1007-13.
127. Murphy, J.M., et al., *Targeting focal adhesion kinase in cancer cells and the tumor microenvironment.* Exp Mol Med, 2020. **52**(6): p. 877-886.
128. Serrels, A., et al., *Nuclear FAK controls chemokine transcription, Tregs, and evasion of anti-tumor immunity.* Cell, 2015. **163**(1): p. 160-73.
129. Gukovsky, I., et al., *Inflammation, autophagy, and obesity: common features in the pathogenesis of pancreatitis and pancreatic cancer.* Gastroenterology, 2013. **144**(6): p. 1199-209.e4.
130. Lowenfels, A.B., et al., *Pancreatitis and the risk of pancreatic cancer. International Pancreatitis Study Group.* N Engl J Med, 1993. **328**(20): p. 1433-7.
131. Lowenfels, A.B. and P. Maisonneuve, *Epidemiology and risk factors for pancreatic cancer.* Best Pract Res Clin Gastroenterol, 2006. **20**(2): p. 197-209.
132. Xue, J., et al., *Alternatively activated macrophages promote pancreatic fibrosis in chronic pancreatitis.* Nat Commun, 2015. **6**: p. 7158.
133. Zheng, L., et al., *Role of immune cells and immune-based therapies in pancreatitis and pancreatic ductal adenocarcinoma.* Gastroenterology, 2013. **144**(6): p. 1230-40.
134. Sakorafas, G.H. and M.G. Sarr, *Pancreatic cancer after surgery for chronic pancreatitis.* Dig Liver Dis, 2003. **35**(7): p. 482-5.
135. Rhim, A.D., et al., *EMT and dissemination precede pancreatic tumor formation.* Cell, 2012. **148**(1-2): p. 349-61.
136. Deng, S., et al., *Chronic pancreatitis and pancreatic cancer demonstrate active epithelial-mesenchymal transition profile, regulated by miR-217-SIRT1 pathway.* Cancer Lett, 2014. **355**(2): p. 184-91.
137. Rhim, A.D., et al., *Detection of circulating pancreas epithelial cells in patients with pancreatic cystic lesions.* Gastroenterology, 2014. **146**(3): p. 647-51.
138. Guerra, C., et al., *Pancreatitis-induced inflammation contributes to pancreatic cancer by inhibiting oncogene-induced senescence.* Cancer Cell, 2011. **19**(6): p. 728-39.
139. Guerra, C., et al., *Chronic pancreatitis is essential for induction of pancreatic ductal adenocarcinoma by K-Ras oncogenes in adult mice.* Cancer Cell, 2007. **11**(3): p. 291-302.
140. Hingorani, S.R., et al., *Preinvasive and invasive ductal pancreatic cancer and its early detection in the mouse.* Cancer Cell, 2003. **4**(6): p. 437-50.

141. Zhu, Y., et al., *Tissue-Resident Macrophages in Pancreatic Ductal Adenocarcinoma Originate from Embryonic Hematopoiesis and Promote Tumor Progression.* Immunity, 2017. **47**(2): p. 323-338.e6.
142. Beatty, G.L., et al., *Exclusion of T Cells From Pancreatic Carcinomas in Mice Is Regulated by Ly6C(low) F4/80(+) Extratumoral Macrophages.* Gastroenterology, 2015. **149**(1): p. 201-10.
143. Adams, S., et al., *Mechano-Immunomodulation: Mechanoresponsive Changes in Macrophage Activity and Polarization.* Ann Biomed Eng, 2019. **47**(11): p. 2213-2231.
144. Jain, N., J. Moeller, and V. Vogel, *Mechanobiology of Macrophages: How Physical Factors Coregulate Macrophage Plasticity and Phagocytosis.* Annu Rev Biomed Eng, 2019. **21**: p. 267-297.
145. Meli, V.S., et al., *Biophysical regulation of macrophages in health and disease.* J Leukoc Biol, 2019. **106**(2): p. 283-299.
146. Wosik, J., et al., *Magnetic Field Changes Macrophage Phenotype.* Biophys J, 2018. **114**(8): p. 2001-2013.
147. Schedin, P. and P.J. Keely, *Mammary gland ECM remodeling, stiffness, and mechanosignaling in normal development and tumor progression.* Cold Spring Harb Perspect Biol, 2011. **3**(1): p. a003228.
148. Northcott, J.M., et al., *Feeling Stress: The Mechanics of Cancer Progression and Aggression.* Frontiers in Cell and Developmental Biology, 2018. **6**: p. 17.
149. Provenzano, P.P. and P.J. Keely, *Mechanical signaling through the cytoskeleton regulates cell proliferation by coordinated focal adhesion and Rho GTPase signaling.* J Cell Sci, 2011. **124**(Pt 8): p. 1195-205.
150. Ray, A., et al., *Stromal architecture directs early dissemination in pancreatic ductal adenocarcinoma.* bioRxiv, 2021: p. 2021.02.19.431984.
151. Panni, R.Z., et al., *Agonism of CD11b reprograms innate immunity to sensitize pancreatic cancer to immunotherapies.* Science Translational Medicine, 2019. **11**(499): p. eaau9240.
152. Zhu, Y., et al., *Tissue-Resident Macrophages in Pancreatic Ductal Adenocarcinoma Originate from Embryonic Hematopoiesis and Promote Tumor Progression.* Immunity, 2017. **47**(2): p. 323-338.e6.
153. Drifka, C.R., et al., *Periductal stromal collagen topology of pancreatic ductal adenocarcinoma differs from that of normal and chronic pancreatitis.* Mod Pathol, 2015. **28**(11): p. 1470-80.
154. Tabdanov, E., et al., *Engineering T cells to enhance 3D migration through structurally and mechanically complex tumor microenvironments.* BioRXiv (Accepted at Nature Communications), 2020. **https://doi.org/10.1101/2020.04.21.051615**.
155. Tabdanov, E.D., et al., *Engineering T cells to enhance 3D migration through structurally and mechanically complex tumor microenvironments.* Nat Commun, 2021. **12**(1): p. 2815.
156. Tabdanov, E.D., et al., *Microtubule-Actomyosin Mechanical Cooperation during Contact Guidance Sensing.* Cell Rep, 2018. **25**(2): p. 328-338 e5.
157. Zaghdoudi, S., et al., *FAK activity in cancer-associated fibroblasts is a prognostic marker and a druggable key metastatic player in pancreatic cancer.* EMBO Molecular Medicine, 2020. **12**(11): p. e12010.

158. Tabdanov, E.D., et al., *Microtubule-Actomyosin Mechanical Cooperation during Contact Guidance Sensing.* Cell Rep, 2018. **25**(2): p. 328-338.e5.
159. Lee, H.O., et al., *FAP-overexpressing fibroblasts produce an extracellular matrix that enhances invasive velocity and directionality of pancreatic cancer cells.* BMC Cancer, 2011. **11**: p. 245.
160. Husemann, Y., et al., *Systemic spread is an early step in breast cancer.* Cancer Cell, 2008. **13**(1): p. 58-68.
161. Hosseini, H., et al., *Early dissemination seeds metastasis in breast cancer.* Nature, 2016. **540**(7634): p. 552-558.
162. Provenzano, P.P., et al., *Contact guidance mediated three-dimensional cell migration is regulated by Rho/ROCK-dependent matrix reorganization.* Biophys J, 2008. **95**(11): p. 5374-84.
163. Ray, A., et al., *Enhanced Directional Migration of Cancer Stem Cells in 3D Aligned Collagen Matrices.* Biophys J, 2017. **112**(5): p. 1023-1036.
164. Bredfeldt, J.S., et al., *Computational segmentation of collagen fibers from second-harmonic generation images of breast cancer.* J Biomed Opt, 2014. **19**(1): p. 16007.
165. Brett, M.E., A.L. Crampton, and D.K. Wood, *Rapid generation of collagen-based microtissues to study cell-matrix interactions.* Technology, 2016. **4**(2): p. 80-87.
166. Crampton, A.L., K.A. Cummins, and D.K. Wood, *A High-Throughput Workflow to Study Remodeling of Extracellular Matrix-Based Microtissues.* Tissue Eng Part C Methods, 2019. **25**(1): p. 25-36.
167. Ray, A., R.K. Morford, and P.P. Provenzano, *Cancer Stem Cell Migration in Three-Dimensional Aligned Collagen Matrices.* Curr Protoc Stem Cell Biol, 2018: p. e57.
168. Ray, A., et al., *Dynamics of 3D carcinoma cell invasion into aligned collagen.* Integr Biol (Camb), 2018. **10**(2): p. 100-112.
169. Kraman, M., et al., *Suppression of antitumor immunity by stromal cells expressing fibroblast activation protein-alpha.* Science, 2010. **330**(6005): p. 827-30.
170. Neesse, A., et al., *Stromal biology and therapy in pancreatic cancer: a changing paradigm.* Gut, 2015. **64**(9): p. 1476-84.
171. Katoh, H. and Y. Fujita, *Epithelial homeostasis: elimination by live cell extrusion.* Curr Biol, 2012. **22**(11): p. R453-5.
172. Slattum, G.M. and J. Rosenblatt, *Tumour cell invasion: an emerging role for basal epithelial cell extrusion.* Nat Rev Cancer, 2014. **14**(7): p. 495-501.
173. Gu, Y., et al., *Defective apical extrusion signaling contributes to aggressive tumor hallmarks.* Elife, 2015. **4**: p. e04069.
174. Ray, A., et al., *Dynamics of 3D carcinoma cell invasion into aligned collagen.* Integr Biol (Camb), 2018.
175. Hendley, A.M., et al., *p120 Catenin Suppresses Basal Epithelial Cell Extrusion in Invasive Pancreatic Neoplasia.* Cancer Res, 2016. **76**(11): p. 3351-63.
176. Zheng, X., et al., *Epithelial-to-mesenchymal transition is dispensable for metastasis but induces chemoresistance in pancreatic cancer.* Nature, 2015. **527**(7579): p. 525-530.
177. Krebs, A.M., et al., *The EMT-activator Zeb1 is a key factor for cell plasticity and promotes metastasis in pancreatic cancer.* Nature Cell Biology, 2017. **19**(5): p. 518-529.
178. Tabdanov, E.D., et al., *Microtubule-Actomyosin Mechanical Cooperation during Contact Guidance Sensing.* Cell Rep, 2018. **25**(2): p. 328-338 e6.

179. Wyckoff, J., et al., *A paracrine loop between tumor cells and macrophages is required for tumor cell migration in mammary tumors.* Cancer Res, 2004. **64**(19): p. 7022-9.
180. Olive, K.P., et al., *Inhibition of Hedgehog signaling enhances delivery of chemotherapy in a mouse model of pancreatic cancer.* Science, 2009. **324**(5933): p. 1457-61.
181. Bement, W.M., *Actomyosin rings: the riddle of the sphincter.* Curr Biol, 2002. **12**(1): p. R12-4.
182. Kubow, Kristopher E., Sarah K. Conrad, and A.R. Horwitz, *Matrix Microarchitecture and Myosin II Determine Adhesion in 3D Matrices.* Current Biology, 2013. **23**(17): p. 1607-1619.
183. Tabdanov, E.D., et al., *Bimodal sensing of guidance cues in mechanically distinct microenvironments.* Nat Commun, 2018. **9**(1): p. 4891.
184. Stokes, J.B., et al., *Inhibition of focal adhesion kinase by PF-562,271 inhibits the growth and metastasis of pancreatic cancer concomitant with altering the tumor microenvironment.* Molecular Cancer Therapeutics. **10**(11): p. 2135-45

185. Tandon, M., et al., *Prolactin Promotes Fibrosis and Pancreatic Cancer Progression.* Cancer Research, 2019. **79**(20): p. 5316.
186. Lachowski, D., et al., *Substrate Rigidity Controls Activation and Durotaxis in Pancreatic Stellate Cells.* Sci Rep, 2017. **7**(1): p. 2506.
187. Chauhan, V.P., et al., *Angiotensin inhibition enhances drug delivery and potentiates chemotherapy by decompressing tumour blood vessels.* Nat Commun, 2013. **4**: p. 2516.
188. Roh-Johnson, M., et al., *Macrophage contact induces RhoA GTPase signaling to trigger tumor cell intravasation.* Oncogene, 2014. **33**(33): p. 4203-12.
189. P, B., et al., *Inflammatory and Innate Immune Cells in Cancer Microenvironment and Progression*. 2015, Springer, Berlin, Heidelberg: Cancer Immunology.
190. Murphy, J.E., et al., *Total Neoadjuvant Therapy With FOLFIRINOX in Combination With Losartan Followed by Chemoradiotherapy for Locally Advanced Pancreatic Cancer: A Phase 2 Clinical Trial.* JAMA Oncol, 2019. **5**(7): p. 1020-1027.

# APPENDIX

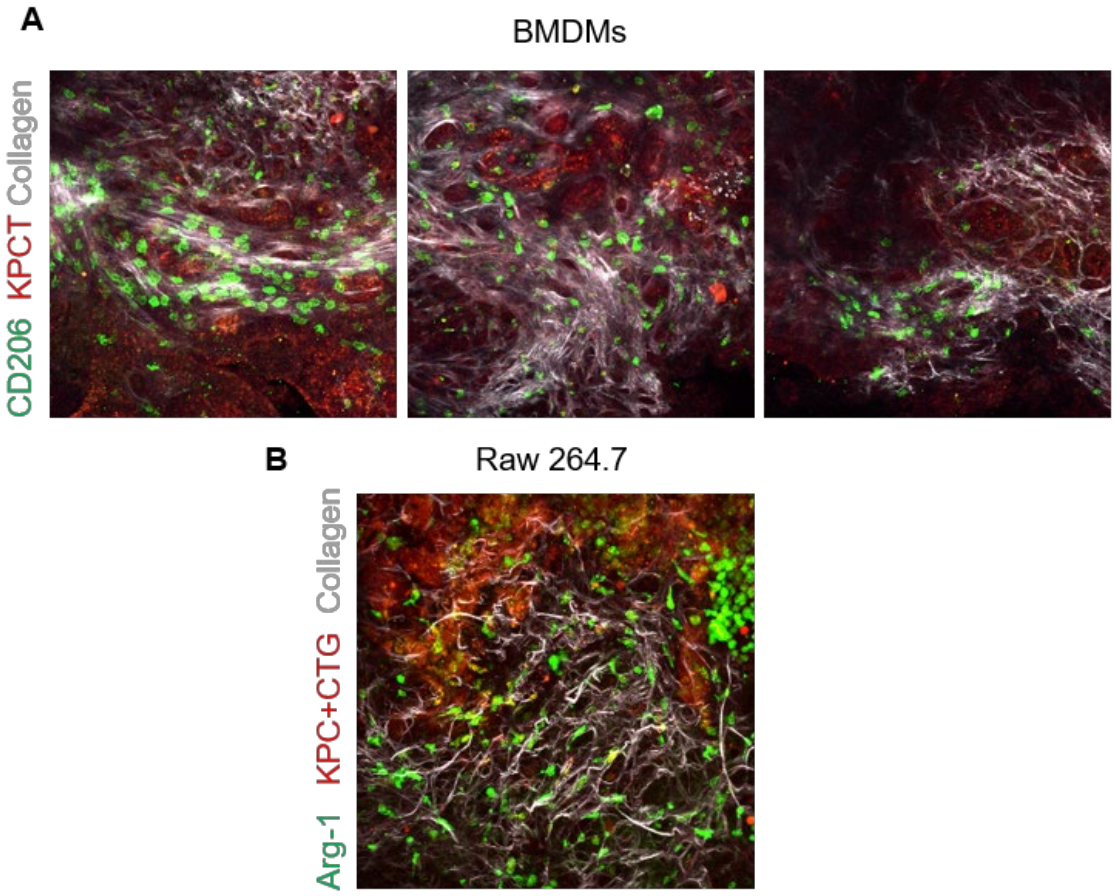


**Supplemental Figure S2.1 Exogenous macrophages home to collagen and express canonical M2 markers. A)** Primary bone marrow derived macrophages were seeded and cultured on live tumor slices for 24 hours, after which cells slices were stained and imaged to assess expression of CD206 and localization relative to collagen. **B)** Immortalized macrophage like line Raw 264.7 were seeded on live tumor slices for 24 hours, after which slices were stained to assess macrophage expression of Arginase-1.

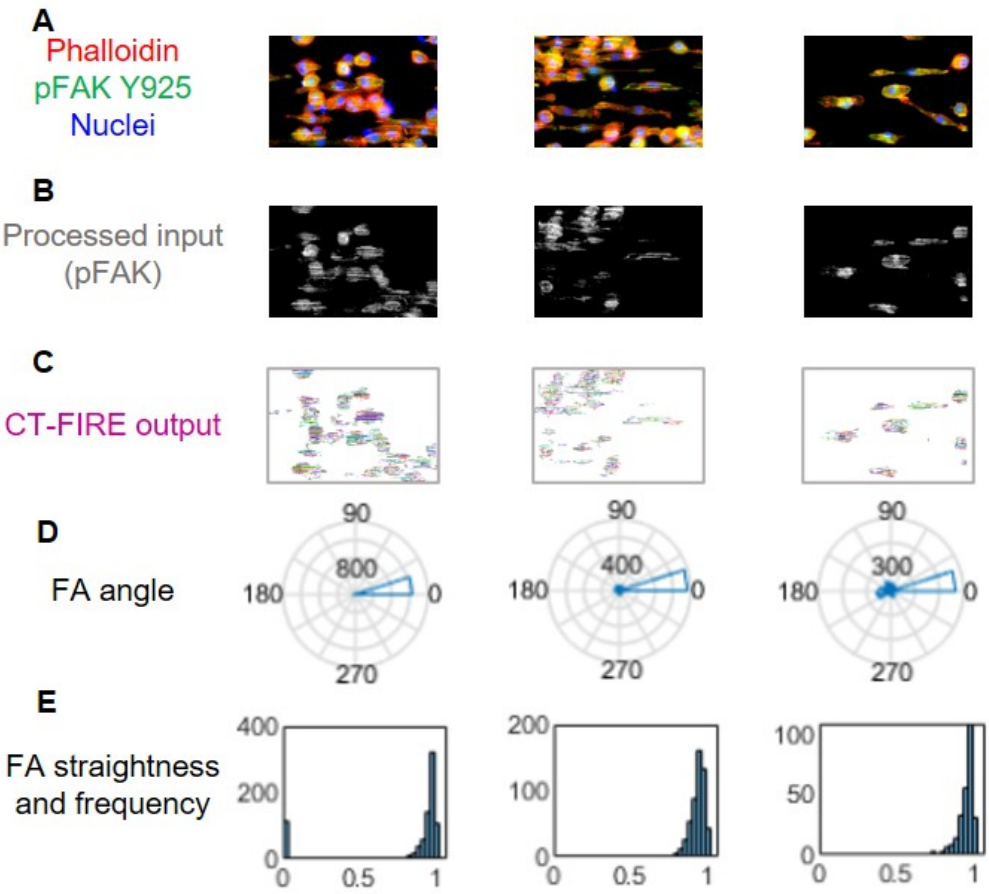


**Supplemental Figure S2.2 Explanation and examples of macrophage focal adhesion characterization. A)** 3 fields of view as examples for quantification. **B)** Processed images from **(A)** depicting image input going into CT-FIRE analysis. **C)** CT-FIRE output masks for characterizing focal adhesion angle **(D)**, where the frequency of the focal adhesion angle is given in the center of the plot (800, 400, and 300 from left to right) with zero degrees being the most frequent orientation, and straightness **(E)** where a 1 on the X-axis represents a perfectly straight and aligned adhesion, and the frequency of the number of adhesions for each measured straightness on the Y-axis.

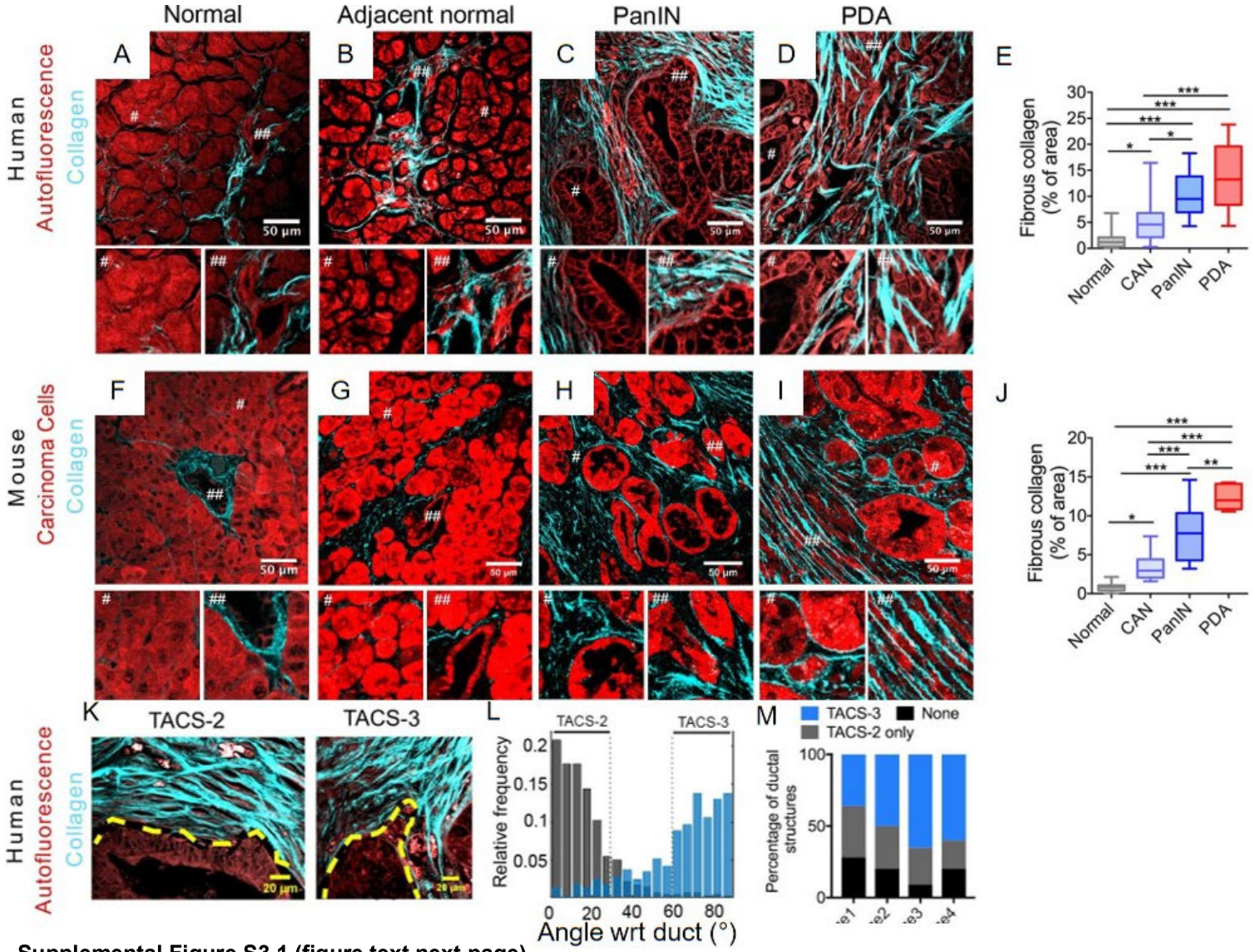


**Supplemental Figure S3.1 (figure text next page).**

**Supplemental Figure S3.1 Fibrous collagen architectures in PDA. (A-D)** LSMPM/SHG of human sample tissue architecture (autofluorescence) and fibrous collagen **(A)** normal, **(B)** cancer-adjacent normal, **(C)** PanIN and **(D)** mature PDA (# and ## are 2X magnifications of the indicated regions). **(E)** Collagen quantification for the data shown in a-d (n=10-21 fields of view across n≥3 patient biopsies). **(F-G)** LSMPM/SHG of *KPCT* or *KPCG* mouse models of PDA for **(F)** normal, **(G)** cancer-adjacent normal, **(H)** PanIN and **(I)** well-differentiated PDA. Note, all tdTomato or zsGreen fluorescence is pseudo-colored red throughout the manuscript for consistency of identifying carcinoma cells. **(J)** Collagen quantification for the data shown in f-I (n=5-12 fields of views across n≥3 mice. **(K-M)** Representative TACS-2 and TACS-3 positive ducts in well-differentiated human PDA depicting parallel and perpendicular alignment of fibrous collagen, with yellow dashed lines indicating ductal boundaries **(K)**, quantified by CT-FIRE **(L)**. **(M)** Frequency of TACS-2 and TACS-3 associated with ductal structures in well-differentiated regions from different stages of human disease (from pathology staged and graded TMA) showing increased prevalence TACS-3 with more advanced disease. Scale bars = 50 μm **(A-D, F-I, K** (right) **)** and 20 μm **(K** (left)**)**, box-whisker plots show min to max with median and interquartile range for e and j; *p<0.05, **p<0.01, ***p<0.001 by the non-parametric Kruskal-Wallis test and Dunn's multiple comparison test.

---

**Supplemental Figure S3.2 Characterization of PDA cell extrusion into periductal collagen architectures**. **(A, B)** Schematic (top left boxes) and images of partial extrusion of carcinoma cells as observed in *KPCT* or *KPCG* tumor sections showing cells extruding into **(A)** TACS-2 and **(B)** TACS-3 architectures in the stroma. Enlarged panels (yellow boxes) depict all three channels (bottom right) or only the fluorescent reporter and nuclei channels (insets). Yellow arrowhead (in **B**) points to an additional cell that is fully extruded and aligned to the collagen fibers. **(C, D)** Quantification of frequency and types of partial cell extrusion in **(C)** PanIN and **(D)** well-differentiated PDA (WD-PDA); II and ⊥ indicates parallel TACS2 and perpendicular TACS3 architectures, respectively; data are mean +/- SD. **(E)** Partial extrusion observed in human well-differentiated PDA samples. Yellow boxes represent the zoomed region showing either all three channels (bottom inset) or only the fluorescent reporter and nuclei channels (top inset). **(F-H)** Fully extruded carcinoma cells invading through the stroma **(F, G)** were observed at similar frequency in PanIN and well-differentiated PDA **(H)** and cells along collagen fibers displayed either an **(F)** elongated and oriented phenotypes (high AR phenotype) or **(G)** a more rounded phenotype with smaller cell diameters (Low AR phenotype); Insets represent zoomed in images, identified with yellow boxes, showing only the fluorescent reporter and nuclei channels. **(I, J)** Morphometric analysis of extruded cells shows a large range of **(I)** aspect ratios and **(J)** diameters (high and low aspect ratios cells are represented in **(F)** and **(G)** respectively. **(K)** Full extrusion of invading cells from ductal structures was observed in human well-differentiated PDA samples; Insets represent zoomed in images identified with yellow boxes showing the fluorescent reporter and nuclei channels, solid yellow arrowhead **(K)** points to an additional, aligned, fully extruded cell and the outlined yellow arrowhead points to one that is rounded and non-aligned. **(L, M)** Cancer adjacent "normal" regions from KPC mice or human disease showing basal extrusions associated with collagen fibers. **(N)** Collagen architecture surrounding ducts in human chronic pancreatitis (CP). **(O)** Frequency of TACS-2 and TACS-3 in association with ductal structures in human CP (Analysis is from 8-33 fields of view from two biopsies per patient from 6 patients with human CP; note, every patient sample presented with ducts that were TACS-3-positive). Scale bars = 20 μm, n >50 fields of view across 11 mice **(C)**, n >20 fields of view across 6 mice **(D and H)**, n=68 cells across 12 mice for **(I)** and **(J)**; data are mean +/- SD.

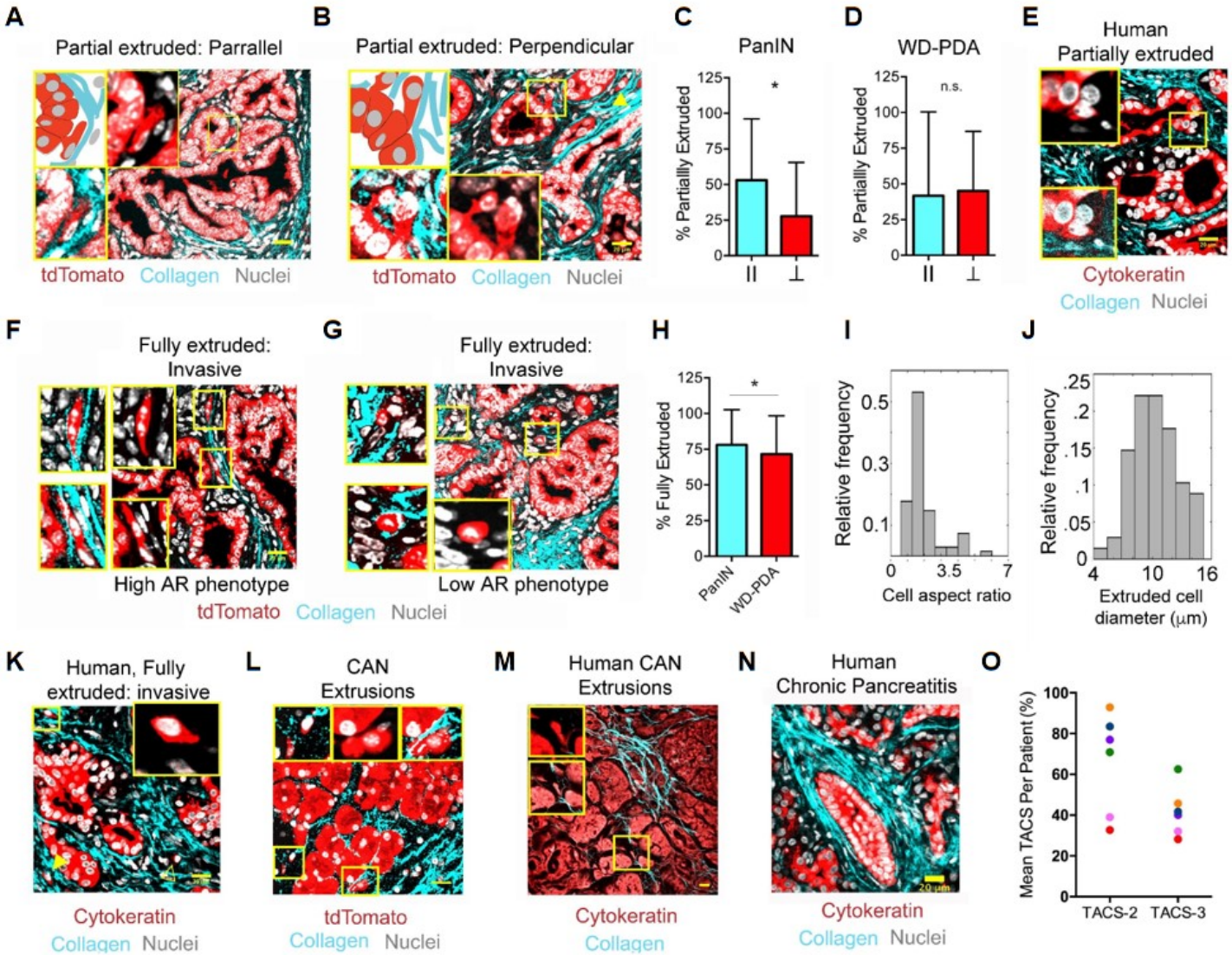


**Supplemental Figure S3.2 (figure text previous page).**

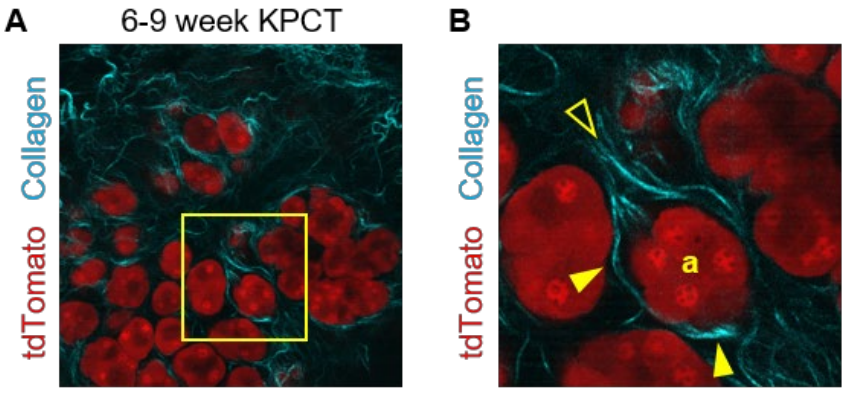


**Supplemental Figure S3.3 TACS may precede appearance of PanINs in young KPCT mice. A)** Live imaging of KPCT pancreas tissue in mice 6-9 weeks of age showing presence of TACS preceding appearance of ductal lesions. Boxed region of interest is magnified in **(B)** to show an acinar cluster (labeled "a") displaying TACS-2 (filled arrow head) and TACS-3 (arrow head outline) architectures.

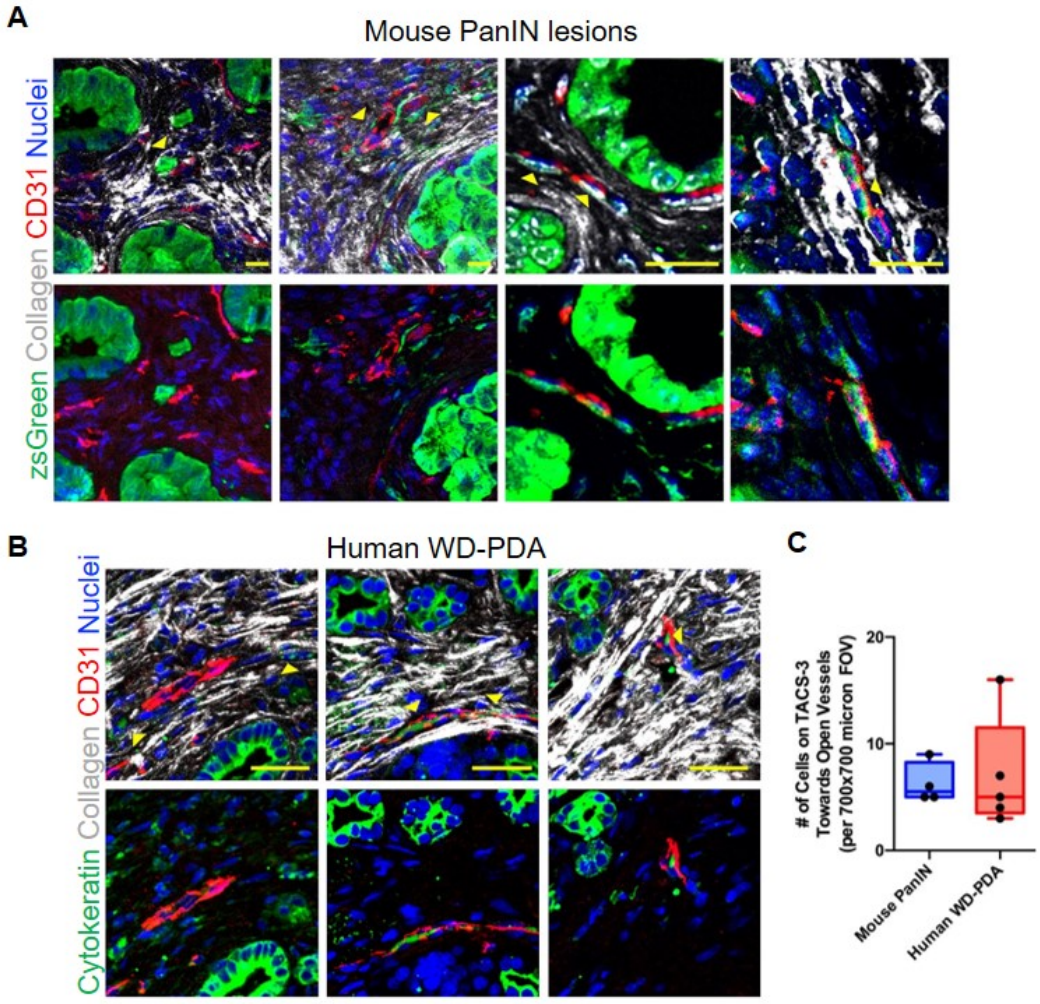


**Supplemental Figure S3.4 Additional examples of extruded cells on aligned collagen interacting with CD31+ vasculature. A)** Extruded cells interacting with vasculature in mPanIN. **B)** Extruded carcinoma cells interacting with vasculature in human PDA. **C)** Quantification of the number of cells per field of view utilizing TACS-3 architectures to migrate toward vasculature in mouse PanIN and human PDA.